# Dipyrrin Complexes as Dyes for Dye-Sensitised Solar Cells

A thesis submitted in partial fulfilment of the
requirements for the degree of

Masters in Science
in Chemistry

at
Massey University, Palmerston North,
New Zealand.

Serena Jade Smalley

2009

# ABSTRACT

## DIPYRRIN COMPLEXES AS DYES FOR DYE-SENSITISED SOLAR CELLS

By Serena Smalley

Supervised by Doctor Shane G. Telfer and Doctor Mark R. Waterland
Institute of Fundamental Sciences, College of Sciences,
Massey University, Palmerston North.

With increasing concerns of global warming and the impending exhaustion of fossil fuels attention is being turned to renewable sources of energy. The sun supplies 3 x $10^{24}$ J per year to the earth which is around $10^4$ times more energy than what the human race consumes. The world's energy needs would be satisfied if a mere 0.1% of the planet's surface was covered with solar cells($\eta$ = 10%)[1], causing the conversion of solar energy (sunlight) into electricity to represent a very practical renewable source.

Past research into solar energy has produced a photovoltaic device, which when coupled with highly coloured coordination compounds, enables this conversion. This device is known as a dye-sensitised solar cell (DSSC). Further research has been conducted into the properties of the dyes, and has shown that highly coloured coordination compounds are able to convert solar energy into electrical energy with the highest efficiencies. The dominant compounds in this area to date have been Grätzel's ruthenium complexes and porphyrins.

However, there exists a class of smaller compounds called dipyrrins, described most simply as "half a porphyrin", which possess many of the attractive qualities for DSSC dyes. Although there are no examples of ruthenium-dipyrrin complexes in the literature, the combination of advantageous properties from both components represent very attractive synthetic targets with huge potential as dyes for DSSCs.

The objectives of this thesis were firstly to develop a series of dipyrrin complexes which would be suitable as dyes for DSSCs; then to fully characterise the complexes and investigate the spectroscopic properties of each complex; and finally to determine the suitability of the complexes as dyes for DSSCs. These objectives were fully met, resulting

in a set of generic target compounds characterised via $^{1}H$ NMR, $^{13}C$ NMR, mass spectrometry (ESI-MS), elemental analysis, and x-ray crystallography. From analyses of the UV-visible, fluorescence, emission, and Raman spectra; and electrochemistry results; the complexes were concluded to be suitable as dyes for DSSC's. An additional bonus is that the syntheses for these complexes are applicable to any dipyrrin, thus aiding future studies into the use of dipyrrins as dyes for DSSC's. This thesis summarises the findings of the above outlined research project.

*Gratzel, M. (2005). Inorganic Chemistry, 44(20), p6481-6851*

# ACKNOWLEDGMENTS

I wish to acknowledge my supervisors Dr Shane Telfer and Dr Mark Waterland for their assistance, advice and patience thorough out the duration of my research project.

I also wish to extend my gratitude to my parents (Steve and Joy Smalley), sisters (Sian and Michaela Smalley), and partner (Alex Cade); particularly during times of frustration and waning motivation. Without the endless supply of loving support and encouragement they gave me this thesis and the laboratory work that went into it would never have come to fruition.

Thanks to the Manawatu branch of the New Zealand Federation for Graduate Women for the financial assistance that allowed me to complete the research component of my Masters in Science. Finally, thanks also to Dr Paul Plieger and his wife Isabel who provided paid work which allowed me to complete the final stages of writing this thesis.

**Acknowledgements for technical assistance:**

*Laboratory Assistance:* Dr Carl Otter for answering my many questions and providing practical assistance in the laboratory.

*Nuclear Magnetic Resonance Spectroscopy*: Dr Pat Edwards for help running NMR experiments, and also assistance in construction of the NMR diagrams in Chapter 2.

*X-Ray Crystallography:* Dr Shane Telfer for collecting data, solving and refining structures, and preparing ORTEP plots. Dr Geoff Jameson who assisted with the interpretation of the x-ray crystal structures.

*Raman Spectroscopy:* Tracey McLean who assisted with collection of spectroscopic data.

*Electrochemistry:* Dr Sivakumar Balakrishnan who assisted with the collection of the electrochemistry data. Dr Simon Hall who assisted with the interpretation of the electrochemistry data.

*Solar Cell Testing*: Dr Wayne Campbell for assistance in the preliminary solar cell testing of my complexes and also for the use of the DSSC animated power point slide which was used as the basis for the DSSC schematic in Chapter 1.

TABLE OF CONTENTS

# LIST OF FIGURES, SCHEMES, TABLES AND EQUATIONS

*Number* *Page*

# ABBREVIATIONSAND SYMBOLS

**acac**. acetylacentone

**bipy**. Bipyridine (2,2'-bipyridine, unless otherwise stated)

**BODIPY**. Borondifluoride dipyrrin

**$CH_3OH$**. Methanol. Also abbreviated to MeOH. Deuterated methanol is represented as MeOD or $CD_3OD$.

**$CHCl_3$**. Chloroform. Deuterated chloroform is represented as $CDCl_3$

**dcbipy**. Dicarboxybipyridine (4,4'-dicarboxy-2,2'-bipyridine, unless otherwise stated)

**DMF**. Dimethylformamide

**DMSO**. Dimethylsulfoxide

**dp**. Dipyrrin

**dpm**. Dipyrromethane

**DSSC**. Dye-sensitised solar cell. Sometimes abbreviated further to DSC

**ESI-MS**. Electrospray ionisation mass spectrometry

**HOMO**. Highest occupied molecular orbital

**HTM**. Hole transport material

**LHE**. Light harvesting efficiency

**LUMO**. Lowest unoccupied molecular orbital

**MC**. Metal centered

**MLCT**. Metal-to-ligand charge transfer

**$molL^{-1}$**. moles per litre, measure of concentration. May be abbreviated further to M, inverse is $Lmol^{-1}$. Also appears in the text as $mmolL^{-1}$ which denotes milimoles per litre.

**$NEt_3$**. Triethylamine

**NMR**. Nuclear magnetic resonance

**phen**. Phenanthroline (1,10-phenanthroline, unless otherwise stated)

**ppm**. Parts per million

**Ru(II)**. Ruthenium(II), $Ru^{2+}$

**SCN**. Thiocyanate

**SEM**. Scanning electron micrograph

**TCO**. Transparent conducting oxide

**TFA**. Trifluroacetic acid

**THF**. Tetrahydrofuran

**$TiO_2$**. Titanium dioxide

**TLC**. Thin layer chromatography

**TnBA**. Tetra-n-butyl ammonium

**UV**. Ultraviolet

**1-T**. Transmittance

**A**. Absorbance

**Bu**. Butyl group i.e $C_4H_9$

**$^{13}$C**. Carbon. In reference to NMR spectroscopy utilising the $^{13}$C isotope of carbon.

**$e^-$**. Electron

**$^1$H**. Proton (hydrogen). In reference to NMR spectroscopy utilising the $^1$H isotope of hydrogen.

***hυ***. Light, photons

**$I^-/I_3^-$**. Iodide/Triiodide

**Jsc**. Short-circuit current (Amps)

**kT**. Boltzman constant ($JK^{-1}$) multiplied by temperature (K)

**M**. generic metal

**Me**. Methyl group i.e $CH_3$

**nm**. Nanometres = $10^9$ m

**Pmax**. The maximum quantity of power supplied (watts)

**Psource**. Quantity of power supplied from the power source (watts)

**R**. generic functional group

**$s^{-1}$**. per second, unit.

**V**. volts – the unit for voltage

**Voc**. Open-circuit voltage (V)

**ΔE**. Change in energy (Joules). Also appears in the text as $\Delta E_n$ where n denotes a number to differentiate the changes in energy of different processes.

**ε**. Molar absorptivity or absorbance coefficient (L $mol^{-1}$ $cm^{-1}$)

$\eta$. Solar cell efficiency (%)

**λex**. Excitation wavelength (nm)

**λmax**. Wavelength maximum or energy maximum (nm)

**μm**. Micrometres = $10^6$ m

# GLOSSARY

**Complex solution**. The volumetric solution containing the quantitative sample of the complex under investigation.

**Dipyrrin**. A compound containing two pyrrole rings joined via a methine (**–C=)** group.

**Free-base**. Refers to the deprotonated dipyrrin, where the proton on the tautomeric pyrrole rings of the body of the dipyrrin has been removed.

**Heteroleptic**. A metal centre bearing two or more different ligands.

**Homoleptic**. A metal centre bearing two or more identical ligands.

**Redox Potential**. A measure, in volts (V), of the affinity of a chemical species for electrons. Indicative of the species ability to gain electrons and thereby be reduced.

**Trituration**. The purification of a solid by using a solid in which the impurity is soluble, but the desired compound is not (or *vice versa*).

*Chapter 1*

# INTRODUCTION

## 1.1. Dipyrrins

Dipyyrins are a group of compounds formally composed of two pyrrole rings fused through a methine (-CH=) group through the 2,2' positions. The general dipyrrin structure with the IUPAC numbering scheme for conventional dipyrrin nomenclature is shown in Figure 1.1[2, 3]. This class of compounds are known by a vast array of names including dipyrrin, dipyrromethene, dipyrrylmethene, pyrrylmethene, pyrromethene, dipyrrolemethene, diaza-*s*-indacene, 2-pyrrol-ylmethylene-*2H*-pyrrolenine, and 2-(*2H*-pyrrol-2-ylidenemethyl)-pyrrole[3]. Dipyrrins can be viewed in the crudest way simply as half a porphyrin (Figure 1.2). Dipyrrin ligands possess a conjugated π system analogous to porphyrins, which endows free-base dipyrrins and dipyrrinato complexes with interesting and useful light absorption, light emission and chiroptical properties[4].

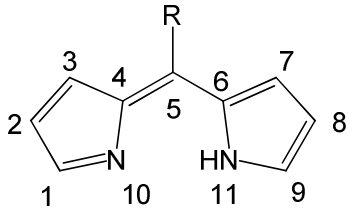


**Figure 1.1** The general dipyrrin structure with the IUPAC numbering scheme for conventional dipyrrin nomenclature.

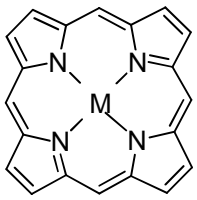


**Figure 1.2** The general structure of a porphyrin, where M denotes a metal centre.

*Meso*-substituted dipyrrins can be prepared easily using a wide range of functionalized aryaldehydes, starting with reagents which are both abundant and commercially available. Preparation is most commonly via a two-step procedure: acid-catalysed condensation of

pyrrole with the arylaldehyde, followed by oxidation of the resulting dipyrromethane. Yields are generally greater than 50% with high purity and are scalable[3]. The resulting symmetrically substituted free-base dipyrrin exists as a tautomer, and are more or less planar with the nitrogen atoms arranged in a *syn*-formation[5]. Free-base dipyrrins are regarded as relatively strong bases and consequently, are often stable in this form. The stability of the free-base dipyrrin depends on the nature and number of substituents, where fully unsubstituted dipyrrin is the least stable. This is due to the susceptibility of the unsubstituted ring to electrophillic and nucleophillic attack [3]. Stability is also reduced when the dipyrrin exists in solution rather than as a solid, but is greatly increased when the dipyrrin is coordinated in a metal complex. Various functional groups may be incorporated on the periphery of complexes of dipyrrinato ligands by substitution on the aryl or pyrrole rings. On kinetically inert complexes, these functional groups can be interconverted using standard synthetic methodologies[2].

Historically, research into dipyrrin chemistry has been in the synthesis of porphyrins[3]. More recently research has been turned to the application of dipyrrins in the formation of charge-neutral chelated complexes with a variety of metal cations and subsequently, dipyrrinato complexes of many transition metal ions have been reported.[3]. Upon deprotonation dipyrrins become monoanionic and are easily coordinated to a broad range of transition metals to form both heteroleptic and homoleptic complexes. Due to the steric interactions between substituents at the 1,9-positions of the dipyrrin, most divalent transition metal cations form chelate complexes with two molecules of dipyrrin to give a square planar complex, e.g. copper (II), palladium (II), zinc (II). Divalent metal exceptions include nickel (II) which forms tetrahedral complexes, while most other transition metal cations form an octahedral complex with three molecules of dipyrrin chelated to a single metal e.g. cobalt (III), indium (III), iron (III) [3]. Dipyrrinatio metalorganic complexes are highly coloured and are often homoleptic. These complexes tend to absorb very strongly in both the ultraviolet and visible regions of the electromagnetic spectrum (particularly when coupled with a $BF_2$ group, otherwise known as BODIPY complexes)[6], and can display intense photoluminesce. As a result dipyrrinato complexes have applications in both light harvesting and energy transfer, making them ideal for use as dyes in dye-sensitised solar cells. However, despite these desirable qualities, to date there is no

published use of transition metal-dipyrrinato complexes as dyes in dye-sensitised solar cells[7].

## 1.2. Ruthenium(II) Complexes

Ruthenium(II) (Ru(II)) complexes are generally stable, diamagnetic, and kinetically inert and have justifiably received great attention for their unparalleled photophysical and photochemical properties. The methodology behind the synthesis of Ru(II) complexes is well developed and there are very few metal ions which possess the same synthetic flexibility. Ru(II) complexes have captured the fascination of a large group of chemists around the world because these particular complexes display a number of interesting and favourable properties. These properties include: decay times of a few microseconds, absorption bands in the spectral range 350-370 nm, a large Stokes shift, and the formation of a metal-to-ligand charge transfer (MLCT) state when the complexes are excited. Usually the lowest excited state, the MLCT is responsible for excited-state electron transfer, emission, or quenching chemistry; and there are metal centred (MC) d-d states that are thermally accessible from the excited MLCT state which provides a dissociative decomposition pathway (Figure 1.3). In addition, the reduced and oxidised species of Ru(II) complexes (for example $[Ru(bipy)_3]^{3+}$ vs. $[Ru(bipy)_3]^{2+}$ vs. $[Ru(bipy)_2(bipy^-)]^+$ [8]) display similar characteristics[9]. As a result of the aforementioned properties there have been numerous studies into both the photochemical and photophysical properties of ruthenium complexes[10-12]. From these studies Ru(II) complexes have found applications in photovoltaics (the generation of electrical energy from sunlight) and water splitting (the generation of hydrogen and oxygen from water using sunlight).

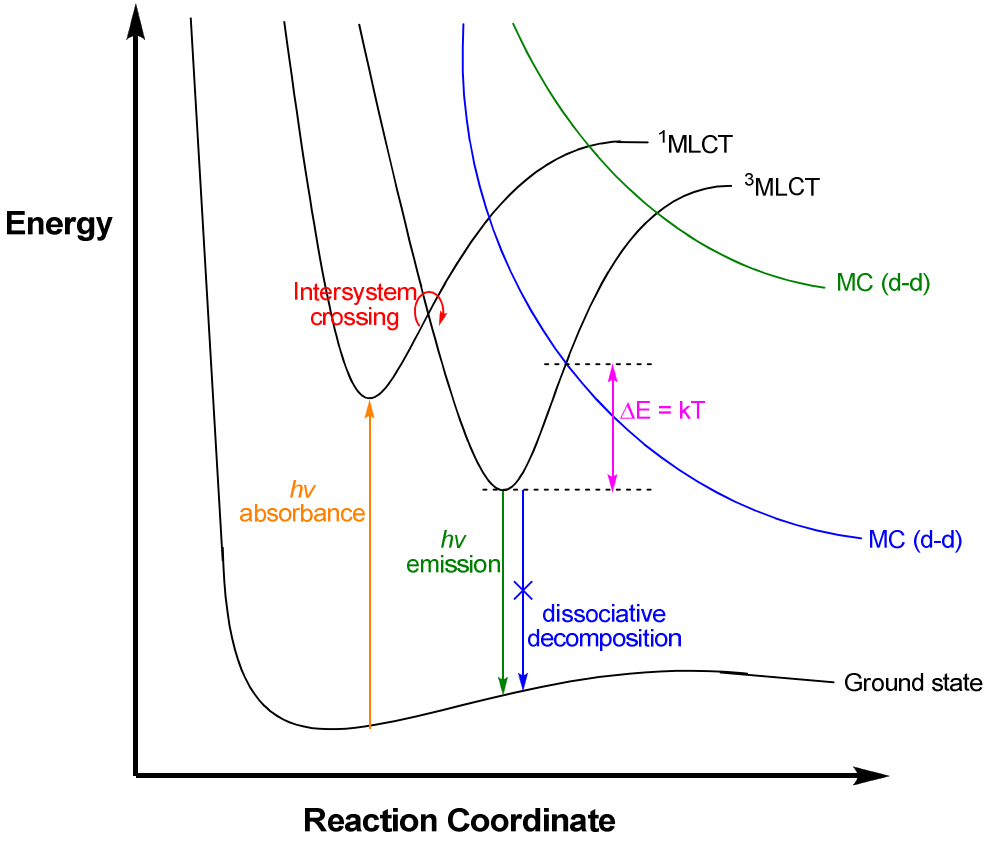


**Figure 1.3** Potential energy diagram for Ruthenium(II) complexes, showing MLCT and MC d-d states.

Ru(II) bipyridyl chemistry has become an extensive area in inorganic research due to the potential application of these particular complexes as building blocks in a wide range of supramolecular devices. In addition, variation of, or modification to the ligands coordinated to the Ru(II) centre can tune the desired properties of Ru(II) bipyridyl complexes. Ru(II) bipyridyl complexes have favourable excited state and redox properties, long lifetimes, and oxidized ruthenium(III) has long-term chemical stability. Consequently, ruthenium bipyridyl complexes have been studied extensively as photosensitizers for homogeneous photocatalytic reactions and dye-sensitization systems[13]. Many of the complexes prepared in these studies conform to the general formula $[Ru(bipy)_2(L)]^{2+}$ where "bipy" is 2,2'-bipyridine and "L" is some other chelating ligand, usually a bis-chelating ligand where both arms possess the identical coordination properties[14].

As ruthenium-dipyrrin complexes could conceivably combine the advantageous properties of ruthenium (II) complexes listed in Chapter 1.2 with those of diprryins listed in Chapter 1.1, they represent very attractive synthetic targets with unsurmountable potential

as functional components in light harvesting and energy transfer systems. However, although dipyrrinato complexes of many transition metal ions have been reported, ruthenium does not feature on this list[7].

## 1.3. Dye-Sensitised Solar Cells

Dye-sensitised solar cells are a relatively new technology, and are only one class of the broad group of photovoltaic devices known as solar cells. The dye-sensitised solar cell (DSSC, or DSC) was invented by Michael Grätzel in 1991, and is a promising method for the conversion of solar radiation into electrical energy on a large scale. DSSCs are advantageous because they offer the prospect of very low cost fabrication without expensive and energy-intensive processes, compatibility with flexible substrates, and a variety of presentations and appearances which make them attractive for both domestic and architectural or decorative applications[1]. In addition, to date DSSCs have already attained conversion efficiencies of up to 11.1% under laboratory conditions[15] compared with 23.0% for a conventional crystalline silicon-type solar cell[16].

The DSSC is essentially a "dye sandwich". It consists of a sensitizer (dye) and an electrolyte sandwiched between an electrode coated in a nanocrystalline, mesoscopic wide-band-gap semiconductor; and a counter electrode. A schematic diagram of a dye-sensitised solar cell is shown in Figure 1.4. A monolayer of the sensitizer is bound to the surface of the semiconductor through an acid functional group. The semiconductor-sensitizer is placed in contact with, and interpenetrated by, a hole-transport material (HTM) such as a redox electrolyte in solution or an organic gel material. This association of the sensitizer as a light absorbing material with the wide-band-gap semiconductor accomplishes the optical absorption and charge separation processes that result in the conversion of solar radiation into electrical energy.

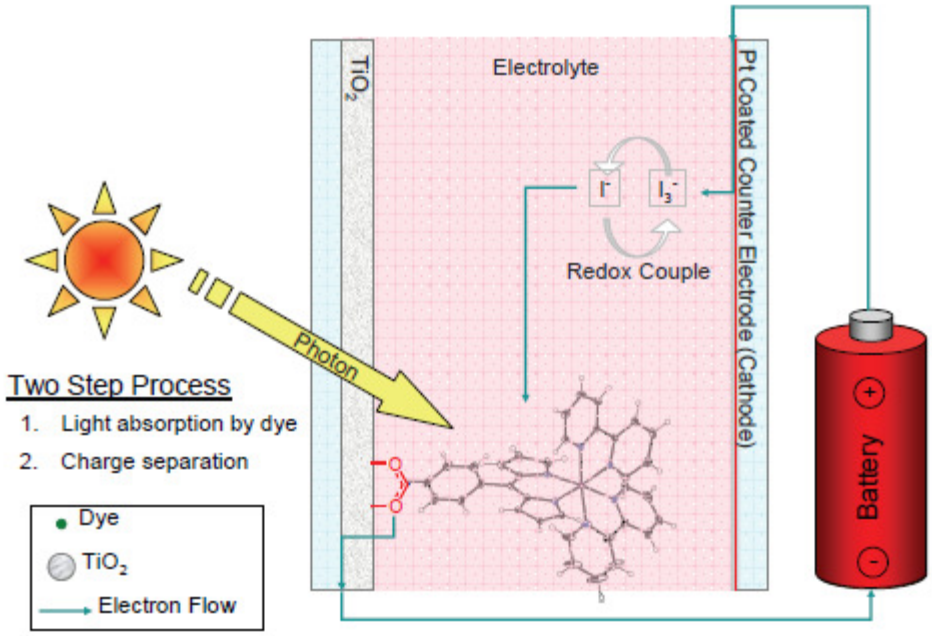


**Figure 1.4** A schematic diagram of a DSSC.

The operation of the DSSC is initiated by the absorption of photons (light) by the dye/sensitizer. The light causes photoexcitation of the dye, which causes the injection of electrons from the excited dye into the conduction band of the $TiO_2$. The ground-state dye is then regenerated through electron donation from (reduction of) the HTM to prevent recapture of the electron injected into the conduction band by the oxidised dye. The HTM is regenerated in turn by reduction at the counter electrode, which is regenerated via electron migration through the circuit: the electron originally ejected from the dye upon photoexcitation. This process is represented diagrammatically by Figure 1.5[13]. The electricity that is generated is produced from the absorbed light by the DSSC overall, but is achieved without any permanent chemical transformations. This means that in theory, this cycle could continue indefinitely without any chemical or environmental consequences. This particular aspect of DSSCs makes them extremely attractive from an ecological perspective.

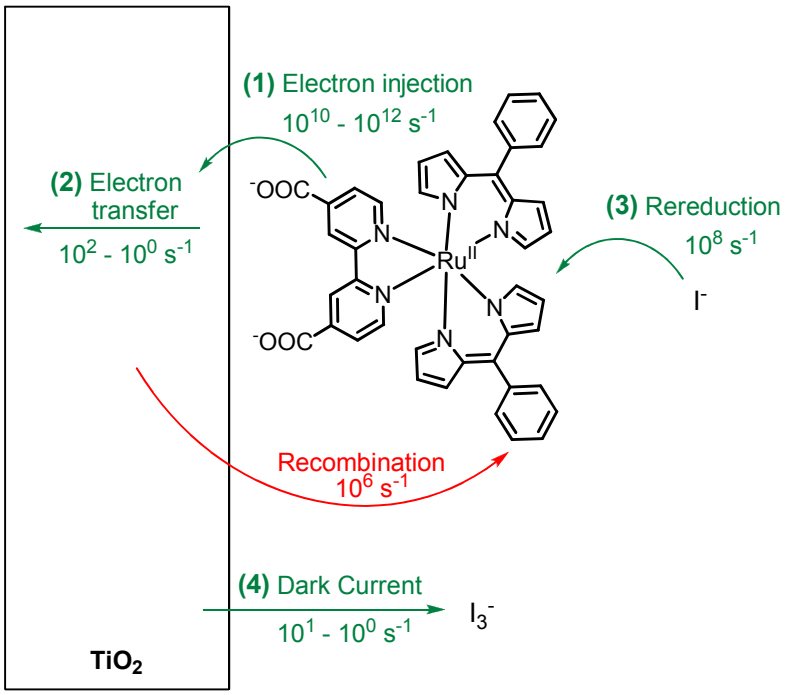


**Figure 1.5** The operation of the DSSC, with typical timescales for each process.

In the nearly two decades since the initial creation of DSSCs there have been multiple investigations into suitable semiconductors, sensitizers, and electrolytes in order to optimise the base efficiency of DSSCs. Several metal oxides have been employed in DSSCs as the semiconductor including $TiO_2$, NiO, ZnO and $Nb_2O_5$. However previous studies[1] have shown $TiO_2$ (anatase) to produce the highest efficiencies. In addition to its high efficiency, $TiO_2$ is also non-toxic, inexpensive and has a high chemical stability under visible irradiation; and accordingly is now the most widely used semiconductor in DSSCs. The substrate for the $TiO_2$ photoeletrode is transparent conducting oxide (TCO)-coated glass. The best TCO materials are those with a low sheet resistance which is independent of the temperature up to 500°C ($TiO_2$ sintering temperature) and high transparency. Fluorine-doped $SnO_2$ is usually used as the substrate in DSSCs. The $TiO_2$ photoelectrode is prepared by coating the TCO material with a $TiO_2$ colloidal solution or paste and then sintered at 450-500°C to give a $TiO_2$ nanoparticle (10-30nm) film ~10μm thick. The nanoparticles cause the film to have an actual surface area with a roughness factor >1000 compared to the apparent surface area, e.g. a 1 $cm^2$, 10μm thick film has an actual surface area of 1000 $cm^2$. As the roughness factor increases, the amount of dye adsorbed in a monolayer to the photoelectrode increases dramatically, which increases the light

harvesting efficiency (LHE) to nearly 100% at the peak absorption wavelength of the dye. The porosity of the $TiO_2$ film is also important for the infiltration of the HTM, that is the HTM must be able to penetrate the film effectively enough to suppress electron recapture from the conduction band of the $TiO_2$ via diffusion of the redox ions into the film[13]. A scanning electron micrograph (SEM) image of a typical nanocrystalline $TiO_2$ film is shown in Figure 1.6[13].

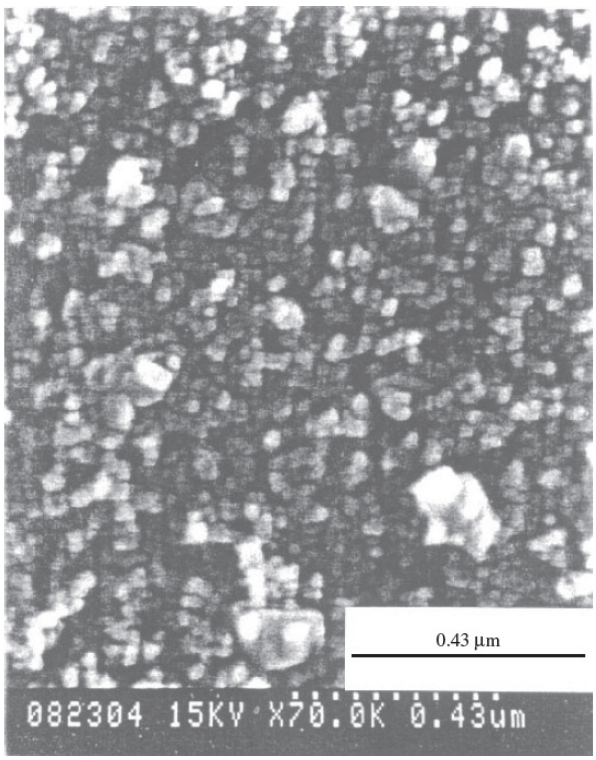


**Figure 1.6** SEM image of a typical nanocrystalline $TiO_2$ film.

Previous studies[17] have shown the optimum HTM to be an electrolyte-couple volatile solvent solution comprising of $I^-/I_3^-$, as it results in DSSC efficiencies at least 2% higher than other HTMs such as $Co^{II}/Co^{III}$ and $SeCN^-/(SeCN)_3^-$ redox couples, hole-conducting organic polymers, small organic molecules, solid inorganic materials, and even $I^-/I_3^-$ in either solid polymer, gel, ionic liquid and plastic crystal systems. However, the downside to the $I^-/I_3^-$ couple is that it is complicated to manufacture and has poor long term stability, so is unsuitable for large-scale use in DSSCs. The performance of the DSSC depends somewhat on the counter cation ($Li^+$, $Na^+$, $K^+$ or $R_4N^+$) to the iodide ion due to the different ion conductivity in the HTM or adsorption on the $TiO_2$ surface, which leads

to a shift of the conduction-band level of the photoelectrode. The ion conductivity is also affected by the viscosity of the HTM, where low-viscosity solvents produce the best results. Basic compounds such as *tert*-butylpyridine have also been known to have been added to HTM to boost DSSC performance. The $I_3^-$ ions in the HTM are formed by the reduction of dye cations by $I^-$ ions and are re-reduced back from $I_3^-$ to $I^-$ ions by the counter electrode, which is usually platinum (coated on TCO substrate or carbon) because of its high electrocatalytic activity[13].

The optimisation of DSSC efficiencies through the use of different sensitizers is a very widely investigated aspect of DSSCs, and is on-going. DSSC sensitizers (referred to from this point forward as 'DSSC dyes', or simply as 'dyes') are usually coordination compounds, and as previously mentioned are the component of the DSSC system that absorbs the sunlight, and then initiates the excited state redox reactions that yield the electrical power. Systematic studies have resulted in a very wide range of dyes, including both mononuclear and polynuclear dyes; dyes based on selective group 7, 8, 10, and 11 metals; and even some purely organic dyes. Despite possessing quite different structures, all of these dyes share a set of attributes, which a dye must conform to in order to be successfully used in solar cells. These attributes include: the ability to bind strongly to $TiO_2$; the ability to strongly absorb solar radiation and to absorb across the whole spectrum (particularly in the visible and near-IR regions); the possession of a suitably high redox potential; and the ability to be stable over many years of exposure to sunlight.

The ability to bind strongly to $TiO_2$ is best achieved through an acidic functional group, most commonly via a carboxylic acid, or alternatively a phosphonic acid group. There are multiple possible binding modes of carboxylic acid groups to $TiO_2$, and these are shown in Figure 1.7[18]. Previous studies[17, 18] have shown that cells with carboxylic acid anchors have the highest cell efficiencies, due to the formation of ester linkages with the surface of the $TiO_2$. These ester linkages cause the anchoring bond to be the strongest of the anchor groups, and also enable improved electronic coupling between the dye and the mesoscopic semiconductor. However, in the presence of water the ester linkage can be hydrolysed, easily displacing the dye, which has serious consequences on the long-term solar cell stability. In addition to providing an efficient anchor in the absence

of water, carboxylic acid groups are also more favourable over alternative functional groups as they promote electronic coupling between the donor levels of the excited dye and the acceptor levels of the $TiO_2$ semiconductor[18].

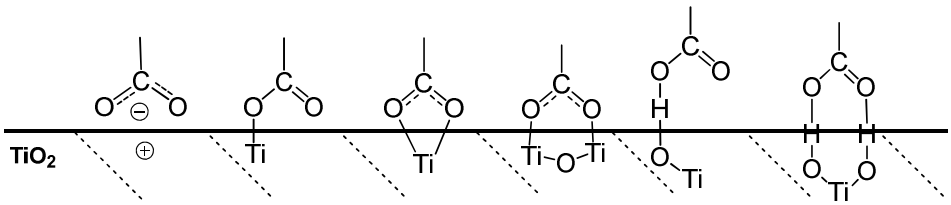


**Figure 1.7** The possible binding modes of carboxylic acid groups to $TiO_2$.

The possession of a suitably high redox potential (LUMO) for efficient charge injection to the $TiO_2$, but a HOMO low enough in energy to allow practically 100% regeneration following excitation is necessary for optimum energy transfer. The ability to transfer electrons into the $TiO_2$ layer must also be considerably faster than the decay of the dye back to its ground state. These attributes are important to help prevent the recapture of electrons injected by the dye into the $TiO_2$ upon excitation. This phenomenon is called recombination (Figure 1.5). Previous studies have shown that cells with ruthenium-polypyridyl dyes, particularly those linked through carboxylic acid groups have the highest cell efficiencies as they undergo ultrafast charge injection (a timescale of picoseconds). A schematic displaying the dynamics of redox processes involved in the conversion of light to electric power by DSSC is shown in Figure 1.8[1, 13].

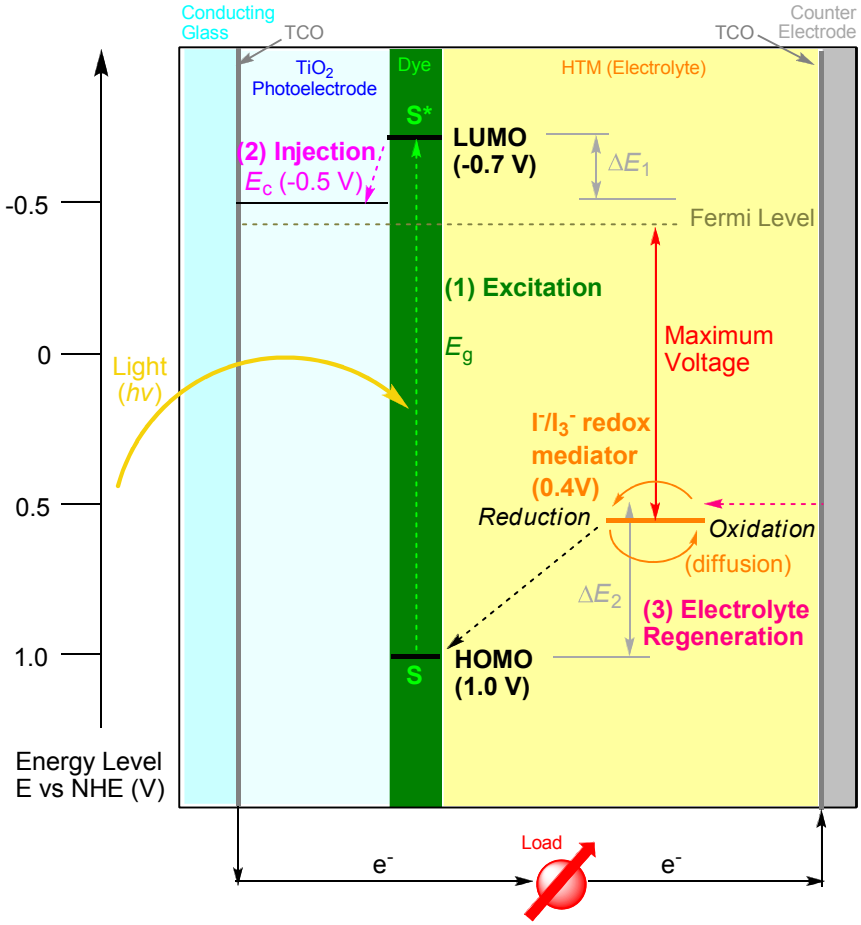


**Figure 1.8** The dynamics of redox processes involved in the conversion of light to electric power by the DSSC.

Past research has shown Grätzel's ruthenium- polypyridyl dyes to satisfy nearly all of these key requirements, with three particular dyes showing efficiencies of greater than ~10%. These are the N719 (the so called 'black' dye), N3, and latest thiocyanate-free dyes (Figure 1.9). These dyes are now manufactured commercially, and are utilised by scientists as the standard to which the efficiencies and spectroscopic properties of new dyes are compared. The UV-Vis absorption spectra of N719 and N3 is shown in Figure 1.10[13], where the two sets of traces correspond to absorbance and transmittance as denoted by the arrows (← and → respectively). The N719 and N3 dyes can absorb over a wide range of the visible and infrared regions of the spectrum respectively, which is what makes them particularly good as DSSC dyes.

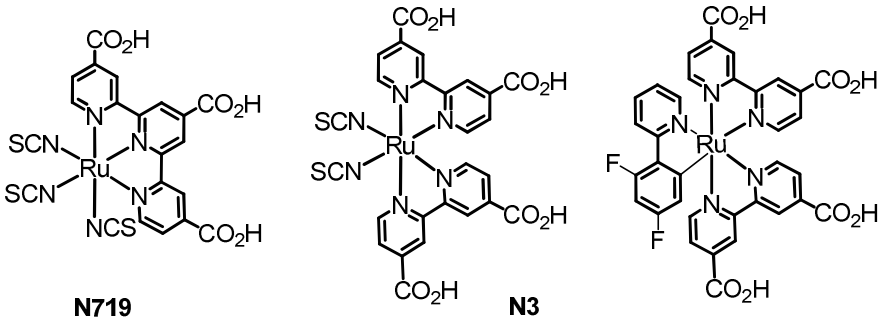


**Figure 1.9** The structures of Grätzel's best DSSC dyes: N719, N3, and the yet unnamed thiocyanate-free dye respectively.

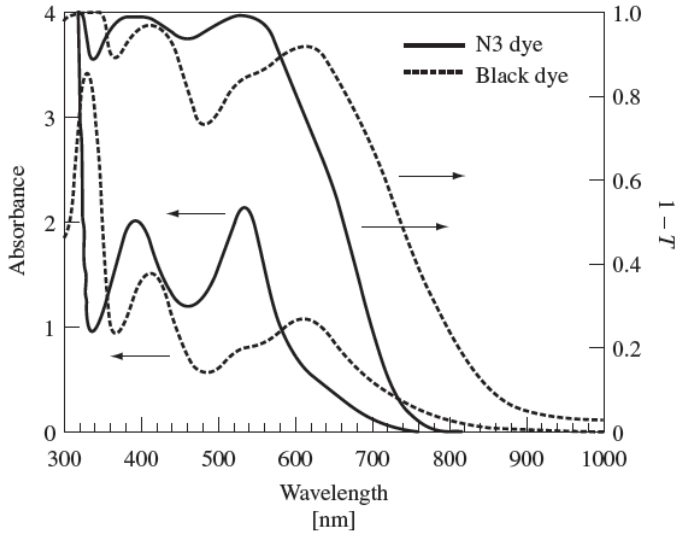


**Figure 1.10** The UV-Visible spectrum of Grätzel's N719 (black) and N3 DSSC dyes.

The most well-known and the most efficient dyes to date are Grätzel's ruthenium-polypyridyl dyes (Figure 1.9) and a group of macrocycles called porphyrins (Figure 1.2**)**.

## 1.4. Research Project Overview

The aim of this research project was threefold:

(1) The first part of this research project was to develop a series of dipyrrin complexes as dyes for DSSCs. These complexes would be simple dipyrrin complexes that in theory

were easy to synthesise. Each of the target complexes would possess all of the attributes of a good DSSC dye, as set out in the DSSC section of this chapter. (1.3). Each of the targets would also be strongly electron donating in the hope of achieving results close to or better than those currently published in the literature for DSSCs.

A set of generic target compounds were identified, composed of one or two dipyrrin ligands and two or one bipyridine ligands, respectively. The intention was for the synthesis of these complexes to be applicable to any dipyrrin, thus aiding future studies into the use of dipyrrins as dyes for DSSCs. Synthesis of subsets of both ruthenium base complexes and different dipyrrins as building blocks was therefore necessary.

The structures for the complete set of target complexes synthesised and discussed in this thesis are shown in Figure 1.11.

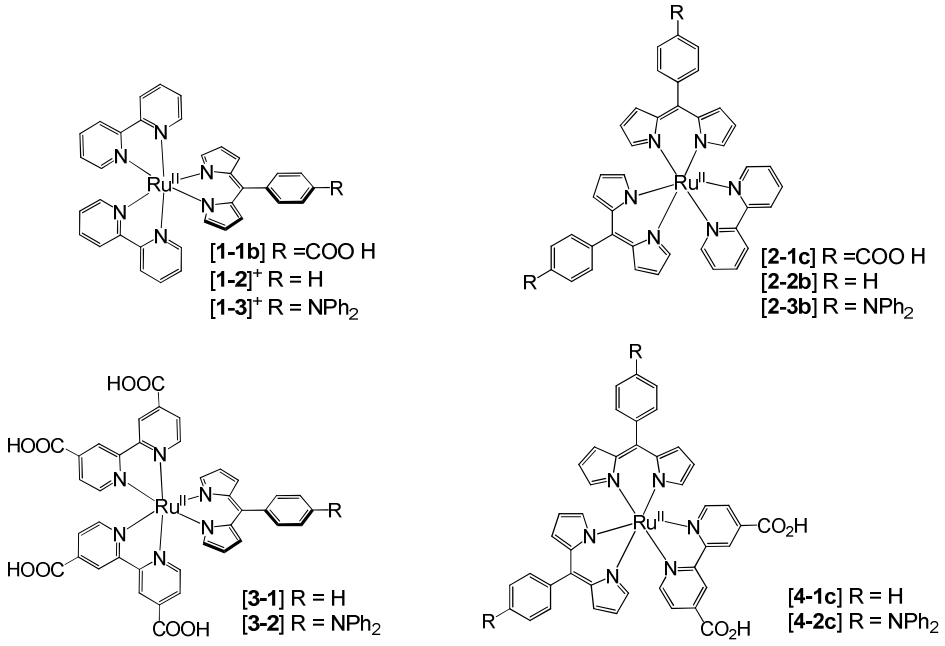


**Figure 1.11** The structures for the complete set of target complexes synthesized and discussed in this thesis.

(2) The second part of this research project was to characterise the complexes and then to investigate the spectroscopic properties of each complex. Characterisation would be achieved using the usual methods: $^{1}H$ NMR, $^{13}C$ NMR, mass spectrometry (ESI-MS), elemental analysis, and x-ray crystallography. Spectroscopic studies would be

conducted by collecting UV-visible, fluorescence, emission, and Raman spectra. Electrochemistry would be investigated and low level calculations would also be performed.

(3) The final part of this research project was to determine the suitability of the complexes as dyes for DSSCs. This would be achieved by constructing informed conclusions from analyses of the spectroscopic data and electrochemistry results. Ultimately assessments of suitable complexes (i.e. those containing a carboxylic acid moiety) would be carried out by integrating solutions of suitable complexes into a photovoltaic device and then measuring the efficiency of each complex to absorb light and convert it to electrical energy. Rational modifications would be made to the structures to attempt to further improve their efficiencies, reconciling every alteration with a logical function. The photovoltaic device conditions such as solvent, electrolyte would also be optimised to yield the highest efficiency possible.

This thesis summarises the findings of the above outlined research project.

*Chapter 2*

# SYNTHESIS OF HETEROLEPTIC DIPYYRIN/BIPYRIDINE COMPLEXES OF RUTHENIUM (II)

## 2.1. Starting Materials

In order to synthesise the target complexes it was first necessary to synthesise the components. On the most part the procedures followed to attain these "building blocks" were either direct reproductions of published methods or were modified versions of literature preparations. The primary source of Ruthenium for all of the target complexes is $RuCl_3 \bullet xH_20$. The synthetic details for all procedures, literature and otherwise, are listed in Chapter 5 of this thesis, with those compounds which were achieved by means of significant deviations from their published counterpart are discussed further in this section.

### 2.1.1. COOMe-dp

The ligand COOMe-dp was synthesized from methyl 4-formylbenzoate by following a modified version of the procedure published by Rohand et al[19], shown in Scheme 2.1. Although the synthesis of this compound had already been published, the second part of the procedure resulted in low yields, so steps were taken to optimise the second step reaction and purification procedures in an effort to increase the yield.

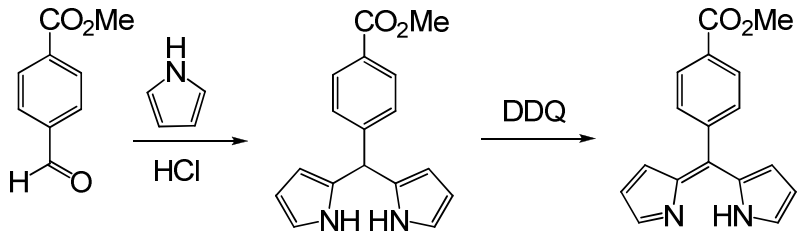


**Scheme 2.1** Synthesis of COOMe-dp.

The majority of literature preparations utilised 2,3-dichloro-5,6-dicyanobenzoquinone (DDQ) to oxidise dipyrromethanes to dipyrrins. However, Rohand et al[19] stated that the use of 2,3,5,6-tetrachloro-1,4-benzoquinone (*p*-chloronil) led to increased yields, due to it

being a milder oxidising agent[19]. Trials conducted using *p*-chloronil led to increased side products and the crude product was much more difficult to purify. This in turn led to alterations in the ratio of DDQ to COOMe-dpm: a reduction in the excess of DDQ in the reaction. The chloroform to acetone solvent ratio was also adjusted, and the introduction of the addition of extra acetone following the oxidising agent to counteract the evaporation of solvent over time and therefore allow the DDQ to remain soluble in the reaction mixture was also introduced. Another new step that was added was the dissolution of crude product in chloroform with subsequent stirring in dichloromethane before washing with chloroform to aid in the removal of intensely coloured side products.

Many problems were encountered with the purification procedure, namely from the use of silica and solubility issues associated with the crude product. These were alleviated somewhat by using dry-packed deactivated alumina instead of silica in the columns, and also by adsorbing the product to alumina before applying to the column. These chromatography techniques were later applied to the dipyrrinato complexes.

Alterations to this reaction were carried out numerous times before the most successful route was achieved. The resulting modified procedure gave a reasonable quantity of product that was of a high purity and matched the spectroscopic data provided in the literature by Rohand et al[19].

### 2.1.2. $Ph_2N$-dp

The ligand $Ph_2N$-dp did not exist in the literature prior to synthesis for this research project. Initially, several unsuccessful attempts were made at synthesising this ligand including the use of hydrochloric acid (successful for both COOMe-dp and Ph-dp) or $InCl_3$ to catalyse the first-step reaction, and the use of DDQ to oxidise the dipyrromethane (second-step reaction). The synthetic method that successfully produced the ligand is illustrated by Scheme 2.2, and is loosely based on the procedure published by Littleret al[20] for dipyrrins with similar functional groups.

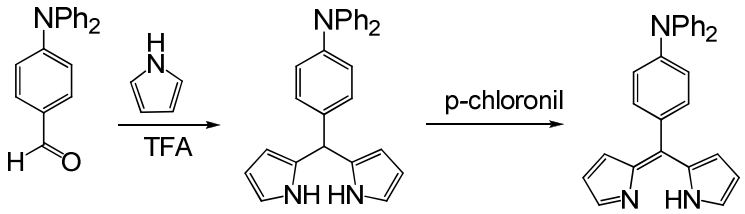


**Scheme 2.2** Synthesis of $Ph_2N$-dp.

The first-step reaction which results in the formation of the dipyrromethane was performed by reacting 4-diphenylaminobenzaldehyde with a sizeable excess of freshly distilled pyrrole in the presence of trifluoroacetic acid (TFA). The dipyrromethane and aldehyde were indistinguishable by thin layer chromatography (TLC) without the use of a dinitrophenylhydrazine (DNP) stain. It was found that the purity of the pyrrole employed in the reaction had a direct correlation with the yield achieved from the procedure, where the use of pyrrole which had been vacuum-distilled immediately prior to performing the dipyrromethane reaction resulted in the highest yield of desired product. The use of freshly distilled pyrrole also reduced the quantity of side products formed in the reaction, therefore resulting in greater ease for purification. It was also realised that purification was necessary to ensure that the second-step reaction would proceed.

DDQ was employed in the second-step reaction at first. NMR studies of small scale reactions indicated that the agent was so strong that it was not only oxidising the dipyrromethane but obliterating it. In terms of strength, *p*-chloronil is a marginally weaker oxidiser than DDQ. An NMR scale reaction where *p*-choronil was substituted in place of DDQ clearly showed changes in peak intensities attributable to the consumption of $Ph_2N$-dpm and formation of $Ph_2N$-dp. This led to reproduction on a larger scale, with triumphant results.

Evidence of the successful formation of the ligand was provided by characterisation via elemental analysis, $^{1}H$ NMR, $^{13}C$ NMR, ESI-MS and UV-visible spectroscopy. The data, which is listed in Chapter 5, was in good agreement with the structure depicted in Scheme 2.2.

## 2.2. Dye One Group Complexes

Dye One Group complexes are a group of bis-bipyridine dipyrrinato complexes i.e. they consist of two bipyridine ligands and one dipyrrin ligand coordinated to a Ru(II) metal centre. There are three complexes in this set, which are differentiated by the functional group (R) on the dipyrrinato ligand: R = COOH [**1-1b**], H [**1-2**]$^+$, and $NPh_2$ [**1-3**]$^+$.

### 2.2.1. Carboxylic Acid-type Dye One: [Ru(bipy)$_2$(COO$^-$-dp)]

Initial attempts made to synthesise this target complex were carried out thermally, first with [Ru(bipy)$_2$Cl$_2$] (based very loosely on a method reported by Sullivan, Salmon & Meyer[21], then with [Ru(bipy)$_2$(CO$_3$)] and later with [Ru(COOMe-dp)(acac)$_2$] (where acac denotes the acetylacetone ligand, $CH_3COCH_2COCH_3$). When it became apparent that conventional heating methods were failing to provide the desired product regardless of the reagents, attention was turned towards utilisation of a microwave synthesiser in combination with a high boiling point solvent. Dimethylformamide (DMF) and ethylene glycol were both trialled, with the latter giving the better results. The proportion of triethylamine in the reaction mixture was also varied before experimentation with several different microwave cycles. The carboxylic acid-type Dye One complex [Ru(bipy)$_2$(COO$^-$-dp)] [**1-1b**] was synthesised via an entirely innovative, two-step reaction; which is illustrated in Scheme 2.3.

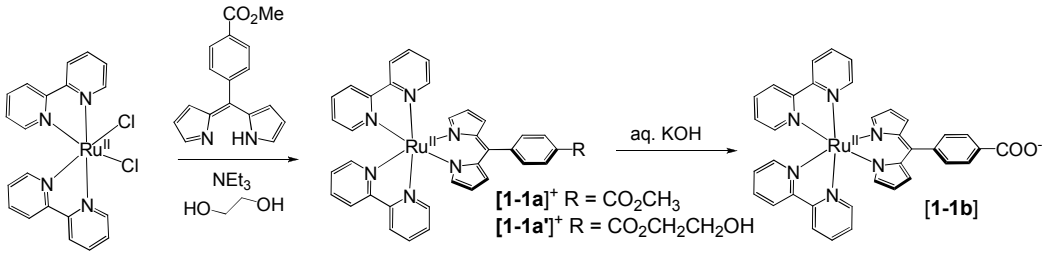


**Scheme 2.3** Synthesis of [Ru(bipy)$_2$(COOH-dp)].

The intermediate product [**1-1a**]$^+$PF$_6$ was obtained as a green solid in good yield by reacting equal equivalents of the ligand COOMe-dp and [Ru(bipy)$_2$Cl$_2$] in ethylene glycol under microwave irradiation for 30 minutes in the presence of one equivalent of base. The use of ethylene glycol as a solvent resulted in a significant degree of transesterification, giving [**1-1a'**]PF$_6$.

Hydrolysis of the ester moieties in aqueous base afforded the complex [Ru(bipy)$_2$(COOH-dp)] (protonated [**1-1b**]). The occurrence of transesterification prior to hydrolysis did not have any adverse effect on the quality and quantity of product that was obtained. This is due to the lack of selectivity in the hydrolysis reaction, where the aqueous base will hydrolyse any ester group regardless of the length of the ester carbon chain. When the carboxyl functional group is deprotonated, the free-base dipyrrin ligand is dianionic (i.e. doubly negative) and therefore the overall complex is neutral (bipyridine is a neutral ligand so $Ru^{2+}$ plus $[COO^-]^{-2}$ equals $[\mathbf{1\text{-}1b}]^{0}$). When this is the case complex [Ru(bipy)$_2$(COO$^-$-dp)] [**1-1b**] conveniently precipitates from the aqueous solution in near total purity. Analytical purity is attained by recrystallising the product from methanol and water.

Complex [Ru(bipy)$_2$(COO$^-$-dp)] [**1-1b**], which is green in the solid state but deep red-orange in solution, was characterized by $^1$H NMR, $^{13}$C NMR, ESI-MS, UV/visible spectroscopy, elemental analysis, and X-ray crystallography. All data are consistent with the structure depicted in Scheme 2.3.

The X-ray crystal structure of [Ru(bipy)$_2$(COO$^-$-dp)] [**1-1b**] is shown in Figure 2.1 as an ORTEP plot, where the thermal ellipsoids are displayed at the 30% level.

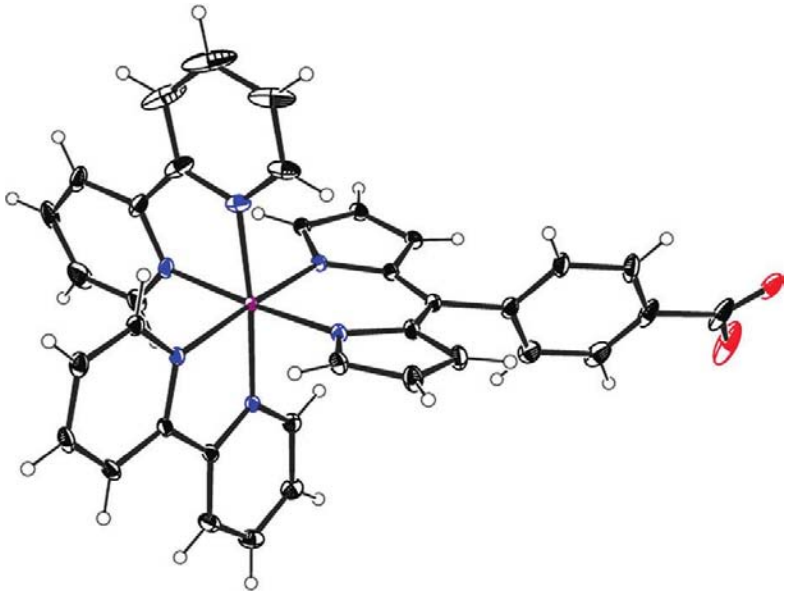

**Figure 2.1** An ORTEP plot showing the molecular structure of [Ru(bipy)$_2$(COOH-dp)] as determined by X-ray crystallography. Thermal ellipsoids are set at the 30% level.

$[Ru(bipy)_2(COO^-\text{-}dp)]\bullet(CH_3OH)\bullet 6H_2O$ crystallizes from the diffusion of methanol vapours into a solution of the complex in methanol in the space group *P*-1. One enantiomer of the complex occupies the asymmetric unit and the geometry at the Ru(II) centre is distorted octahedral. The Ru-$N_{bipy}$ bond lengths fall in the range 2.047(2)-2.058(2) Å, while the Ru-$N_{dipyrrin}$ bond lengths are longer at 2.062(2) and 2.062(4) Å. The phenyl ring is twisted 71.5° out of the plane of the dipyrrin ligand, while the deprotonated carboxylato group twists 15.0° out of the plane of the phenyl ring. The C-O bond distances of the carboxylato group (1.260(8) and 1.263(7) Å) are consistent with it being deprotonated, thus rendering $[Ru(bipy)_2(COO^-\text{-}dp)]$ [**1-1b**] neutral. The carboxylato groups of neighbouring complexes are linked into an infinite network by hydrogen bonds to common methanol molecules, as shown by Figure 2.2.

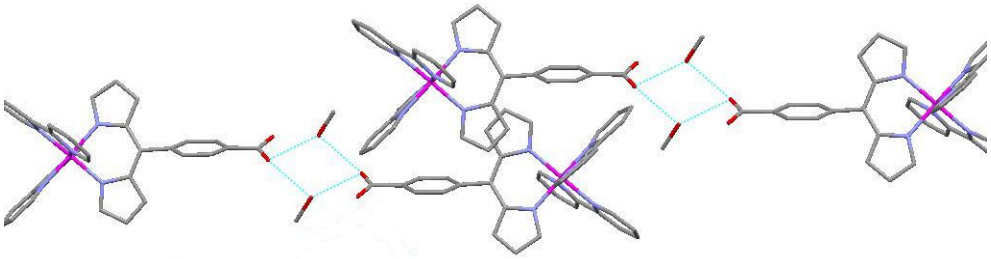

**Figure 2.2** A segment of the infinite hydrogen-bonding network formed between common methanol molecules and the carboxylate groups of neighbouring $[Ru(bipy)_2(COOH\text{-}dp)]$ molecules.

The hydrogen bonds linking $[Ru(bipy)_2(COO^-\text{-}dp)]$ [**1-1b**] molecules and methanol (represented by the turquoise lines in Figure 2.2) form a parallelogram where opposite bond distances and bond angles are equal, but adjoining distances and angles are not. The length of the bond formed between $O_{dipyrrin}\cdots H\text{-}O_{methanol}$ is 2.791(-) and 2.799(-) Å. This distance is consistent with the bond being a hydrogen bond, as it falls well within the limits for the length of a hydrogen bond (1.8-3.5 Å) (A normal covalent bond is ~0.96 Å, while anything greater than 3.5 Å would be considered a dipole-dipole interaction)[22, 23]. The bond angles centred over the methanol molecules are 113.4°, more than twice those centred over the dipyrrin molecules, which are 66.6°.

NMR and UV-visible data collated for [Ru(bipy)$_2$(COO$^-$-dp)] [**1-1b**] are discussed in detail in Chapter 3 of this thesis, while ESI-MS and elemental values along with the NMR and UV-visible values are listed in Chapter 5.

## 2.2.2. Phenyl-type Dye One: [Ru(bipy)$_2$(Ph-dp)]

Following the success of the carboxylic acid-type Dye One complex [Ru(bipy)$_2$(COO$^-$-dp)] [**1-1b**], it was tested whether or not the same methodology could be applied to different dipyrrin ligands, by substituting Ph-dp for COOMe-dp and replicating the successful synthetic procedure described in Chapter 2.2.2. The proton in place of the ester functional group on the dipyrrin ligand meant that transesterification was not possible and hydrolysis was redundant, resulting in a straightforward, one-step reaction. This reaction, which is illustrated in Scheme 2.4, successfully afforded the complex [Ru(bipy)$_2$(Ph-dp)] [**1-2**]$^+$.

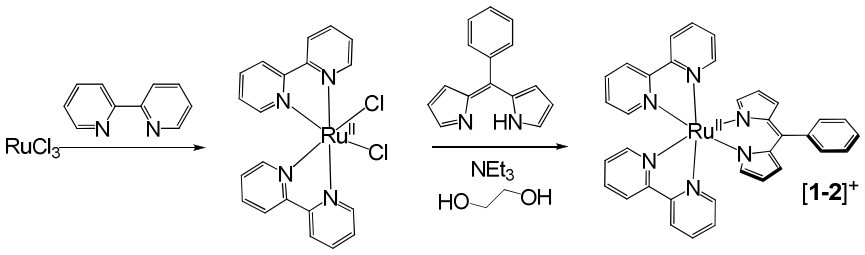


**Scheme 2.4** Synthesis of [Ru(bipy)$_2$(Ph-dp)].

Complex [**1-2**]$^+$ was obtained as a green solid in good yield by reacting equal equivalents of the ligand Ph-dp and [Ru(bipy)$_2$Cl$_2$] in ethylene glycol under microwave irradiation for 30 minutes in the presence of one equivalent of base. The complex is positively charged overall because the phenyl group on the dipyrrin is neutral, making the free-base ligand monoanionic (bipyridine is a neutral ligand so $Ru^{2+}$ plus $[Ph\text{-}dp]^{-1}$ equals [**1-2**]$^{+1}$).

The purification procedure for the phenyl-type Dye One complex [Ru(bipy)$_2$(Ph-dp)]$^+$ [**1-2**]$^+$ differs significantly from that for the carboxylic acid-type Dye One [Ru(bipy)$_2$(COO$^-$-dp)] [**1-1b**] for two reasons: the difference in properties which arises from the absence of a functional group on the dipyrrin in the latter complex; and the resulting overall charge on the complex. The precipitate formed from the addition of

$NH_4PF_6$ to the crude product was too fine to collect by filtration, so the salt was extracted into an organic phase, dried, and the solvent removed. Trituration with diethyl ether from acetonitrile failed to generate the second precipitate, so purification was achieved instead by a series of columns over different media. The first column was over an anionic Sephadex resin which was expected to retain the positively charged complex while allowing any impurities to flow through. This was not the case: instead the impurities were retained and near-pure complex was collected. The second column was over neutral lipophilic Sephadex which draws on polarity to separate molecules. This column also rejected the complex, holding instead all of the additional impurities. The final column was carried out over neutral alumina, which removed any remaining uncharged and stubborn charged contaminants. Complex $[Ru(bipy)_2(Ph\text{-}dp)]^+$ $[\mathbf{1\text{-}2}]^+$ which, like complex $[Ru(bipy)_2(COO^-\text{-}dp)]$ [**1-1b**], is green in the solid state but orange-red in solution, was characterized by $^1H$ NMR, $^{13}C$ NMR, ESI-MS, UV/visible spectroscopy and elemental analysis. All data are consistent with the structure depicted in Scheme 2.4.

NMR and UV-visible data are discussed in detail in Chapter 3 of this thesis, while ESI-MS and elemental values along with the NMR and UV-visible values are listed in Chapter 5. X-ray crystallography was not possible, as crystals did not grow despite multiple attempts with a variety of solvent combinations.

### 2.2.3. Diphenylamino-type Dye One: $[Ru(bipy)_2(Ph_2N\text{-}dp)]$

The success of the phenyl-type Dye One complex $[Ru(bipy)_2(Ph\text{-}dp)]$ $[\mathbf{1\text{-}2}]^+$, strongly suggested that the same innovative microwave irradiation-based methodology could be applied to different dipyrrin ligands, with the exception that purification procedures would need to be altered according to the dipyrrin ligand that was coordinated. Subsequently, the route was applied to a third dipyrrin with the goal of synthesising another Dye One group complex. Without an ester group transesterification cannot occur in the course of the reaction, making hydrolysis again redundant, and thus the same straightforward, one-step procedure that afforded $[Ru(bipy)_2(Ph\text{-}dp)]$ $[\mathbf{1\text{-}2}]^+$ was repeated for the ligand $Ph_2N$-dp. This resulted in the synthesis of the diphenylamino-type Dye One complex $[Ru(bipy)_2(Ph_2N\text{-}dp)]$ $[\mathbf{1\text{-}3}]^+$, which is illustrated in Scheme 2.5.

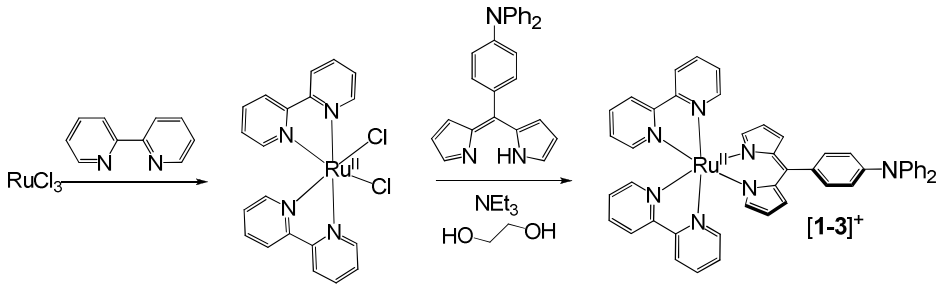


**Scheme 2.5** Synthesis of [Ru(bipy)$_2$(Ph$_2$N-dp)].

Complex [Ru(bipy)$_2$(Ph$_2$N-dp)] [**1-3**]$^+$ was obtained as a green solid in good yield by reacting equal equivalents of the ligand Ph$_2$N-dp and [Ru(bipy)$_2$Cl$_2$] in ethylene glycol under microwave irradiation for 30 minutes in the presence of one equivalent of base.

The neutral diphenylamino functional group causes the dipyrrin ligand to be negative and therefore the overall end product to be positively charged (bipyridine is a neutral ligand so $Ru^{2+}$ plus [Ph$_2$N-dp]$^{-1}$ equals [**1-3**]$^{+1}$). This likens the complex considerably to the phenyl-type Dye One complex [Ru(bipy)$_2$(Ph-dp)]$^+$ [**1-2**]$^+$, and so the purification procedure is the same, up to and including the column chromatography over anionic sephadex. The purity of the diphenylamino-type Dye One complex [Ru(bipy)$_2$(Ph$_2$N-dp)] ([**1-3**]$^+$) at this point is substantially better than that for the phenyl-type Dye One complex [Ru(bipy)$_2$(Ph-dp)] [**1-2**]$^+$ at the same point, so much so that further purification is not required. Complex [Ru(bipy)$_2$(Ph$_2$N-dp)] [**1-3**]$^+$, which is again green in the solid state but orange-red in solution, was characterized by $^1$H NMR, $^{13}$C NMR, ESI-MS, UV/vis spectroscopy and elemental analysis. All data are consistent with the structure depicted in Scheme 2.5. NMR and UV-visible data are discussed in detail in Chapter 3 of this thesis, while ESI-MS and elemental values along with the NMR and UV-visible values are listed in Chapter 5. X-ray crystallography was not possible, as crystals did not grow despite multiple attempts with a variety of solvent combinations.

## 2.3. Dye Two Group Complexes

Dye Two Group complexes are a group of bipyridine bis-dipyrrinato complexes i.e. they consist of one bipyridine ligand and two dipyrrin ligands coordinated to a Ru(II) metal centre. There are three complexes in this set, which are differentiated by the functional

group (R) on the dipyrrinato ligand: R = COOH [**2-1c**], H [**2-2b**], and $NPh_2$ [**2-3b**]. Unlike the Dye One Group Complexes, the Dye Two Group complexes are all neutral.

### 2.3.1. Carboxylic Acid-type Dye Two: [Ru(bipy)(COOH-dp)$_2$]

The first attempt at the synthesis of this complex was very loosely based on procedures outlined by Oki & Morgan[24], however due to the insolubility of the reagents in toluene and the high impurity of the dipyrrin sample used, the initial reaction was unsuccessful.. The next two attempts followed the same general procedure except that the toluene was replaced with acetone. However it was not possible to isolate the product in both cases, because each time the acetone was evaporated. Miraculously, the burnt remains clearly showed the presence of the desired complex by $^1$H NMR, and were subsequently combined and purified via an anion exchange column. Initially the column was deemed a failure, but it was discovered a significant period of time later when rinsing the column with acetone that pure complex had been obtained. A small quantity of pure product was collected, which was reacted with dcbipy for the first [Ru(dcbipy)(COOMe-dp)$_2$] (Dye Four) trials (see Chapter 2.4 of this thesis).

Following what was believed to be an unsuccessful anion exchange column, this reaction was attempted in a microwave synthesiser. But the target product remained unattainable despite trying a combination of different solvents and microwave cycles, so attention was turned back to the thermal reaction. A survey of published procedures for various complexes derived from [Ru(dmso)$_4$Cl$_2$] revealed that most had employed absolute ethanol as the solvent. This led to the successful synthetic procedure, which is illustrated in Scheme 2.6.

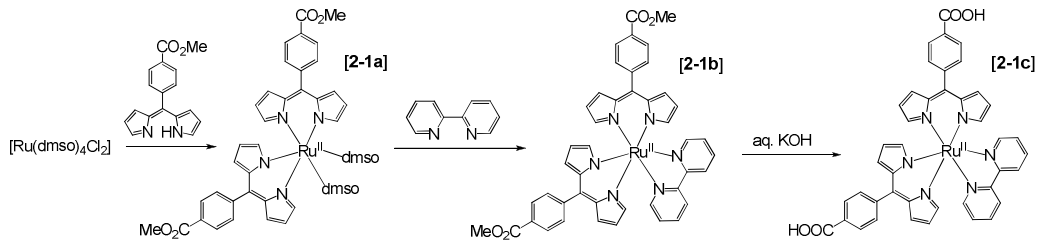


**Scheme 2.6** Synthesis of [Ru(bipy)(COOH-dp)$_2$].

The intermediate complex [Ru(dmso)$_2$(COOMe-dp)$_2$] [**2-1a**] was obtained in good yield by thermally reacting two equivalents of the ligand COOMe-dp with one equivalent of

$[Ru(dmso)_4Cl_2]$ in absolute ethanol. Purification via column chromatography on deactivated dry-packed alumina afforded a fine red-brown solid, which was orange-coloured in solution. When trialling this intermediate reaction it was initially thought that the target product to be isolated was $[Ru(COOMe\text{-}dp)(dmso)_2Cl_2]^-$ or $[Ru(COOMe\text{-}dp)_2Cl_2]^{2-}$ depending on the equivalents of dipyrrin in the reaction mixture. It was not realised until much later that the compound was in fact $[Ru(dmso)_2(COOMe\text{-}dp)_2]$. This is because each dipyrrin ligand was displacing one chloride and one dimethylsulphoxide (dmso) ligand rather than displacing the dmso ligands and leaving the chlorides. This is due to the charge of the ligands: because the deprotonated dipyrrin ligand is negatively charged, it displaces the anionic chloride ligands from the Ru(II) "building block", whereas a neutral ligand will preferentially displace the dmso ligands.

On this basis it was thought that the dmso ligands would be easily displaced by the neutral bipyridine. Indeed, the intermediate $[Ru(dmso)_2(COOMe\text{-}dp)_2]$ [**2-1a**] could be cleanly converted into $[Ru(bipy)(COOMe\text{-}dp)_2]$ [**2-1b**] via a direct reaction with 2,2'-bipyridine at elevated temperatures. It is necessary to exclude all solvent from the reaction in order for it to proceed. Complex $[Ru(bipy)(COOMe\text{-}dp)_2]$ [**2-1b**] was isolated as a metallic turquoise solid and characterized by $^1H$ NMR, $^{13}C$ NMR, ESI-MS, UV-visible spectroscopy, and elemental analysis. All data are consistent with the structure depicted in Scheme 2.6.

Hydrolysis of the ester moieties in aqueous base afforded the complex $[Ru(bipy)(COOH\text{-}dp)_2]$ [**2-1c**]. Two equivalents of tetra-n-butyl ammonium (TnBA) hydroxide is required to isolate the product, which occurs as a salt with the TnBA cation ($Bu_4N^+$) upon deprotonation by the hydroxide anions. Extraction into organic solvent followed by washing with a substantial excess of water and finally recrystallisation affords analytically pure $[Ru(bipy)(COOH\text{-}dp)_2]$ [**2-1c**] in its neutral (protonated) form. The details surrounding the transformation of $[Ru(bipy)(COOH\text{-}dp)_2]$ [**2-1c**] from anionic to neutral during the purification procedure are not certain, but the protonation of the anionic complex by a minority of water molecules in the washing step is a viable explanation. The water molecules which, to enable protonation of $[Ru(bipy)(COOH\text{-}dp)_2]$ [**2-1c**], become hydroxide ions upon loss of a proton and could subsequently form ionic interactions with the now released TnBA cation ($Bu_4N^+$). This would regenerate

TnBA hydroxide which, due to being water soluble, would be washed away freely in the washings.

The overall complex is neutral when the carboxyl functional group on both dipyrrin ligands is protonated because the free-base dipyrrin ligand is neutral in its protonated form (and bipyridine is a neutral ligand, so $Ru^{2+}$ plus 2x$[COOH\text{-}dp]^{-1}$ equals [**2-1c**]$^{0}$). The carboxylic acid-type Dye Two complex [Ru(bipy)$(COOH\text{-}dp)_2$] [**2-1c**] was isolated as a metallic green solid and characterized by $^{1}H$ NMR, $^{13}C$ NMR, ESI-MS, UV-vis spectroscopy, and elemental analysis. All data are consistent with the structure depicted in Scheme 2.6.

The X-ray crystal structure of [Ru(bipy)$(COOH\text{-}dp)_2$] [**2-1c**] is shown in Figure 2.3 as an ORTEP plot, where the thermal ellipsoids are displayed at the 30% level.

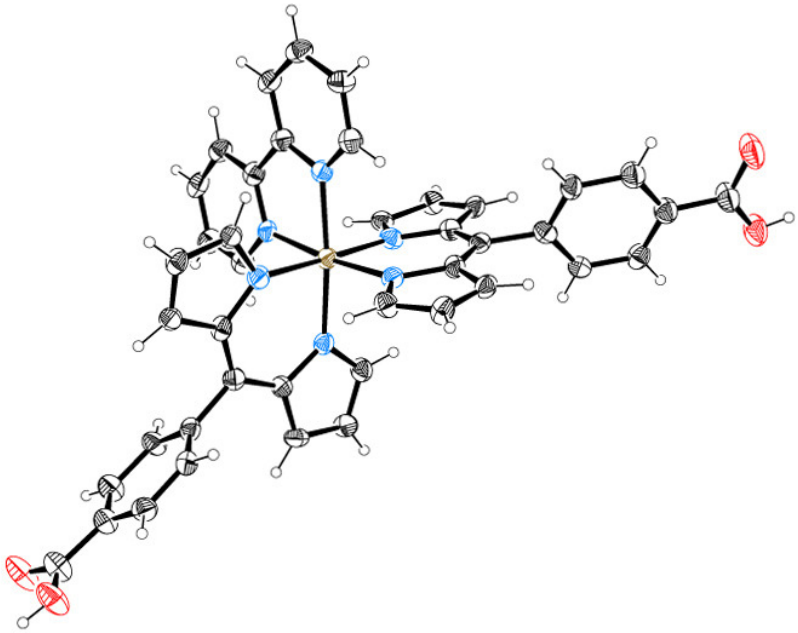

**Figure 2.3** An ORTEP plot showing the molecular structure of [Ru(bipy)$(COOH\text{-}dp)_2$] as determined by X-ray crystallography. Thermal ellipsoids are set at the 30% level.

[Ru(bipy)$(COOH\text{-}dp)_2$]•$(C_5H_{12})$ crystallizes from the diffusion of pentane vapours into a solution of the complex in acetone in the space group *Pbcn*. The asymmetric unit is defined by half of one enantiomer of the complex, which sits on a two-fold rotation

axis. The geometry around the Ru(II) centre is approximately octahedral; however one of the dipyrrinato ligands is bending away from the plane in which the ruthenium atom and the nitrogen donor atoms lie. The Ru-$N_{dipyrrin}$ bond lengths fall in the range 2.052(8)-2.063(8) Å, while the Ru-$N_{bipy}$ bond lengths are shorter at 2.023(8). The shorter Ru-$N_{bipy}$ bond length is presumably due to the greater propensity of bipyridine to engage in π-backbonding. The phenyl ring is twisted 69.5° out of the plane of each dipyrrin ligand, while the protonated carboxylato group twists 179.5° out of the plane of each phenyl ring. The C-O bond distances of the carboxylato group (1.269(13) and 1.277(12) Å) are consistent with it being protonated, thus rendering [Ru(bipy)(COOH-dp)$_2$] [**2-1c**] neutral. The two carboxyl groups located on the periphery of each [Ru(bipy)(COOH-dp)$_2$] [**2-1c**] complex form a hydrogen bond with neighbouring complexes via a cyclic dimer motif, which links complexes of alternating handedness into zigzag chains that propagate through out the crystal structure (Figure 2.4).

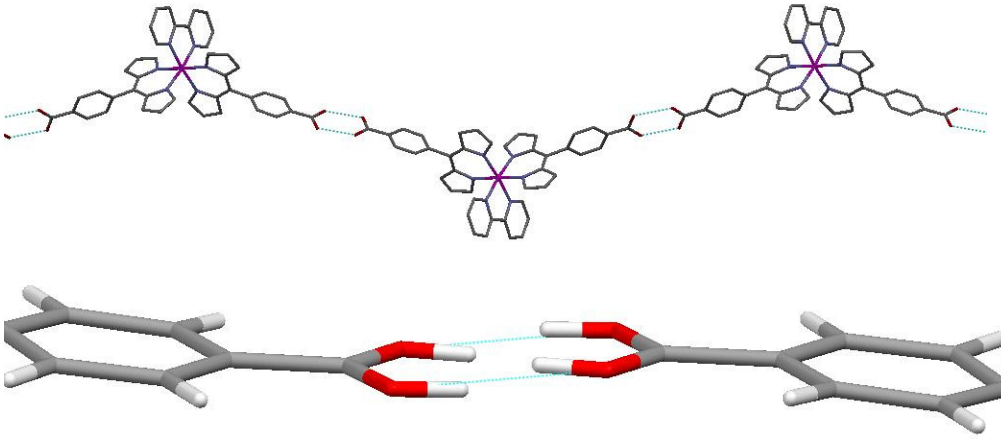

**Figure 2.4** A segment of the infinite hydrogen-bonding network formed between the carboxylic acid groups of neighbouring [Ru(bipy)(COOH-dp)$_2$] molecules.

The hydrogen bonds linking neighbouring [Ru(bipy)(COOH-dp)$_2$] [**2-1c**] molecules (represented by the turquoise lines in Figure 2.4) form a dimer. The length of the bond formed between the carboxylic acid groups is 2.634(-) Å. This distance is consistent with the bond being a hydrogen bond, as it falls well within the limits for the length of a hydrogen bond (1.8-3.5 Å) (A normal covalent bond is ~0.96 Å, while anything greater than 3.5 Å would be considered a dipole-dipole interaction)[22, 23]. The carboxylic acid group on each dipyrrin ligand of the [Ru(bipy)(COOH-dp)$_2$] [**2-1c**] molecule appears as

four sides of a pentagon. The pair of each 'pentagons' from the neighbouring [Ru(bipy)(COOH-dp)$_2$] [**2-1c**] molecules sit out of the plane formed by the hydrogen bonds, where one carboxylic acid group sits above the plane while the opposite carboxylic acid group sits below the plane. This phenomenon is clearly shown in Figure 2.4. The bond angles centred on the upper half of each carboxylic acid 'pentagon' are equivalent, as are the bond angles centred on the lower half of each carboxylic acid 'pentagon'. However, the upper bond angles differ slightly from those for the lower half: the two upper bond angles, centred over the oxygen atom, are 120.5°, whereas the two lower bond angles, also centred over the oxygen atom, are 116.0°.

NMR and UV-visible data collated for [Ru(bipy)(COOH-dp)$_2$] [**2-1c**] are discussed in detail in Chapter 3 of this thesis, while ESI-MS and elemental values along with the NMR and UV-visible values are listed in Chapter 5.

As the monodentate dmso ligands on the intermediate [Ru(dmso)$_2$(COOH-dp)$_2$] [**2-1a**] should be readily displaced by any neutral chelating ligand, [Ru(dmso)$_2$(COOH-dp)$_2$] [**2-1a**] is expected to be a useful intermediate for the synthesis of various bis- and tris-complexes of Ru(II), including tris-dipyrrinato complexes.

### 2.3.2. Phenyl-type Dye Two: [Ru(bipy)(Ph-dp)$_2$]

Following the success of the carboxylic acid-type Dye Two complex [Ru(bipy)(COOH-dp)$_2$] [**2-1c**], it was tested whether or not the same methodology could be applied to different dipyrrin ligands, by substituting Ph-dp for COOMe-dp and replicating the successful synthetic procedure discussed in Chapter 2.3.2. Analogous to the Dye One group complexes hydrolysis was again redundant, resulting in a simple, two-step reaction. This reaction, which is illustrated in Scheme 2.7, successfully afforded the complex [Ru(bipy)(Ph-dp)$_2$] [**2-2b**].

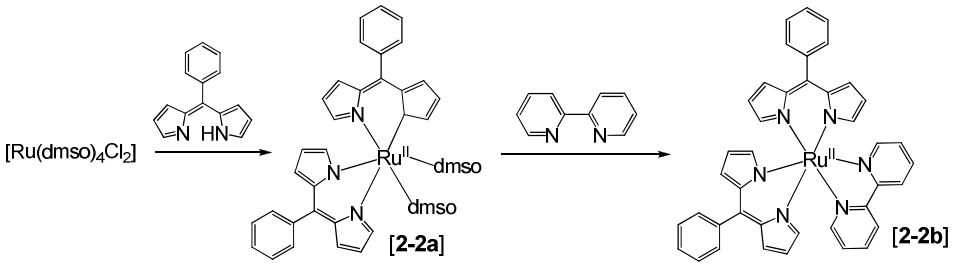


**Scheme 2.7** Synthesis of [Ru(bipy)(Ph-dp)$_2$].

The intermediate complex [Ru(dmso)$_2$(Ph-dp)$_2$] [**2-2a**] was obtained in good yield by thermally reacting two equivalents of the ligand Ph-dp with one equivalent of [Ru(dmso)$_4$Cl$_2$] in absolute ethanol. Purification via column chromatography on deactivated dry-packed alumina afforded a fine red-brown solid, which was orange-coloured in solution. The intermediate [Ru(dmso)$_2$(Ph-dp)$_2$] [**2-2a**] was cleanly converted into [Ru(bipy)(Ph-dp)$_2$] [**2-2b**] via a direct reaction with 2,2'-bipyridine at elevated temperatures in the crucial absence of any solvent. The complex is neutral overall because the phenyl group on the dipyrrin is neutral, making the free-base ligand negatively charged (bipyridine is a neutral ligand so $Ru^{2+}$ plus 2x$[Ph\text{-}dp]^{-1}$ equals $[\mathbf{2\text{-}2b}]^{0}$).

The behaviour of the phenyl-type Dye Two complex [Ru(bipy)(Ph-dp)$_2$] [**2-2b**] is so similar to that of the carboxylic acid-type Dye Two complex [Ru(bipy)(COOH-dp)$_2$] [**2-1b**] that there was little deviation necessary from the processes that purify the latter. The exception was the necessity of a further purification step for [Ru(bipy)(Ph-dp)$_2$] [**2-2b**] involving the centrifugation of the precipitate formed during the recrystallisation, suspension in hexane and collection by filtration. This extra step was necessary because the recrystallised solid was too fine to facilitate collection by filtration. The phenyl-type Dye Two complex [Ru(bipy)(Ph-dp)$_2$] [**2-2b**] was isolated as a metallic green solid and characterized by $^{1}$H NMR, $^{13}$C NMR, ESI-MS, UV-visible spectroscopy, elemental analysis, and X-ray crystallography. All data are consistent with the structure depicted in Scheme 2.7.

The X-ray crystal structure of [Ru(bipy)(Ph-dp)$_2$] [**2-2b**] is shown in Figure 2.5 as an ORTEP plot, where the thermal ellipsoids are displayed at the 30% level.

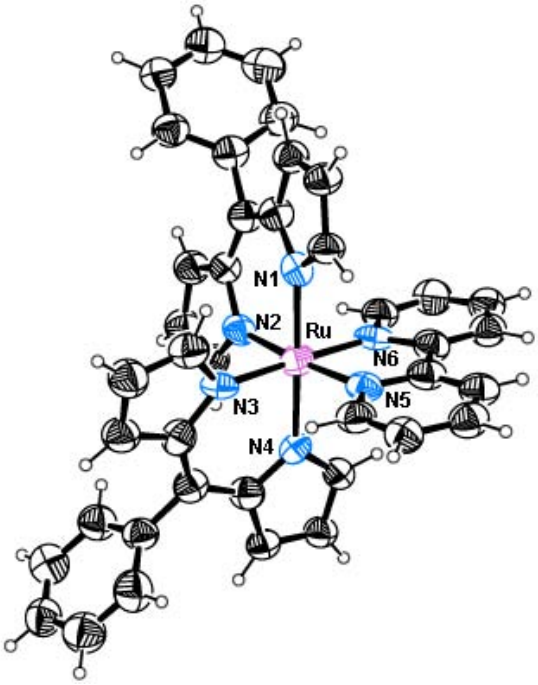


**Figure 2.5** An ORTEP plot showing the molecular structure of [Ru(bipy)(Ph-dp)$_2$] as determined by X-ray crystallography. Thermal ellipsoids are displayed at the 30% level.

[Ru(bipy)(Ph-dp)$_2$] [**2-2b**] crystallizes from the diffusion of methanol vapours into a solution of the complex in chloroform in the space group $P2_1c$. The asymmetric unit is occupied by one enantiomer of the complex, and the geometry around the Ru(II) centre is approximately octahedral, where the two dipyrrin ligands are twisting slightly out of the plane in which the ruthenium atom and the nitrogen donor atoms lie. The Ru-$N_{dipyrrin}$ bond lengths fall in the range 1.992(11)-2.045(11) Å, while the Ru-$N_{bipy}$ bond lengths are marginally longer (2.062(2) and 2.062(4) Å). One phenyl ring is twisted 71.5° out of the plane, while the other is twisted 91° out of the plane of the their respective dipyrrin ligands.

### 2.3.3. Diphenylamino-type Dye Two: [Ru(bipy)(Ph$_2$N-dp)$_2$]

The success in the synthesis of the phenyl-type Dye Two complex [Ru(bipy)(Ph-dp)$_2$] [**2-2b**], strongly suggested that the same innovative "molten bipy" methodology could be applied to different dipyrrin ligands, with the advantage that unlike the Dye One group complexes, purification procedures could be virtually unchanged regardless of the dipyrrin ligand that was coordinated. Subsequently, the route was applied to a third dipyrrin with

the goal of synthesising another Dye Two group complex. The same simple, two-step reaction procedure that afforded [Ru(bipy)(Ph-dp)] [**2-2b**] was repeated for the ligand $Ph_2N$-dp, which illustrated by Scheme 2.8, resulted in the synthesis of the complex [Ru(bipy)($Ph_2N$-dp)$_2$] [**2-3b**].

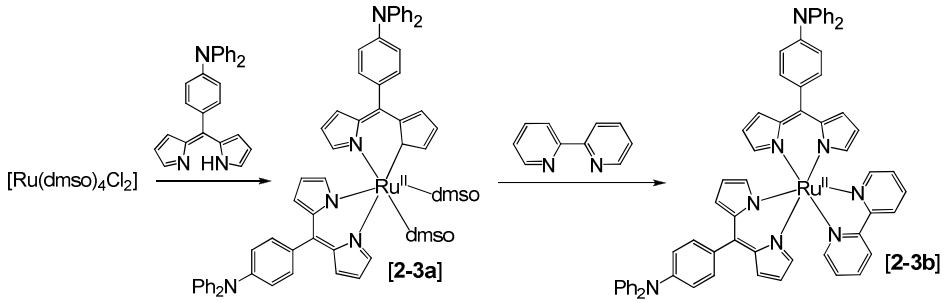


**Scheme 2.8** Synthesis of [Ru(bipy)($Ph_2N$-dp)$_2$].

The diphenylamino-type Dye Two complex [Ru(bipy)($Ph_2N$-dp)$_2$] [**2-3a**] was obtained in good yield by thermally reacting two equivalents of the ligand $Ph_2N$-dp with one equivalent of [Ru(dmso)$_4$Cl$_2$] in absolute ethanol. Purification via column chromatography on deactivated dry-packed alumina afforded a fine red-brown solid, which was orange-coloured in solution. The intermediate [Ru(dmso)$_2$($Ph_2N$-dp)$_2$] [**2-3a**] was cleanly converted into [Ru(bipy)($Ph_2N$-dp)$_2$] [**2-3b**] via a direct reaction with 2,2'-bipyridine at elevated temperatures in the crucial absence of any solvent.

The neutral diphenylamino functional group causes the dipyrrin ligand to be negative and therefore the overall end product to be neutral (bipyridine is a neutral ligand so $Ru^{2+}$ plus 2x[$Ph_2N$-dp]$^{-1}$ equals [**2-3b**]$^{0}$). This likens the complex considerably to the phenyl-type Dye Two complex [Ru(bipy)(Ph-dp)$_2$] [**2-2b**], causing the behaviour of [Ru(bipy)($Ph_2N$-dp)$_2$] [**2-3b**] to be so similar to both [Ru(bipy)(COOH-dp)$_2$] [**2-1b**] and [Ru(bipy)(Ph-dp)$_2$] [**2-2b**] and that an identical purification procedure can be followed, up to and including the column chromatography over neutral alumina. The purity of [Ru(bipy)($Ph_2N$-dp)$_2$] [**2-3b**] at this point is notably substandard compared to that for both the ester- and phenyl-type Dye Two complexes at the same point, so much so that further purification is absolutely essential. Total purification of [Ru(bipy)($Ph_2N$-dp)$_2$] [**2-3b**] is achieved by means of a further two chromatography columns. The first was over neutral lipophilic sephadex which draws on size exclusion to separate molecules. This column allowed the free-flow of the complex, leaving behind additional impurities on the

column. The second and final column was carried out over neutral alumina, which removed any remaining contaminants before analytically pure product was eluted.

The diphenylamino-type Dye Two complex [Ru(bipy)($Ph_2$N-dp)$_2$] [**2-3b**] was isolated as a metallic green solid and characterized by $^1$H NMR, $^{13}$C NMR, ESI-MS, UV-visible spectroscopy, and elemental analysis. All data are consistent with the structure depicted in Scheme 2.8. NMR and UV-visible data are discussed in detail in Chapter 3 of this thesis, while ESI-MS and elemental values along with the NMR and UV-visible values are listed in Chapter 5. X-ray crystallography was not possible, as crystals did not grow despite multiple attempts with a variety of solvent combinations.

## 2.4. Dye Three Group Complexes

Dye Three Group complexes are a group of bis-bipyridine dipyrrinato complexes i.e. they consist of two bipyridine ligands and one dipyrrin ligand coordinated to a Ru(II) metal centre. The Dye Three Group complexes are the same as the Dye One Group complexes except that the bipyridine ligands are replaced by dicarboxybipyridine ligands in the Dye Three Group complexes. There are two complexes in this set, which are differentiated by the functional group (R) on the dipyrrinato ligand: R = H [**3-1**], and $NPh_2$ [**3-2**].

Unfortunately, due to time constraints, it was not possible to synthesise this group of complexes. The proposed method is shown below in Scheme 2.9 (next page), where the "building block" material [Ru(dcbipy)$_2$Cl$_2$] can be obtained by following the procedure published by Grätzel et al[25].

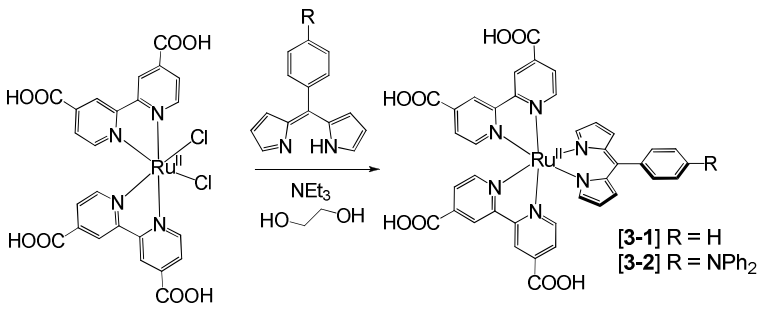


**Scheme 2.9** Proposed synthesis of the Dye Three group complexes: [Ru(dcbipy)$_2$(Ph-dp)] and [Ru(dcbipy)$_2$($Ph_2$N-dp)].

Should the above methodology fail, an alternative high-temperature thermal reaction involving ethylene glycol may also be a feasible pathway. This reaction is reported in Bessho et al[26].

## 2.5. Dye Four Group Complexes

Dye Four Group complexes are a group of bipyridine bis-dipyrinato complexes i.e. they consist of one bipyridine ligand and two dipyrrin ligands coordinated to a Ru(II) metal centre. The Dye Four Group complexes are the same as the Dye Two Group complexes except that the bipyridine ligands are replaced by dicarboxybipyridine ligands in the Dye Four Group complexes. There are two complexes in this set, which are differentiated by the functional group (R) on the dipyrrinato ligand: R = H [**4-1b**], and $NPh_2$ [**4-2b**], however only the first of the two complexes in this set was successfully synthesised. When the carboxylic acid groups on the dicarboxybipyridine ligand are protonated the Dye Four Group complexes are neutral.

### 2.5.1. Phenyl-type Dye Four: [Ru(dcbipy)(Ph-dp)$_2$]

Due to the low yield and low purity of the Ph-dp ligand, the synthetic method for the Dye Four group complexes was developed using the ligand COOMe-dp, which was of high purity and in abundance. The very first trial was conducted using the anion exchange column product from the intermediate [$Ru(dmso)_2(COOMe\text{-}dp)_2$] [**2-1a**] (see Chapter 2.3.1) with one equivalent of dicarboxybipyridine (dcbipy) under an inert atmosphere. Concurrently an *in situ* reaction was also set up, which involved the synthesis of the intermediate material then addition of dicarboxybipyridine without isolating the intermediate beforehand. Some success was had with both reactions but the products were lost during the purification step when they precipitated on a column. When more [$Ru(dmso)_2(COOMe\text{-}dp)_2$] [**2-1a**] became available the reaction was repeated, but without success.

A different approach was taken for the next trial reaction, which involved the use of a ruthenium-cymene dimer [(*p*-cymene)$RuCl_2]_2$ (where cymene has the molecular formula

$C_{10}H_{14}$) as the base complex. The dimer was reacted with dicarboxybipyridine, and then this new complex was reacted *in situ* with COOMe-dp in the presence of base. The first step was very successful but multiple attempts failed to coordinate the dipyrrin to the ruthenium. This reaction was based on that used by Gratzel to synthesise the famous N3 dye[27].

At this point it was decided that due to its abundance, trials would be conducted with bipyridine until success was achieved, at which time the successful trial would then be applied to the less abundant but similarly structured dicarboxybipyridine. Details for these trails are provided in Chapter 2.3.1 of this thesis. Following the overwhelming success of the "molten bipy" reaction that gave [Ru(bipy)(COOMe-dp)$_2$] [**2-1b**], the bipyridine was substituted for dicarboxybipyridine and the methodology was repeated. Although the literature stated that the melting point of dicarboxybipyridine was much higher than bipyridine (dicarboxybipyridine melts at >360°C compared with bipy at 70-73°C[28], it was observed that the orange [Ru(dmso)$_2$(COOMe-dp)$_2$] appeared to be melting first, and it was hoped that the dicarboxybipyridine would dissolve into the molten complex, and initiate a reaction. Unfortunately this was not the case and even after an extended period of time at elevated temperatures both compounds remained in solid form. The next attempt at this reaction involved dissolving the reagents and then removing the solvent on a rotary-evaporator to give a film. Due to the insolubility of dicarboxybipyridine in any solvent this procedure was not possible.

It was proposed that the melting points of other bipyridine derivatives similar to dicarboxybipyridine but with different melting points, could be manipulated post-coordination to give dicarboxybipyridine. This was explored. The melting point for the dialdehydebipyridine derivative CHO-bipy was reported as 188°C[28], while the melting point for the octadecyl ester derivative was reported as 87°C, and the longer chain dihydrocholesteryl ester derivative was reported as 280-285°C[29]. These compounds all melt at significantly lower temperatures than dicarboxybipyridine. On this basis it was believed that a medium chain ester derivative such as the docosonate ester derivative COOR-bipy would have a melting point on the scale between that for bipyridine and dicarboxybipyridine, and would therefore be a feasible prospect for a "molten bipy" reaction. In addition, the ester was particularly attractive as an alternative chelating ligand as it is easily hydrolysed to give the desired carboxylic acid functional groups. Although

the octadecyl ester derivative had a known melting point and was identified to be suitable, 1-octadecanol was not readily available; whereas there was immediate access to docosonol. This is the reasoning behind why the docosonate ester was implicated. Following the success of the "molten bipy" reaction between the ester-type intermediate $[Ru(dmso)_2(COOMe\text{-}dp)_2]$ [**2-1a**] and the docosonate ester derivative (COOR-bipy), the methodology was repeated with the phenyl-type intermediate $[Ru(dmso)_2(Ph\text{-}dp)_2]$ [**2-2a**]. This resulted in the successful synthetic procedure, which is illustrated in Scheme 2.10.

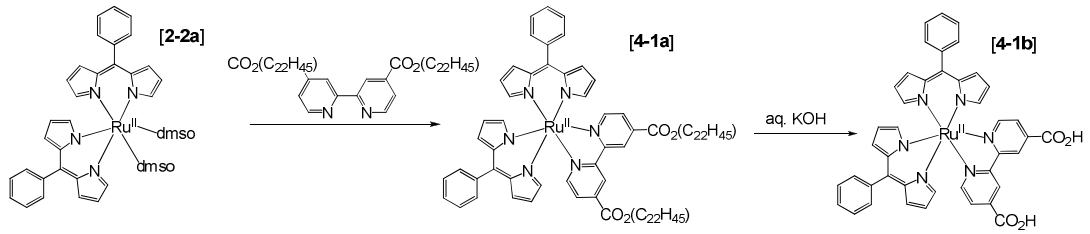


**Scheme 2.10** Synthesis of $[Ru(dcbipy)(Ph\text{-}dp)_2]$.

Complex $[Ru(COOR\text{-}bipy)(Ph\text{-}dp)_2]$ [**4-1a**] was obtained in good yield by directly reacting the intermediate $[Ru(dmso)_2(Ph\text{-}dp)_2]$ [**2-2a**] with COOR-bipy at elevated temperatures. Like the "molten bipy" reaction which generates the Dye Two group complexes, clean conversion occurs and it is necessary to exclude all solvent from the reaction in order for it to proceed. Complex $[Ru(COOR\text{-}bipy)(Ph\text{-}dp)_2]$ [**4-1a**] was isolated as a metallic green solid.

Hydrolysis of the ester moieties in aqueous base afforded the phenyl-type Dye Four complex $[Ru(dcbipy)(Ph\text{-}dp)_2]$ [**4-1b**]. TnBA hydroxide is required to isolate the product, which occurs as a salt. The complex $[Ru(dcbipy)(Ph\text{-}dp)_2]$ [**4-1b**] is extracted as a thick oil, which precipitates upon addition of pentane. The resulting solid was nearly pure, except that a very large amount of residual TnBA remained associated with the salt. Further cycles of washing with water, extracting into organic solvent, and exposure to a drying agent reduced the residual ammonium base, but only by a fraction. The residual base also caused the product to be very hygroscopic. Recrystallisation from the same solvent combination as that which purifies both $[Ru(bipy)(COOH\text{-}dp)_2]$ [**2-1b**] and $[Ru(bipy)(Ph\text{-}dp)_2]$ [**2-2b**] (which have very similar structures to $[Ru(dcbipy)(Ph\text{-}dp)_2]$ [**4-1b**]), was hoped to also take the complex to analytical purity but was not able to remove the residual ammonium base. Other solvent combinations were also ineffective.

The phenyl-type Dye Four complex [Ru(dcbipy)(Ph-dp)$_2$] [**4-1b**] was isolated as a metallic green solid and characterized by $^{1}$H NMR, $^{13}$C NMR, and ESI-MS. ESI-MS data is consistent with the structure depicted in Scheme 2.10, whereas the NMR spectra clearly show peaks attributable to the presence of remaining TnBA hydroxide. UV-visible and Raman spectra were also recorded, which were indicative of the desired complex shown in Scheme 2.10, but not accurate due to the imprecise mass in the solutions. These are discussed briefly in Chapter 3. The growth of crystals was not attempted, also due to the high degree of impurity.

*Chapter 3*

# SPECTROSCOPIC ANALYSIS AND ELECTROCHEMISTRY

Several techniques were employed to investigate the spectroscopic properties including NMR, UV-visible and Raman spectroscopy. The electrochemistry for each complex was also examined. Collectively, the results of the spectroscopic and electrochemical studies were used to ascertain whether the target complexes possessed the correct attributes to act as suitable dyes in DSSCs. For some sections of this chapter the Dye Two group complexes referred to in the discussion also includes the ester-type complex [**2-1a**].

## 3.1. $^{1}$H and $^{13}$C NMR Spectral Study

Nuclear Magnetic Resonance spectroscopy (NMR) is the technique which exploits the magnetic properties of certain nuclei (including $^{1}$H, $^{2}$H, $^{10}$B, $^{11}$B boron, $^{13}$C, $^{14}$N, $^{15}$N nitrogen, $^{19}$F fluorine, $^{17}$O oxygen, $^{31}$P phosphorus, $^{35}$Cl chlorine, $^{29}$Si silicon, $^{23}$Na sodium, among many others) to elucidate structural information about a chemical substance. NMR is a useful technique for identifying the structure of a substance that has been produced from a synthetic process, and/or the level of purity that the substance may be at. In addition, NMR may also be used for a more specific purpose to study the effects of varying the functional group connected to a ligand on the behaviour of other components in the same coordination complex.

Heteroleptic dipyrrin/bipyridine complexes in particular are suitable for examination by $^{1}$H NMR spectroscopy because their spectra are comparatively simple. There is no observable coupling between the groups of bipyridyl and dipyrrinato protons, and very little overlap of resonances (deduced from COSY experiments). The diamagnetic complexes of Ru(II) with the ligands COOMe-dp/COOH-dp, Ph-dp and $Ph_2N$-dp, as well as the free-base ligands themselves have been studied. The effects of varying the functional group connected to the dipyrrin ligand of each dye group on the behaviour of the bipyridine ligand and the body of the dipyrrin ligand has been investigated for the complexes in this thesis using two different isotopes: $^{1}$H and $^{13}$C. The reasoning behind

studying these particular components as that both of the bipyridine and dipyrrin ligands are incorporated in varying proportions into all of the target complexes discussed in this thesis and are recordable by $^{1}H$ and $^{13}C$ NMR; which makes for a uncomplicated yet interesting comparison. Two simultaneous investigations were conducted: where the peak positions for key common components was traced and compared across the three complexes within each dye group including intermediate materials; and where the peaks positions for key common components was traced and compared across the three dye groups for each dipyrrin ligand, also including intermediate materials. The findings from two of these investigations are detailed in this chapter, with the dipyrrin peaks assigned with the aid of Falk[5].

### 3.1.1. Dye One Group Complexes

Figure 3.1 shows the $^{1}H$ NMR spectra for the free-base dipyrrin COOMe-dp (top), and the Dye One group complex [Ru(bipy)$_2$(COO$^-$-dp)] [**1-1b**] (bottom).

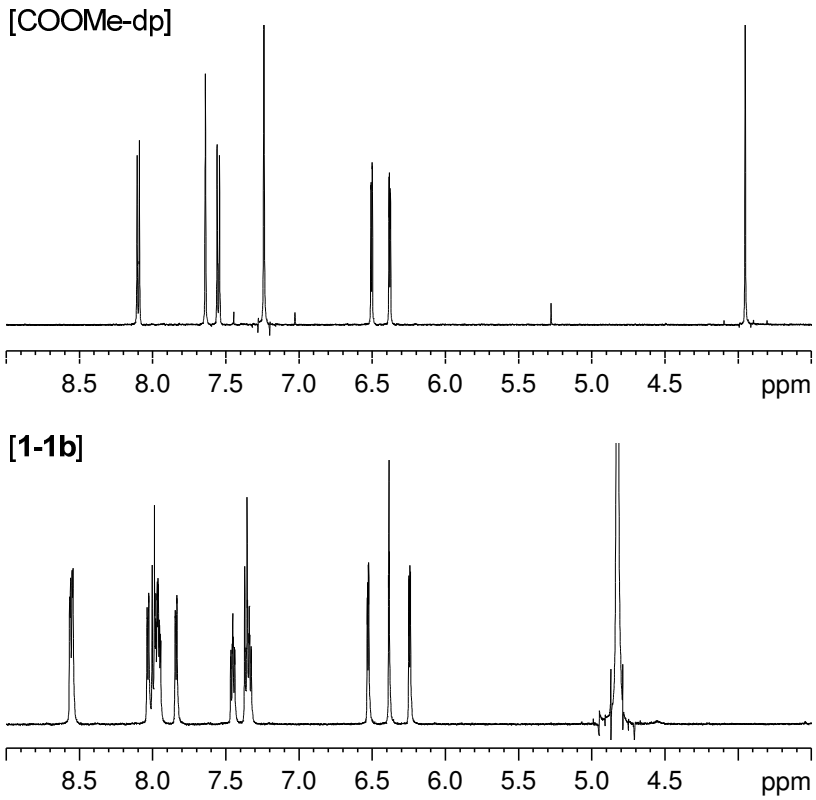


**Figure 3.1** $^{1}H$ NMR spectra for the formation of [Ru(bipy)$_2$(COO$^-$-dp)] [**1-1b**] from COOMe-dp.

The peaks in the free-base dipyrrin spectrum (Figure 3.1, top) may be assigned to (from left to right): the first pair of aromatic protons from the central phenyl ring (closest to functional group) **D1**, a singlet proton from the pyrrole ring (closest to nitrogen atom) **D3**, the second pair of aromatic protons from the central phenyl ring **D2**, $CDCl_3$, two doublet protons from the pyrrole rings (where the former peak **D4** is closer to the nitrogen atom than the latter **D5**), and the set of methyl protons from the ester group. These assignments are based on the integrals calculated for each peak and from their expected behaviour according to their chemical environment e.g. if proximal to an electronegative atom such as nitrogen would be expected to appear downfield of the spectrum (ie at a higher chemical shift value) due to deshielding.

A clear conversion is observed in the difference between the two spectra, providing clear evidence for the formation of the carboxylic acid-type Dye One group complex $[Ru(bipy)_2(COO^-\text{-dp})]$ [**1-1b**]. Firstly, the appearance of bipyridine peaks in the spectrum for $[Ru(bipy)_2(COO^-\text{-dp})]$ [**1-1b**], supports successful coordination of the dipyrrin to the ruthenium building block $[Ru(bipy)_2Cl_2]$. Well-defined triplet peaks attributable to the bipyridine protons appear at *ca.* 8.5, 7.5 and 7.4 ppm. There is a prominent shift in the position of phenyl group protons in the dipyrrin ligand from *ca.* 7.5 and 8.1 ppm in the free-base dipyrrin to *ca.* 7.8 and 8.0 ppm in the $[Ru(bipy)_2(COO^-\text{-dp})]$ [**1-1b**] complex, and the two pyrrolic protons *ca.* 6.5 ppm move apart slightly. The most significant signal movement is that displayed by the singlet pyrrolic peak which travels drastically upfield from *ca.* 7.6 ppm in the free-base dipyrrin to *ca.* 6.4 ppm in the $[Ru(bipy)_2(COO^-\text{-dp})]$ [**1-1b**] complex. This indicates a rotation of the pyrrole rings from a transoid conformation in the free ligand to a cisoid conformation once coordinated. The absence of the methyl proton peak at 3.9 ppm in the $^1$H NMR spectra for the complex $[Ru(bipy)_2(COOMe\text{-dp})]PF_6$ [**1-1a**] (not shown) indicates that hydrolysis of the functional group from the ester to the carboxylic acid has successfully occurred. There is a marginal shift in all peak positions in the spectra for complex $[Ru(bipy)_2(COO^-\text{-dp})]$ [**1-1b**] in contrast to the free-base dipyrrin, which may be due to the use of *d*-methanol as the solvent as opposed to *d*-chloroform for solubility reasons.

A comparison of the $^1$H NMR spectra for Ph-dp and $[Ru(bipy)_2(Ph\text{-dp})]^+$ $[\mathbf{1\text{-}2}]^+$ is nearly identical to that conducted for COOMe-dp and $[Ru(bipy)_2(COO^-\text{-dp})]$ [**1-1b**]. The only difference is that the chemical shift values for the Ph-dp and $[Ru(bipy)_2(Ph\text{-dp})]^+$ $[\mathbf{1\text{-}2}]^+$

signals are slightly higher with the exception of the two doublet pyrrolic peaks which remain the same. The small shift downfield for the Ph-dp and $[Ru(bipy)_2(Ph\text{-}dp)]^+$ [**1-2**]$^+$ signals is likely to be due to the minor deshielding effect the ester group has upon COOMe-dp and $[Ru(bipy)_2(COO^-\text{-}dp)]$ [**1-1b**]. Another significant difference in the spectra for $[Ru(bipy)_2(Ph\text{-}dp)]^+$ [**1-2**]$^+$ compared to $[Ru(bipy)_2(COO^-\text{-}dp)]$ [**1-1b**] is that there are no ester functional groups in the former complex, so peaks attributable to the methyl protons are not present.

A comparison of the $^1$H NMR spectra for $Ph_2N$-dp and $[Ru(bipy)_2(Ph_2N\text{-}dp)]^+$ [**1-3**]$^+$ (shown in Figure 3.2) also displays several similarities to the other Dye One group complexes. Again a clear conversion is observed in the difference between the two spectra, providing clear evidence for the formation of the Dye One group complex $[Ru(bipy)_2(Ph_2N\text{-}dp)]^+$ [**1-3**]$^+$. Well-defined triplet peaks attributable to the bipyridine protons appear at *ca.* 8.7, 7.6 and 7.5 ppm. The position of the peaks for the protons attached to the phenyl group in the centre of the dipyrrin ligand are again significantly shifted, this time from about 7.4 ppm in the free-base dipyrrin to 8.1 ppm in the complex $[Ru(bipy)_2(Ph_2N\text{-}dp)]^+$ [**1-3**]$^+$. Resonances corresponding to the diphenylamino group protons for the complex relative to the free-base dipyrrin remained constant at *ca.* 7.1 and 7.2 ppm. This lack of movement in contrast to the rest of the signals for the same ligand is expected due to the large distance of the group from the metal centre. The most significant signal movement is still that displayed by the singlet pyrrolic peak which travels drastically upfield from *ca.* 7.7 ppm in the free-base dipyrrin to *ca.* 6.5 ppm in the $[Ru(bipy)_2(Ph_2N\text{-}dp)]^+$ [**1-3**]$^+$ complex.

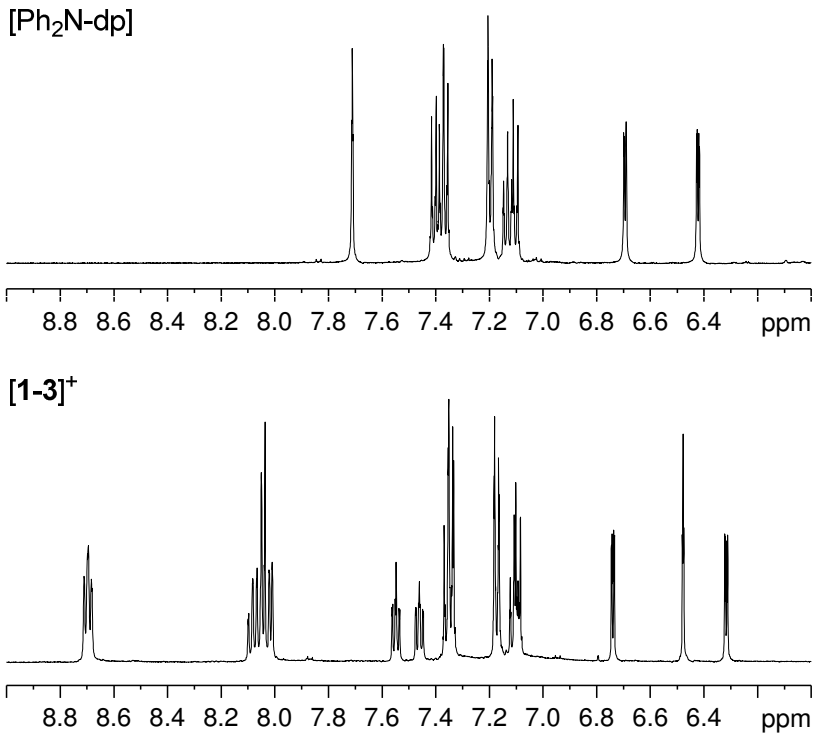


**Figure 3.2** $^{1}$H NMR spectra for the formation of $[Ru(bipy)_2(Ph_2N\text{-}dp)]^+$ [**1-3**]$^+$ from $Ph_2N$-dp.

Because of the lack of coupling and overlapping resonances, by running COSY experiments on each compound it is possible to track the movement of the common chemically equivalent sets of protons in each spectrum. This allows the comparison of the relative shifts of each set from one Dye One group complex to another on the basis that changes in the chemical shift of each set of protons should be directly related to the distance to and type of functional group attached to the dipyrrin ligand, and subsequently the influence the atoms involved may have on the rest of the complex. The chemically equivalent proton sets common to each of the Dye One complexes that were chosen for the study included: each of the bipyridine protons, the pyrrolic protons on the dipyrrin, and the aromatic protons on the central phenyl group of the dipyrrin. The bipyridine sets are labelled **B1**, **B2**, **B3**, **B4** according to the proximity of each proton set to the nitrogen atom on the bipyridine moiety, where **B1** is the closest; and the dipyrrin sets are labelled **D1**, **D2**, **D3, D4, D5** where **D1** and **D2** are the phenyl protons, **D3** is the singlet pyrrolic peak and **D4** and **D5** are the doublet pyrrolic peaks. Figure 3.3 clearly shows the results of this examination, in the form of a summary of the relative chemical shifts of the phenyl and bipyridine protons.

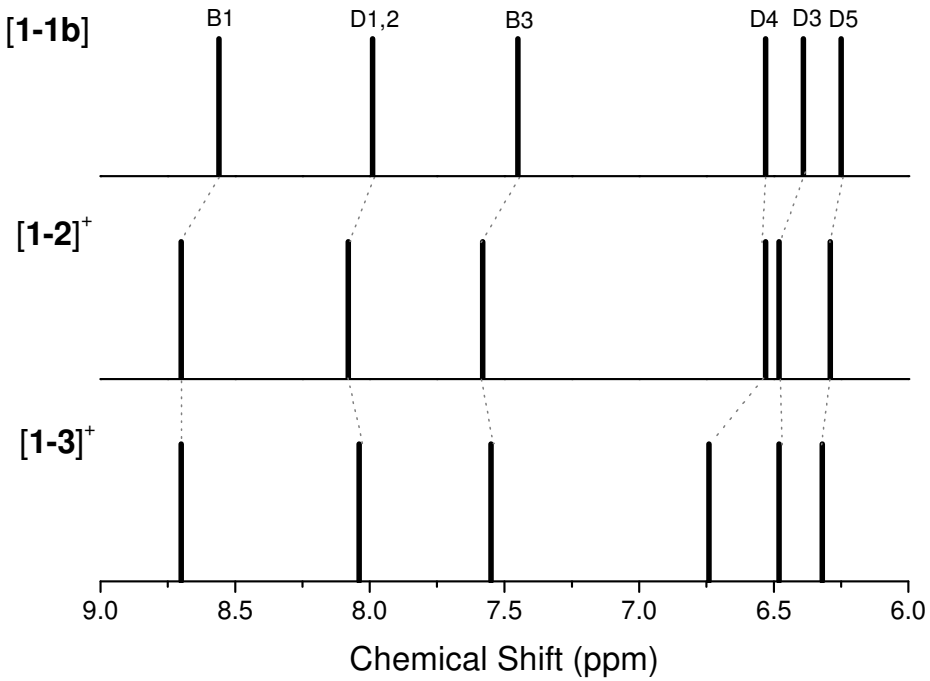


**Figure 3.3** Summary of the relative chemical shifts for selected resonances in the three Dye One group complexes from $^1$H NMR spectra.

As anticipated there is a significant difference in the peak positions for each chemically equivalent set of protons common to each of the three Dye One group complexes. Interestingly, there is negligible difference between the signal positions for the resonances for each of the bipyridine peaks (**B1**, **B2**, **B3**, **B4**) and for the phenyl protons (**D1** and **D2**) for $[Ru(bipy)_2(Ph\text{-}dp)]^+$ [**1-2**]$^+$ and $[Ru(bipy)_2(Ph_2N\text{-}dp)]^+$ [**1-3**]$^+$. There is however a noticeable discrepancy when comparing these two complexes to $[Ru(bipy)_2(COO^-\text{-}dp)]$ [**1-1b**], where the signals for **B1**, **B2**, **B3**, **B4, D1, D2,** and **D5** all appear 1 ($\pm$0.5) ppm downfield in the spectra for the phenyl type ($[Ru(bipy)_2(Ph\text{-}dp)]^+$ [**1-2**]$^+$) and diphenylamino type ($[Ru(bipy)_2(Ph_2N\text{-}dp)]^+$ [**1-3**]$^+$) complexes compared to the same carboxylate type ($[Ru(bipy)_2(COO^-\text{-}dp)]^+$ [**1-1b**]) complex. A similar trend is observed for the singlet pyrrolic proton **D3** except that the shift is in the opposite direction. In contrast the doublet pyrrolic proton **D4** follows the inverse trend, where there is negligible difference between the signals observed in $[Ru(bipy)_2(COO^-\text{-}dp)]$ [**1-1b**] and $[Ru(bipy)_2(Ph\text{-}dp)]^+$ [**1-2**]$^+$, and the same signal is shifted downfield by not just one but 2.5 ppm in $[Ru(bipy)_2(Ph_2N\text{-}dp)]^+$ [**1-3**]$^+$.

The direction of movement is a result of shielding and deshielding effects upon the protons where movement is upfield (to a lower chemical shift value) and downfield (to a higher chemical shift value) respectively. The ring currents of the bipyridyl ligands will have a significant effect on the direction of movement for some of the dipyrrin protons, because those protons will be located in close proximity to the faces of the bipyridine ligands.

The magnitude of the change in relative chemical shift is due to the sensitivity of the protons. The most sensitive protons, and therefore those expected to have larger relative shifts, are those protons that are closest to the nitrogen atom of the pyrrole ring. This is due to the metal ion being bonded to the nitrogen atoms, which causes the protons to be very much more sensitive to the metal ion than other protons. This is the reasoning behind why the movement for the pyrrolic protons is so much greater than for the phenyl protons, and also explains the huge jump for the singlet pyrrolic peak upon coordination. A stepwise effect may also be observed, whereby the closer the positioning of the proton to the nitrogen atoms, the more sensitive and therefore the proportional change in relative chemical shift value.

The likely explanation for such a significant movement of all signals for the protons in the diphenylamino type complex in particular relative to those for the same protons in the other Dye One group complexes is most likely due to the greater propensity of the diphenylamino group for electron donation compared to the other functionalities, which results from the addition of two highly conjugated phenyl rings and a fully occupied nitrogen atom.

### 3.1.2. Dye Two Group Complexes

Figure 3.4 shows the $^{1}$H NMR spectra for the free-base dipyrrin COOMe-dp at the top, the intermediate complex [Ru(dmso)$_2$(COOMe-dp)$_2$] [**2-1a**] (middle), and the carboxylic acid-type Dye Two group complex [Ru(bipy)(COOH-dp)$_2$] [**2-1c**] (bottom).

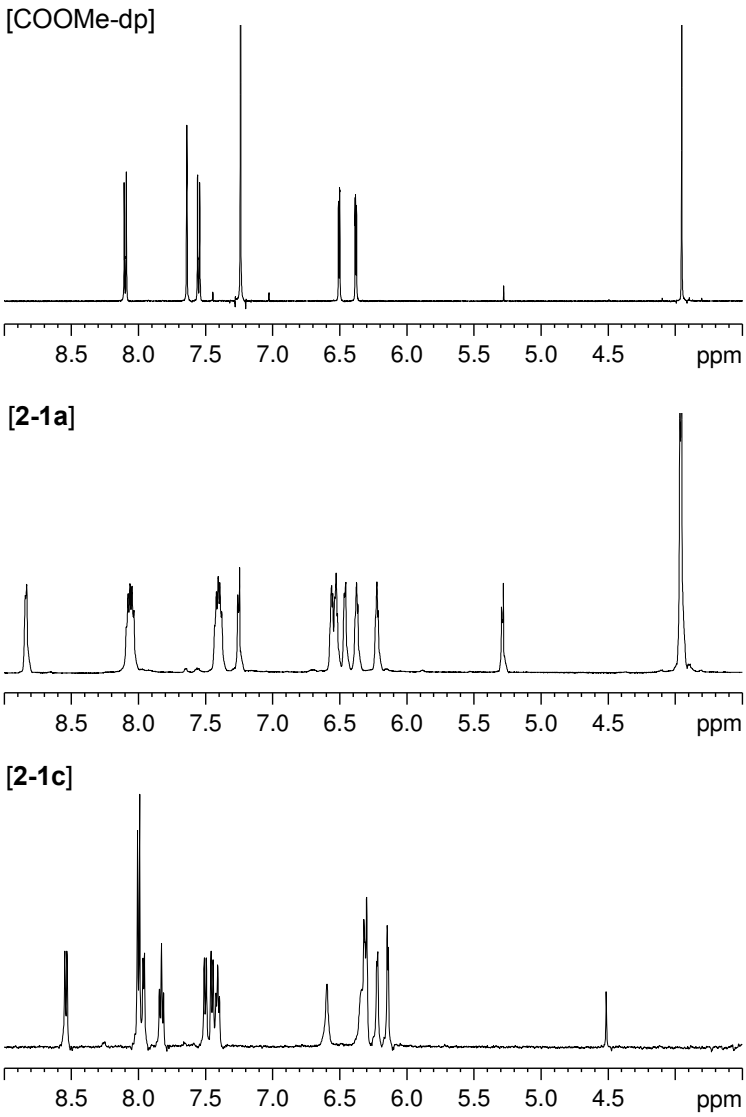


**Figure 3.4** $^{1}$H NMR spectra for the formation of [Ru(bipy)(COOH-dp)$_2$] [**2-1c**] from COOMe-dp, via an ester-dmso intermediate.

The peaks in the free-base dipyrrin spectrum have already been discussed in the previous subsection (3.1.1) of this chapter.

A clear conversion to the intermediate ester-dmso complex [Ru(dmso)$_2$(COOMe-dp)$_2$] [**2-1a**] is observed in the difference between the two spectra. An axis of symmetry is created when each dipyrrin ligand replaces a chloride and dmso ligand connected to the Ru(II) metal centre. The axis of symmetry lies straight through the core of each dipyrrin ligand, so that one side of the ligand is influenced by the neighbouring dipyrrin ligand and the other is influenced by the flanking dmso ligands that remain after coordination. This

symmetry plane is the reason why two complete collections of dipyrrin signals are observed. For the purpose of explaining the signals observed for these two separate collections of chemically equivalent protons, they have been arbitrarily labelled **Dn**, and **Dn'**, where **Dn'** is always the right-hand signal. There is little difference in the chemical shift values for the two collections of phenyl protons; hence the peaks appear as two quadruplets rather than four discrete sets of doublets. Both phenyl proton collections shift upfield slightly (proton sets **D2** and **D2'** move twice the distance upfield than **D1** and **D1'** where the latter are those belonging to the upper phenyl protons i.e. those closest to the ester functionality) but barely change position in proportion to the more significant changes of the other proton sets upon coordination to the metal centre. The split in the doublet pyrrolic peaks is more substantial, where the two proton collections **D4**, **D5** and **D4'**, **D5'** are obviously distinct: **D4** moves downfield to 6.6 ppm with **D5** remaining in the same position at 6.4 ppm; while **D4'** moves very slightly upfield with **D5'** moving downfield to 6.2 ppm, with all movements relative to the same proton signals in the free-base dipyrrin (6.5 and 6.4 ppm for **D4** and **D5** respectively). The space between the two pyrrolic doublet signals is also marginally larger between **D4'**, **D5'** compared to **D4**, **D5**. However, the most conspicuous feature of the spectrum is by far the movement in the position of the singlet pyrrolic peak, which is split in two opposite directions upon coordination of the dipyrrin ligands: from 7.6 ppm in the free-base dipyrrin to 8.8 ppm for **D3** and 6.5 ppm for **D3'** in the ester-dmso intermediate. The appearance of methyl peaks consistent with those found in dmso at *ca.*2.6 ppm also supports the formation of $[Ru(dmso)_2(COOMe\text{-}dp)_2]$ [**2-1a**].

The same trends as those described here for $[Ru(dmso)_2(COOMe\text{-}dp)_2]$ [**2-1a**] are observed for the formation of the dmso intermediates $[Ru(dmso)_2(Ph\text{-}dp)_2]$ [**2-2a**] (the phenyl-type intermediate) and $[Ru(dmso)_2(Ph_2N\text{-}dp)_2]$ [**2-3a**] (the diphenylamino-type intermediate), providing evidence that these two complexes were also successfully synthesised. Even the chemical shift values are only marginally different, with the only distinction being the very slight movement upfield and greater separation of the signals for $[Ru(dmso)_2(Ph\text{-}dp)_2]$ [**2-2a**] relative to $[Ru(dmso)_2(COOMe\text{-}dp)_2]$ [**2-1a**], which is repeated for the $[Ru(dmso)_2(Ph_2N\text{-}dp)_2]$ [**2-3a**] signals relative to $[Ru(dmso)_2(Ph_2N\text{-}dp)_2]$ [**2-2a**].

The difference between the second and bottom spectra provides clear evidence for the formation of the Dye Two group complex [Ru(bipy)(COOH-dp)$_2$] [**2-1c**]. Firstly, the appearance of bipyridine peaks in the spectrum for [Ru(bipy)(COOH-dp)$_2$] [**2-1c**], supports successful coordination of the dipyrrin to the ester-dmso intermediate complex. [Ru(dmso)$_2$(COOMe-dp)$_2$] [**2-1a**]. Peaks assignable to the bipyridine protons appear at *ca.* 7.8 and 7.4 ppm; and the signal assigned to the methyl group of the dmso ligands simultaneously disappears. The replacement of the two dmso ligands by bipyridine alters the chemical environment of the second collection of protons to be very similar to the first collection, thus the difference between the two collections of signals is substantially reduced and it appears in the spectrum that the plane of symmetry through the dipyrrin ligand is lost. There is a prominent shift in the position of phenyl group protons in the dipyrrin ligand that causes the two "quadruplets" to split into two sets of two doublets. The pyrrolic protons shift downfield very slightly, and the space between each of them narrows. The two singlet pyrrolic peaks are now so extremely similar that the signal for **D3** travels drastically downfield resulting in the resonance actually overlapping that given for **D3'**. The absence of the methyl proton peak at 3.9 ppm in the $^1$H NMR spectra for the complex [Ru(bipy)(COOH-dp)$_2$] [**2-1c**] indicates that hydrolysis of the functional group from the ester to the carboxylic acid has successfully occurred. There is a marginal shift in all peak positions in the spectra for complex [Ru(bipy)(COOH-dp)$_2$] [**2-1c**] in contrast to the free-base dipyrrin and the intermediate complex [Ru(dmso)$_2$(COOMe-dp)$_2$] [**2-1a**], which may be due to the use of *d*-dmso as the solvent as opposed to *d*-chloroform for solubility reasons.

The same trends as those described here for [Ru(bipy)(COOH-dp)$_2$] [**2-1c**] are observed for the formation of the Dye Two group complexes [Ru(bipy)(Ph-dp)$_2$] [**2-2c**] (the phenyl-type complex) and [Ru(bipy)(Ph$_2$N-dp)$_2$] [**2-3c**] (the diphenylamino-type complex), providing evidence that these two complexes were also successfully synthesised. In contrast to the transformation of all other complexes and intermediates from their predecessors, the positions for the signals for all three Dye Two group complexes are virtually identical, with the exception of the signals belonging to the functionalities for each complex.

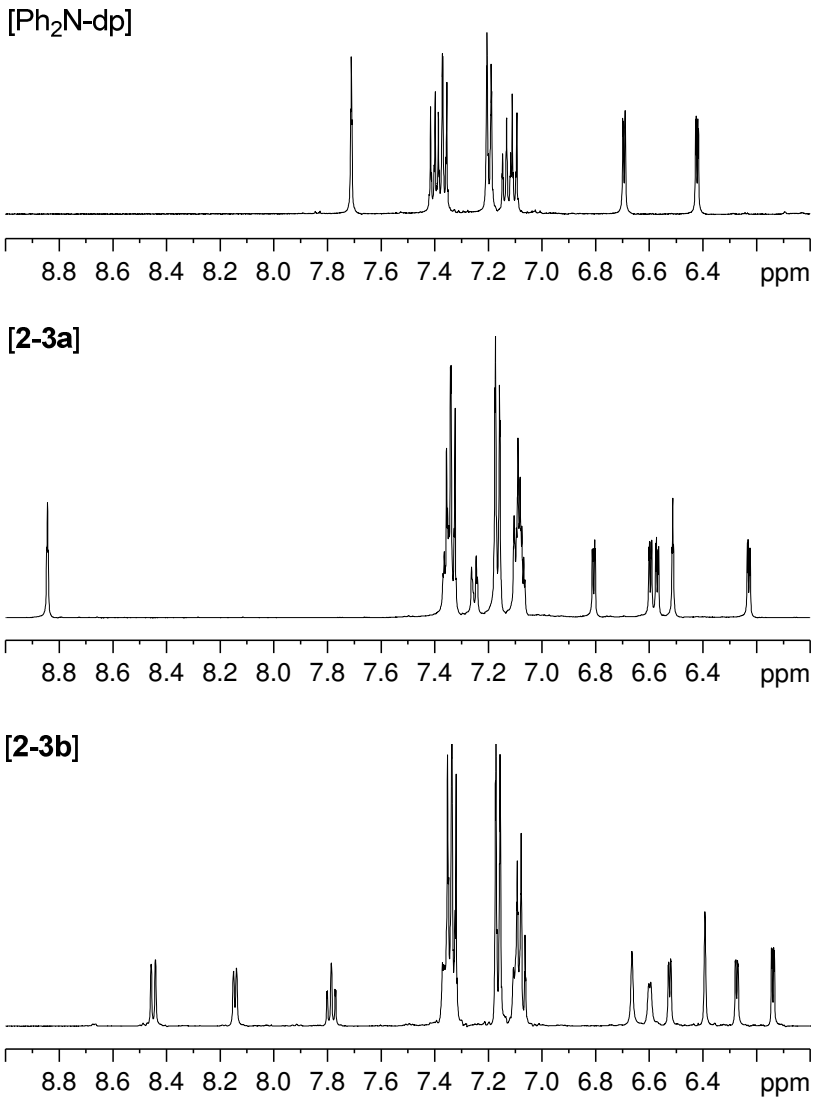


**Figure 3.5** $^{1}$H NMR spectra for the formation of [Ru(bipy)($Ph_2$N-dp)$_2$] [**2-3**] from $Ph_2$N-dp, via a diphenylamino-dmso intermediate.

Because of the lack of coupling and small degree of overlapping resonances, by running COSY experiments on each compound it is possible to track the movement of some of the common chemically equivalent sets of protons in each spectrum. This allows the comparison of the relative shifts of each set from one Dye Two Group complex to another on the basis that changes in the chemical shift of each set of protons should be directly related to the distance to and type of functional group attached to the dipyrrin ligand, and subsequently the influence the atoms involved may have on the rest of the complex. The chemically equivalent proton sets common to each of the Dye Two complexes that were chosen for the study included: each of the bipyridine protons, the

pyrrolic protons on the dipyrrin, and the aromatic protons on the central phenyl group of the dipyrrin. The bipyridine sets are labelled **B1**, **B2**, **B3**, **B4** according to the proximity of each proton set to the nitrogen atom on the bipyridine moiety, where **B1** is the closest; and the dipyrrin sets are labelled **D1**, **D2**, **D3, D4, D5** where **D1** and **D2** are the phenyl protons, **D3** is the singlet pyrrolic peak and **D4** and **D5** are the doublet pyrrolic peaks. Figure 3.3 clearly shows the results of this examination, in the form of a summary of the relative chemical shifts of the phenyl and bipyridine protons.

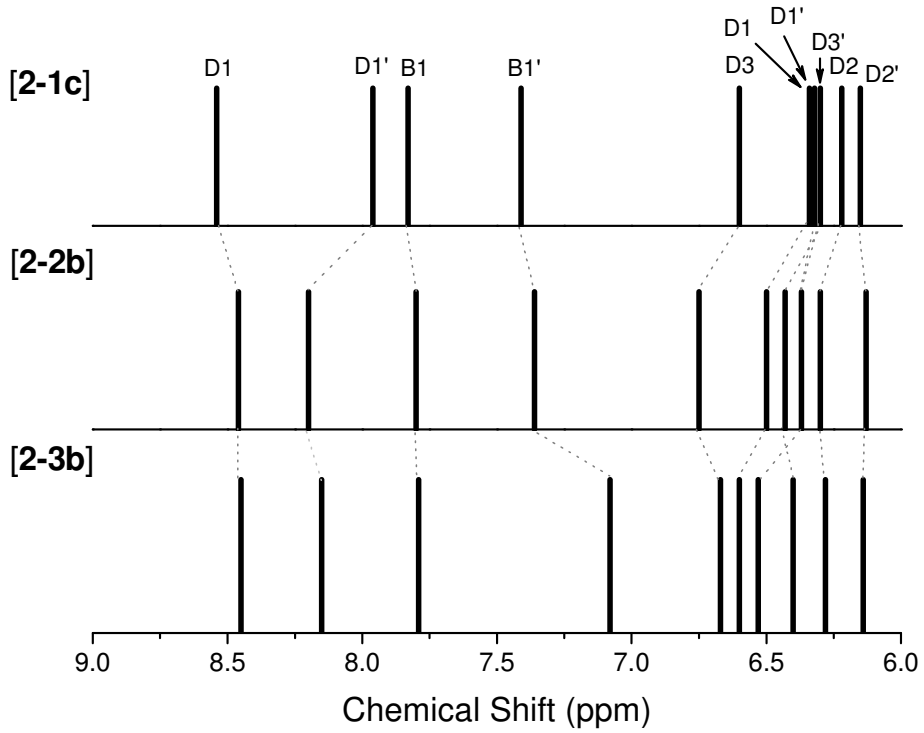


**Figure 3.6** Summary of the relative chemical shifts for selected resonances in the three Dye Two group complexes from $^1$H NMR spectra.

There is virtually no difference in the relative chemical shift values for the first bipyridine protons (**B1**, **B2**,) and dipyrrinato phenyl protons (**D1**, **D2**) in each of the phenyl- and diphenylaimino-type Dye Two group complexes [Ru(bipy)(Ph-dp)$_2$] [**2-2b**] and [Ru(bipy)(Ph$_2$N-dp)$_2$] [**2-3b**], respectively. The same signals are virtually identical for the carboxylate-type complex [Ru(bipy)(COOH-dp)$_2$] [**2-1c**] as well, except that one of the phenyl protons appears downfield 2 ppm. More significant differences are apparent when inspecting the latter bipyridine protons (**B3**, **B4**) and the pyrrolic protons (**D3**, **D4**, **D5**).

Firstly, the separation between the bulk of the signals narrows moving from [Ru(bipy)(COOH-dp)$_2$] [**2-1c**] to [Ru(bipy)(Ph-dp)$_2$] [**2-2b**] to [Ru(bipy)(Ph$_2$N-dp)$_2$] [**2-3b**], which causes some resonance overlap in the diphenylamino-type Dye Two complex [Ru(bipy)(Ph$_2$N-dp)$_2$] [**2-3b**]. Secondly, the order of the signals is consistent across the complexes, with the exception of on pyrrolic doublet (thought to be **D3'**) which appears upfield of the pyrrolic singlet in [Ru(bipy)(COOH-dp)$_2$] [**2-1c**] but downfield of the singlet in [Ru(bipy)(Ph-dp)$_2$] [**2-2b**]. Finally, any signals that are slightly shifted only travel marginally downfield (i.e. to a higher chemical shift value) in a stepwise fashion from [Ru(bipy)(COOH-dp)$_2$] [**2-1c**] to [Ru(bipy)(Ph-dp)$_2$] [**2-2b**] to [Ru(bipy)(Ph$_2$N-dp)$_2$] [**2-3b**], likely to be due to the tendency of electron donating groups (such as the diphenylamino functionality) to have a deshielding effect on neighbouring protons.

The same explanation may be provided for the magnitude of the change in relative chemical shift and the greater degree of movement for the diphenylamino-type complex compared to same protons in the other Dye Two group complexes as was provided for the Dye One group complexes. The magnitude of change in position is due to the sensitivity of the protons, whereby the most sensitive protons, (and therefore those expected to have larger relative shifts), are those protons that are closest to the nitrogen atom of the pyrrole ring. This is due to the metal ion being bonded to the nitrogen atoms, which causes the protons to be very much more sensitive to the metal ion than other protons. This is the reasoning behind why the movement for the pyrrolic protons is so much greater than for the phenyl protons in the dipyrrin, and also explains the huge jump for the two isomeric singlet pyrrolic peaks upon coordination in the intermediate complexes. A stepwise effect may also be observed, whereby the closer the positioning of the proton to the nitrogen atoms, the more sensitive and therefore the proportional change in relative chemical shift value. This is the case for the pyrrolic doublet protons.

## 3.2. UV-Visible Spectroscopic Analysis

UV-visible spectroscopy is the measurement of the quantity of photons absorbed by a substance as a function of wavelength in the ultraviolet and visible regions of the electromagnetic spectrum. The absorption of light in the ultraviolet and visible ranges:

10-400 nm and 380-760 nm respectively. UV-visible spectroscopy is a useful technique for quantitatively determining how strongly a chemical substance absorbs light at a given wavelength, particularly coloured solutions such as conjugated compounds or solutions of transition metal ions. The molar absorptivity (ε, L $mol^{-1}$ $cm^{-1}$) is calculated from the Beer-Lambert Law given by $A = \varepsilon c l$ (Equation 3.1): where A is the measured absorbance, *l* is the pathlength through the sample (cm), and c is the concentration of the absorbing substance ($molL^{-1}$).

The electronic transitions that chemical molecules undergo may be recognized from the shapes and positions of the bands that are observed in the spectra acquired from UV-visible spectroscopy, thereby providing information on the structure of the chemical substance under scrutiny.

The strength of light absorption was investigated for each complex using UV-visible spectroscopy. Solutions of known, precise concentration were prepared, and a small sample of each used to fill a 1 mm pathlength quartz cell. The quartz cell was placed in a UV-visible spectrometer (equipment details are provided in Chapter 5) the absorbance recorded over the range 300-900 nm, and then the molar absorptivity for each complex was calculated. The traces recorded are accredited solely to the absorbance of each complex because the spectra were baseline corrected, that is both the baseline and solvent spectrum were automatically subtracted by the spectrometer. All molar absorptivity values were calculated from the Beer-Lambert Law described earlier, and are referred to on the spectra in this thesis as the absorbance coefficient. Assignments were made on the basis of the well-documented optical transitions in $[Ru(bipy)_3]^{2+}$.

The purpose of the UV-visible spectroscopic analysis in this thesis is to determine what types of electronic transitions are occurring within the dye complexes, and to test the strength and span of absorption across the UV-visible region of the electromagnetic spectrum; and then to use this information to help ascertain whether the complexes would be suitable as dyes in DSSCs.

### 3.2.1. Dye One Group Complexes

Figure 3.7 (next page) illustrates the UV-visible spectra recorded for each of the Dye One group complexes.

Two distinct absorption bands are observed in the visible region of the UV-visible spectra for each Dye One group complex which may be likened to the Soret-band (around 400 nm) and Q-band (around 525 nm) that are characteristic of porphyrin UV-visible absorbance spectra[30]. The energy maxima for the absorption bands for each Dye One group complex occur at the same wavelength (± 1-3 nm) and the bandwidths and shapes of these absorption bands are also nearly identical. There is some variation in the molar absorptivity, which is to be expected due to the difference in electron donating properties of each of the three functionalities.

There is a broad peak centred at a wavelength of 525 nm. This peak originates from the transfer of charge occurring between the Ru(II) metal centre and the bipyridine ligand: a metal-to-ligand charge-transfer, or an MLCT transition. The MLCT transition is the transition that occurs between the highest occupied molecular orbital (HOMO) and the lowest unoccupied molecular orbital (LUMO) in the complex. The HOMO and LUMO consist of the d-orbitals of the ruthenium and the π* orbital of the ligand, respectively. The HOMO level is shifted negatively by the bipyridine ligand which leads to a red shift i.e. a shift to a lower energy in the absorption spectrum of the complex. This red shifting of the absorption is advantageous because this also contributes electron acceptance from reduced redox iodide ions ($I^-$) from the electrolyte HTM in the course of DSSC operation. Similar shifts are seen in analogous halide and oxalate complexes[31] and can be rationalized on the basis of anionic, weakly $\pi$-accepting ligands raising the energies of the Ru(II) d orbitals. These are known as a d$\pi$-$\pi$* transition. The MLCT transition in the Dye One group complexes is also red-shifted with respect to the wavelength of the same transition in the well-documented complex $[Ru(bipy)_3]^{2+}$ (MLCT of $[Ru(bipy)_3]^{2+}$ occurs at 443 nm[32].

There is an intense, narrow, higher energy peak centred at *ca.* 460 nm which can be assigned to a $S_o \rightarrow S_1$ ($\pi$-$\pi$*) transition of the dipyrrin ligand. As the bandwidth and

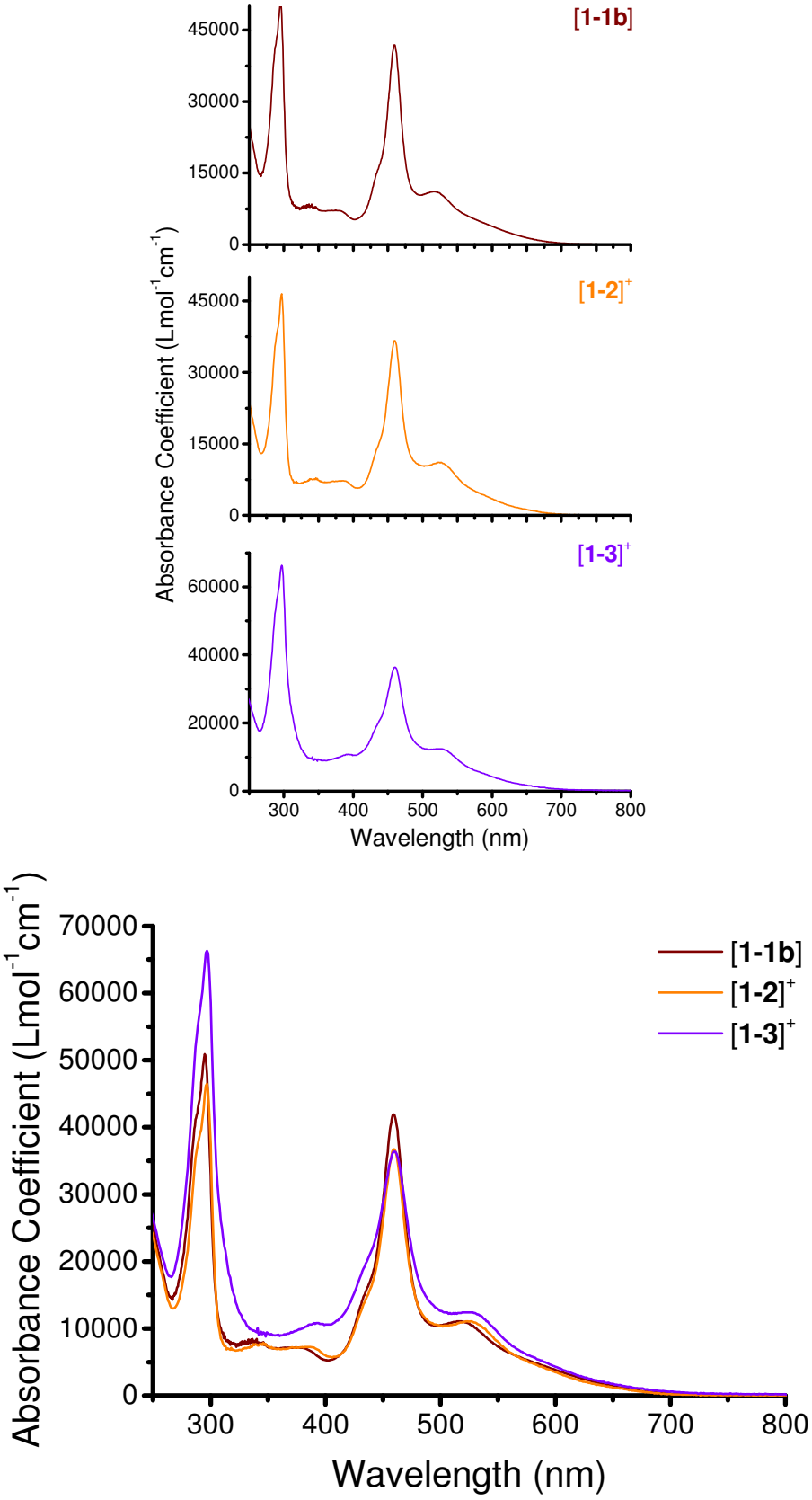


**Figure 3.7** UV-visible absorption spectra for the Dye One group complexes.

position of the peak is not altered by the variation of the dipyrrinato functionality we may presume that it is relatively insensitive to the identity of the coligands (and probably also the identity of the metal centre) and therefore is an intraligand transition i.e. it takes place internally within the dipyrrin. Both the relatively narrow bandwidth and the position of this peak are diagnostic of this type of transition.

There are also two bands displayed in the higher energy UV region of the absorbance spectra for the Dye One group complexes. A second broad band appears at 346 nm and a second sharp peak at 297 nm. The broad band is less obvious than the analogous peak in the visible region, while the sharper peak has a slightly higher intensity than its analogous visible region band. It is not possible to assign these bands to a particular transition, but it is believed that the latter peak ($\lambda_{max}$ = 297 nm) is attributable to the dipyrrin, as it appears in the absorbance spectra for the free-base dipyrrin ligands (not shown here) and is not documented for $[Ru(bipy)_3]^{2+}$.

Although the shapes and positions are the same, the intensity of the absorption bands differs slightly among the three Dye One group complexes. The intensities for the carboxylate-type complex $[Ru(bipy)_2(COO^-\text{-dp})]$ [**1-1b**] and phenyl-type complex $[Ru(bipy)_2(Ph\text{-dp})]^+$ [**1-2**]$^+$ are virtually the same, but the molar absorptivity for the diphenylamino-type complex $[Ru(bipy)_2(Ph_2N\text{-dp})]^+$ [**1-3**]$^+$ is noticeably greater. This is most like explainable once again by the superior predisposition of the diphenylamino group for electron donation.

The simple appearance of the absorption spectrum of the Dye One group complexes as the superposition of a $\pi$-$\pi^*$ dipyrrin transition and a separate d$\pi$-$\pi^*$ MLCT transition suggests that the two chromophores are largely uncoupled; that is, the orbitals involved in these transitions are distinct and located in different spatial regions of the complex.

### 3.2.2. Dye Two Group Complexes

Figure 3.8 (next page) illustrates the UV-visible spectra recorded for each of the Dye Two group complexes.

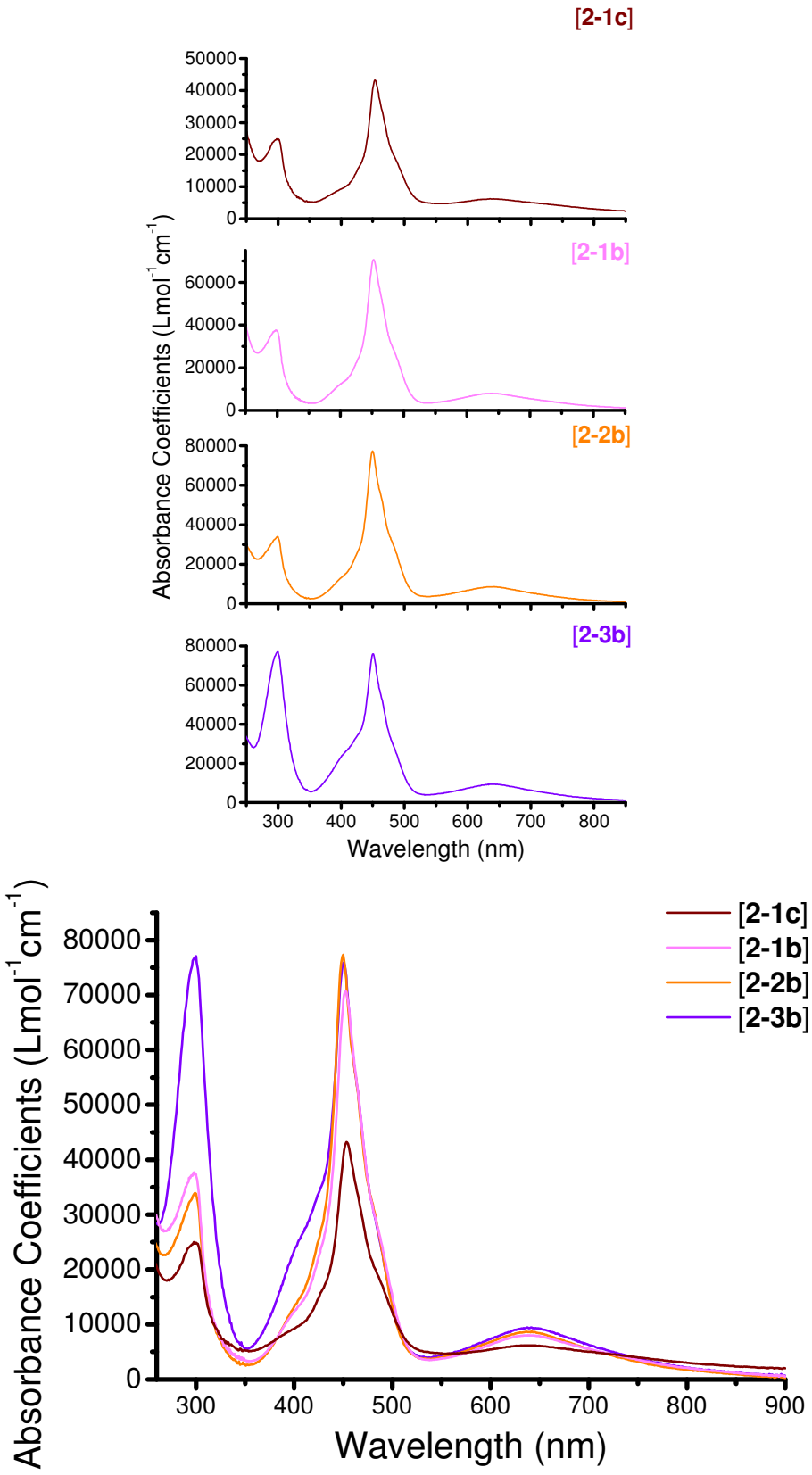


**Figure 3.8** UV-visible absorption spectra for the Dye Two group complexes.

There are several similarities between the absorption spectra for the Dye Two group complexes and the Dye One group complexes. Two distinct absorption bands are also observed in the visible region of the UV-visible spectra for each Dye Two group complexes which may again be likened to the Soret-band (around 400 nm) and Q-band (around 525 nm) that are characteristic of porphyrin UV-visible absorbance spectra[30]. The energy maxima for the absorption bands for each Dye Two group complex also occur at the same wavelength (margin is slightly larger at ± 2-4 nm) and the bandwidths and shapes of these absorption bands are also nearly identical. There is very little variation in the molar absorptivity for the Dye Two group complexes despite differences in the electron donating properties of each of the three functionalities. The exception to this is the carboxylic acid-type complex which has a molar absorptivity half that of the rest of the Dye Two group complexes, but this is thought to be due to solubility issues that are encountered with the compound despite re-recording the spectra in a range of different solvents.

The lowest energy visible region peak is again very broad but with the energy maxima centred at a longer wavelength of *ca.* 635 nm. The origin of this peak is the same as in the Dye One group complexes: from an MLCT transition, which arises from the transfer of charge occurring between the Ru(II) metal centre and the bipyridine ligand. This transition is also red-shifted with respect to $[Ru(bipy)_3]^{2+}$ (MLCT of $[Ru(bipy)_3]^{2+}$ occurs at 443 nm)[32] and, like the Dye One group complexes, can be rationalized on the basis of anionic, weakly $\pi$-accepting ligands raising the energies of the Ru(II) d orbitals, known as a d$\pi$-$\pi^*$ transition.

The higher energy visible region peak is also an intense narrow band, but is centred at a wavelength of *ca.* 450 nm – slightly blue-shifted with respect to its Dye One counterpart. This band can again be assigned to a $S_o \rightarrow S_1$ ($\pi$-$\pi^*$) transition of the dipyrrin ligand. We may again presume that the peak is relatively insensitive to the identity of the coligands (and probably also the identity of the metal centre) and therefore is an intraligand transition i.e. it takes place internally within the dipyrrin because the bandwidth and position of the peak is not altered by the variation of the dipyrrinato functionality. As mentioned for the Dye One group complexes both the relatively narrow bandwidth and the position of this peak are diagnostic of this type of transition.

There is only one band displayed in the higher energy ultraviolet region of the absorbance spectra for the Dye Two group complexes at *ca.* 300 nm – the same wavelength as the Dye One group complexes. However there is considerable variation in the molar absorptivity values for this particular peak. For the ester, carboxylic acid and phenyl-type complexes ([Ru(bipy)(COOMe-dp)$_2$] [**2-1b**], [Ru(bipy)(COO$^-$-dp)$_2$] [**2-1c**], and [Ru(bipy)$_2$(Ph-dp)] [**2-2b**] respectively) the height of the peak in the UV region is less than that in the visible region, where the difference is substantially larger in the case of the ester and phenyl-type complexes. For the diphenylamino-type complex [Ru(bipy)$_2$(Ph$_2$N-dp)] [**2-3b**] a "mirror effect" is seen in that both the values for the molar absorptivity for the UV and visible region dipyrrinato peaks are nearly indistinguishable. In contrast, the broader peak observed at *ca.* 346 nm in the spectra for the Dye One group complexes appears non-existent in the spectra for the Dye Two group complexes. This is most likely because the molar absorptivity values for the Dye Two group complexes are comparatively lower than those for the Dye One group complexes. Like for the Dye One group complexes it is not possible to assign these bands to a particular transition, but it is again believed that the peak with $\lambda_{max}$ centred at 297 nm is attributable to the dipyrrin, for the same reasons already mentioned in 3.2.1.

The simple appearance of the absorption spectrum of the Dye Two group complexes as the superposition of a $\pi$-$\pi^*$ dipyrrin transition and a separate d$\pi$-$\pi^*$ MLCT transition suggests that the two chromophores are largely uncoupled; that is, the orbitals involved in these transitions are distinct and located in different spatial regions of the complex.

### 3.2.3. Cross-Examination of the Dye Group Complexes

Table 3.1 summarises the energy maxima and absorption coefficients for the two assigned bands (those appearing in the visible region) in each of the UV-visible spectra.

| | $\lambda_{max}$ ($\varepsilon$ x$10^4$) | |
|---|---|---|
| **Complex** | **dp** | **MLCT** |
| Dye One Group Complexes: | | |
| **[1-1b]** | 459 (4.19) | 516 (1.11) |
| **[1-2]$^+$** | 460 (3.67) | 525 (1.10) |
| **[1-3]$^+$** | 460 (3.64) | 524 (1.24) |
| Dye Two Group Complexes: | | |
| **[2-1b]** | 454 (4.32) | 635 (6.21 x$10^3$) |
| **[2-1c]** | 453 (7.07) | 638 (8.05 x$10^3$) |
| **[2-2b]** | 450 (7.73) | 642 (8.72 x$10^3$) |
| **[2-3b]** | 451 (7.59) | 641 (9.47 x$10^3$) |
| Dye Four Group Complexes: | | |
| **[4-1b]** | 451 | 640 |

**Table 3.1** Energy maxima and absorbance coefficients for key complexes ($\lambda_{max}$ stated in nm and $\varepsilon$ (in brackets) stated in Lmol-1 cm$^{-1}$).

It is clear from comparing the values in Table 3.1 that the MLCT absorption band is progressively red shifted in going from $[Ru(bipy)_3]^{2+}$ to the Dye One group complexes to the Dye Two group complexes, where the energy maximum occurs for the Dye One group complexes at *ca.* 525 nm compared with *ca.* 640 nm for the Dye Two group complexes. In contrast, as the ratio of bipyridine to dipyrrin ligands is inverted (from 2:1 to 1:2) the wavelength of the band assigned to the intraligand dipyrrin ($\pi$-$\pi$*) transition remains unchanged. Interestingly it is also apparent from Table 3.1 that substituting the bipyridine ligand for a carboxylic acid derivative of the same ligand (as is the case in the Dye Four group complex $[Ru(dcbipy)(Ph\text{-}dp)_2]$ [**4-1b**]) does not have any effect on either transition.

White light such as sunlight is composed of a broad range of wavelengths encompassing the ultraviolet, visible and infrared regions of the electromagnetic spectrum. When white light passes through a coloured substance a fraction of the light is reflected while the remaining wavelengths are absorbed. It is the diametrically opposite colour to the reflected wavelength that is perceived by the naked eye. This relationship is illustrated by the colour wheel shown in Figure 3.9.

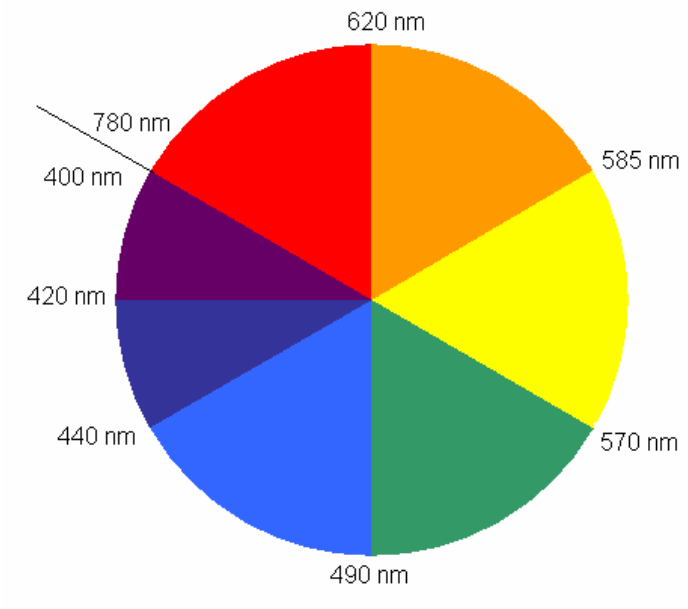


**Figure 3.9** Colour wheel illustrating the relationship between perceived colour and the wavelength that is actually reflected.

Figure 3.10 is a photograph of samples of each of the key complexes synthesised in this research project, both as solid samples and in solution. All solutions were made up with dry, analytical dichloromethane, with the exception of $[Ru(bipy)_2(COO^-\text{-}dp)]$ [**1-1c**] which was made up with analytical dimethylsulphoxide. On the basis of the theory outlined above for the division of white light and the values stated in Table 3.1 for the visible region of each spectra (i.e. the values for $dp_2$ and $MLCT_2$) the colours observed in Figure 3.10 can be rationalised.

**Figure 3.10** Samples of each of the key Dye One (left) and Dye Two (right) complexes both as solid samples (front) and in solution (back).

It is notable that the Dye One complexes are a different colour in solution to the colour they appear as in solid form. The Dye Two group complexes do not possess this characteristic. The free-base diphenylamino-type dipyrrin $Ph_2N$-dp is solvatochromic (i.e. is different colours in different solvents), appearing purple in methanol but intensely yellow in acetone; however upon coordination to the Ru(II) metal centre loses this characteristic.

The absorption bands observed in the visible region for the Dye Two complexes all appear at ~460 and ~520 nm The fact that not just one but two energy maxima are characteristic of the Dye One group complexes can be simplified by applying elementary wave theory from any first year physics course, which dictates that two individual waves occurring concurrently are accumulative. Application of this fundamental theory results in a combined wavelength of ~490 nm. The absorption of light at this wavelength renders a substance a red-orange colour. This is consistent with the colour displayed by each of the Dye One group complex solutions.

The absorption bands observed in the visible region for the Dye One complexes all appear at ~450 and ~640 nm The fact that not just one but two energy maxima are characteristic of the Dye Two group complexes can be simplified by applying elementary wave theory from any first year physics course which dictates that two individual waves occurring concurrently are accumulative. Application of this fundamental theory results in a combined wavelength of ~545 nm. The absorption of light at this wavelength renders a substance a deep red colour. However, from Figure 3.10 this is clearly not the colour that is being reflected. In examining the wavelength of each individual transition it is noted that the absorption of light of a range of wavelengths that encompasses the series of MLCT transition around 640 nm renders a substance green in colour. This is consistent with the colour displayed by each of the Dye Two group complex solutions. It may be deduced from this observation that although not reflected in the molar absorptivity data, the MLCT absorption is significantly stronger than the dipyrrin absorption, thus giving rise to the unexpected colour in solution. This is advantageous for application to DSSCs as this positioning is closer to the bipyridine ligands, which in the Dye Three and Dye Four group complexes is the site closest to the $TiO_2$ layer, and therefore would aid electron injection. Aside from this fascinating phenomenon, further interest is added to the Dye Two in that green Ru(II) complexes are not common.

## 3.3. Resonance Raman Spectroscopic Analysis

When light interacts with a material the photons which comprise the light may be absorbed, scattered, or pass straight through the material without interacting with it. Raman Spectroscopy is a technique for which information about the vibrations of molecules within a chemical substance is collected from scattered photons, thereby providing structural information about the chemical substance[33].

Intense Raman scattering occurs from vibrations which cause the electron cloud around a molecule to become polarized. If only the electron cloud polarization is involved in the scattering, then the dominant process of elastic scattering will occur, called Rayleigh scattering. Rayleigh scattering is the dominant process because most photons scatter that way. However if nuclear motion is induced then the process is inelastic, resulting in the energy of the scattered photon differing by one vibrational unit from the incident photon. This is Raman scattering (both Stokes $h(\upsilon_o-\upsilon_{ex})$ and anti-Stokes $h(\upsilon_o+\upsilon_{ex})$ scattering). Raman spectroscopy may be likened to infrared absorption (which is also a vibrational spectroscopy technique) except that usually symmetric vibrations give the greatest Raman scattering whereas the most intense absorptions in infrared spectroscopy are due to asymmetric vibrations. The two techniques are in fact complimentary and are often employed in unison[33].

Resonance Raman spectroscopy is a specialised branch of Raman spectroscopy in which electronic information in addition to vibrational information may be collected from a sample. It is a useful technique for assigning electronic transitions as vibrational modes of chromophores that resonate at the Raman excitation wavelengths which are selectively enhanced. Most often employed for the analysis of coloured compounds, resonance Raman is growing in popularity due to its ability to give extremely informative *in situ* analysis for particular species, including porphyrins[33]. In some cases resonance effects may even be exploited to selectively observe a particular scatterer in a complex matrix[34]. The process for which to obtain resonance Raman scattering is much the same as that for conventional Raman scattering. That is, a laser beam with an excitation frequency close to that of the electronic transition of interest is directed at a sample, and then the energy changes required to cause nuclear motion are identified. Identification is achieved by using a single frequency of radiation to irradiate the sample and detecting the

radiation one vibrational energy unit different from the incident beam that is scattered from the sample. Absorption will, unavoidably, also occur and may cause photodegradation of the sample. Sample damage is often visible to the naked eye as a colour change or black spot, and may be determined analytically by comparing and contrasting molar absorptivity values[33].

Resonance Raman spectra were recorded at multiple excitation wavelengths for each complex of interest. The excitation wavelengths were chosen according to the positions that the peaks appeared in the UV-visible region, and were provided by lasers (equipment details are provided in Chapter 5). Multiple windows were recorded for some excitation wavelengths, and all windows at all wavelengths were calibrated using cyclohexane. Photon collection was achieved using a 180° backscattering geometry. Photodegradation was minimised by employing a spinner to ensure that any one fraction of the sample did not remain exposed to the laser bean for the whole period of analysis, and every sample was checked for photodegradation by monitoring the molar absorptivity values via UV-visible spectroscopy prior to, and immediately after, laser beam exposure. In the occurrence of any change in values (which would suggest sample damage) the samples were replaced by fresh ones.

In this thesis the purpose of the resonance Raman spectroscopic analysis is to confirm the peak assignments made in the UV-visible spectroscopic analysis and to support the reasoning that the complexes would be suitable as dyes in DSSCs.

### 3.3.1. Dye One Group Complexes

Resonance Raman experiments were conducted on solutions of complexes $[Ru(bipy)_2(COO^-\text{-dp})]$ [**1-1b**], $[Ru(bipy)_2(Ph\text{-dp})]^+$ [**1-2**]$^+$, and $[Ru(bipy)_2(Ph_2N\text{-dp})]^+$ [**1-3**]$^+$. Spectra were acquired at two or three excitation wavelengths corresponding to the bands in the visible region of the afore-mentioned absorption spectra (Chapter 3.2.1). Wavelengths of 458 and 488 nm correspond to the intense dipyrrin absorption at *ca.* 460 nm, whereas a wavelength of 514nm corresponds to the band at *ca.* 525 nm which is attributed to an MLCT. The resonance Raman spectra that are observed at these wavelengths for each of the Dye One group complexes are shown in Figure 3.11 (next page).

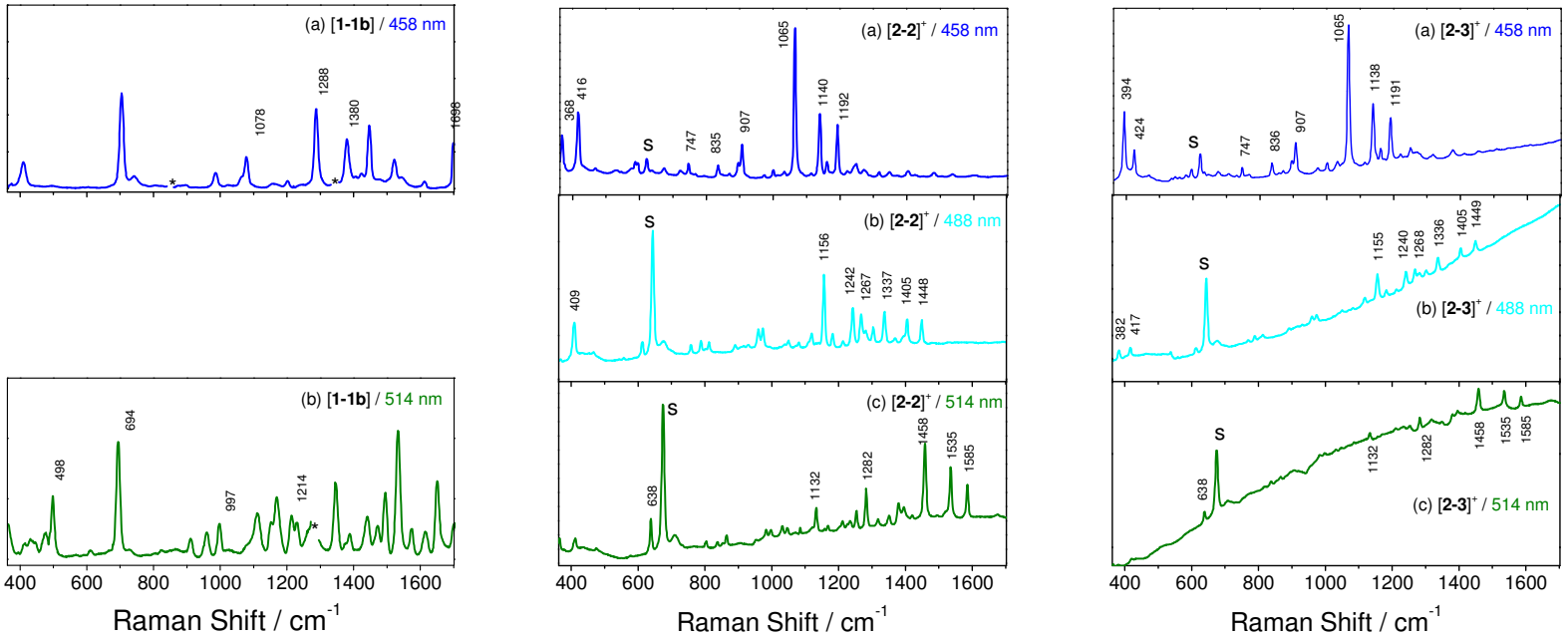


**Figure 3.11** Resonance Raman spectra of $[Ru(bipy)_2(COO^-\text{-}dp)]$ [**1-1b**] in methanol and $[Ru(bipy)_2(Ph\text{-}dp)]^+$ [**1-2**]$^+$ and $[Ru(bipy)_2(Ph_2N\text{-}dp)]^+$ [**1-3**]$^+$ in dichloromethane at stated excitation wavelengths. S denotes a solvent band, and asterisks denote where laser lines have been removed.

The observed Raman spectra from the excitation wavelengths of 458 and 488 nm, and 514 nm are distinctly different, and therefore must arise from dissimilar vibrational modes. Evidence that the longer excitation wavelength (514 nm) is indeed associated with vibrational modes of the Ru-bipy MLCT chromophores as was predicted, is provided by the qualitative similarity to the resonance Raman spectrum of $[Ru(bipy)_3]^{2+}$. Conversely, the shorter excitation wavelengths (458 and 488 nm) both result in resonant enhancement of dipyrrin vibrational modes. These observations confirm the origin of the two absorption bands and lend further weight to a localized, non-interacting depiction of the dipyrrin and MLCT chromophores as was outlined in Chapter 3.2.1. It is also unsurprising that the peak assignments and Raman shift values are nearly identical for each of the three dipyrrinato functional groups, due to the lack of differentiation between the absorption spectra for the three complexes.

### 3.3.2. Dye Two Group Complexes

Resonance Raman experiments were conducted on solutions of complexes $[Ru(bipy)(COOMe\text{-}dp)_2]$ [**2-1b**], $[Ru(bipy)(COOH\text{-}dp)_2]$ [**2-1c**], $[Ru(bipy)(Ph\text{-}dp)_2]$ [**2-2b**], and $[Ru(bipy)(Ph_2N\text{-}dp)_2]$ [**2-3b**]. Spectra were acquired at two or four excitation wavelengths corresponding to the bands in the visible region of the afore-mentioned absorption spectra (Chapter 3.2.2). Wavelengths of 458 and 488 nm correspond to the intense dipyrrin absorption at *ca.* 450 nm, whereas wavelengths of 514 and 633 nm correspond to the band at *ca.* 640 nm which is attributed to MLCT. The resonance Raman spectra that are observed at these wavelengths for each of the Dye Two group complexes are shown in Figure 3.12 (next page).

Remarkably different spectra were again observed for the excitation wavelengths of 458 and 488 nm versus those for the excitation wavelengths of 514 and 633 nm, and therefore must also arise from dissimilar vibrational modes.

The spectra arising from the two low energy excitation wavelengths (514 and 633 nm) both exhibit distinct parallels with the resonance Raman spectrum of $[Ru(bipy)_3]^{2+}$. This implies that the absorption band of the Dye Two group complexes at around 640 nm also involves a Ru(II)-to-bipy MLCT transition. Conversely, the shorter excitation wavelengths (458 and 488 nm) both result in resonant enhancement

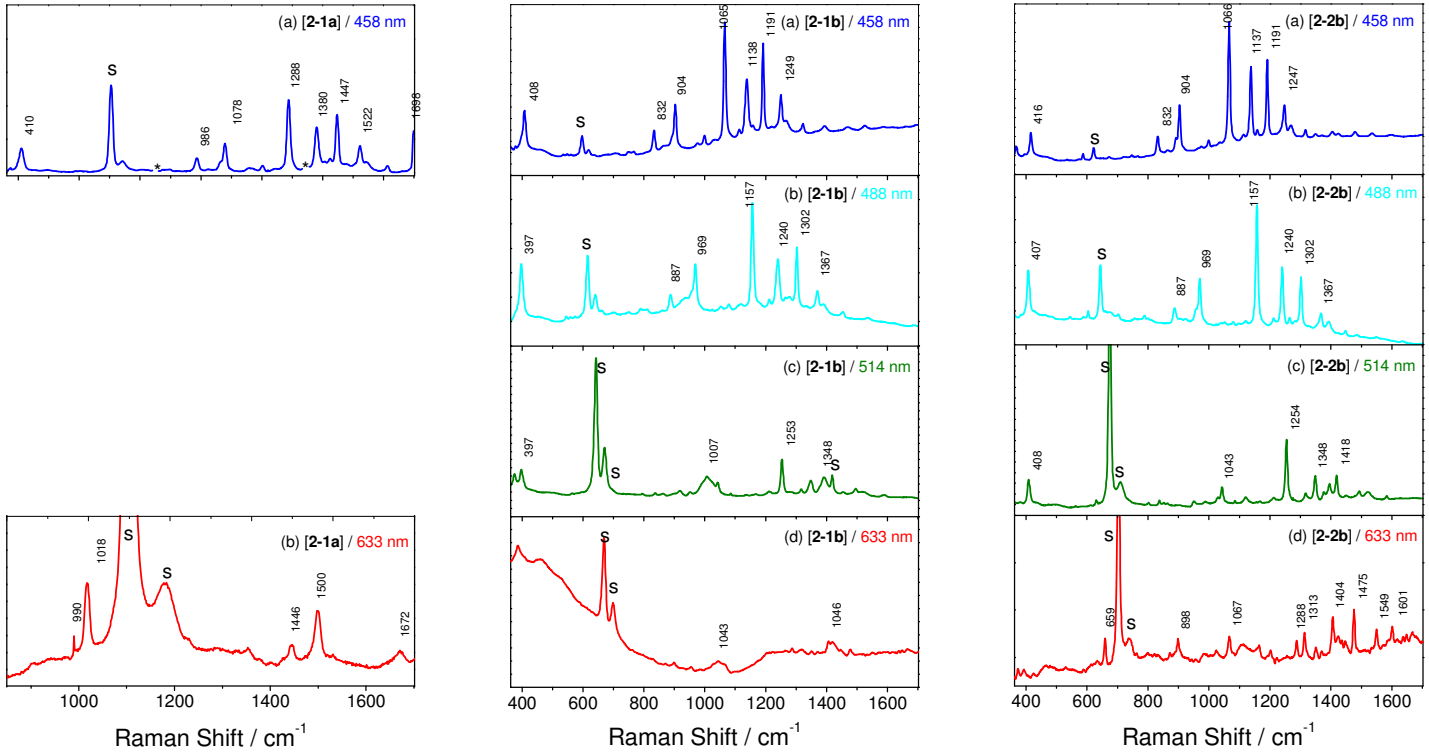


**Figure 3.12** Resonance Raman spectra of [Ru(bipy)(COOH-dp)$_2$] [**2-1c**] in dmso and [Ru(bipy)(COOMe-dp)$_2$] [**2-1b**], [Ru(bipy)(Ph-dp)$_2$] [**2-2b**], [Ru(bipy)(Ph$_2$N-dp)$_2$] [**2-3b**] and [Ru(dcbipy)(Ph-dp)$_2$] [**4-1b**] in dichloromethane at stated excitation wavelengths. S denotes a solvent band, and asterisks denote where laser lines have been removed.

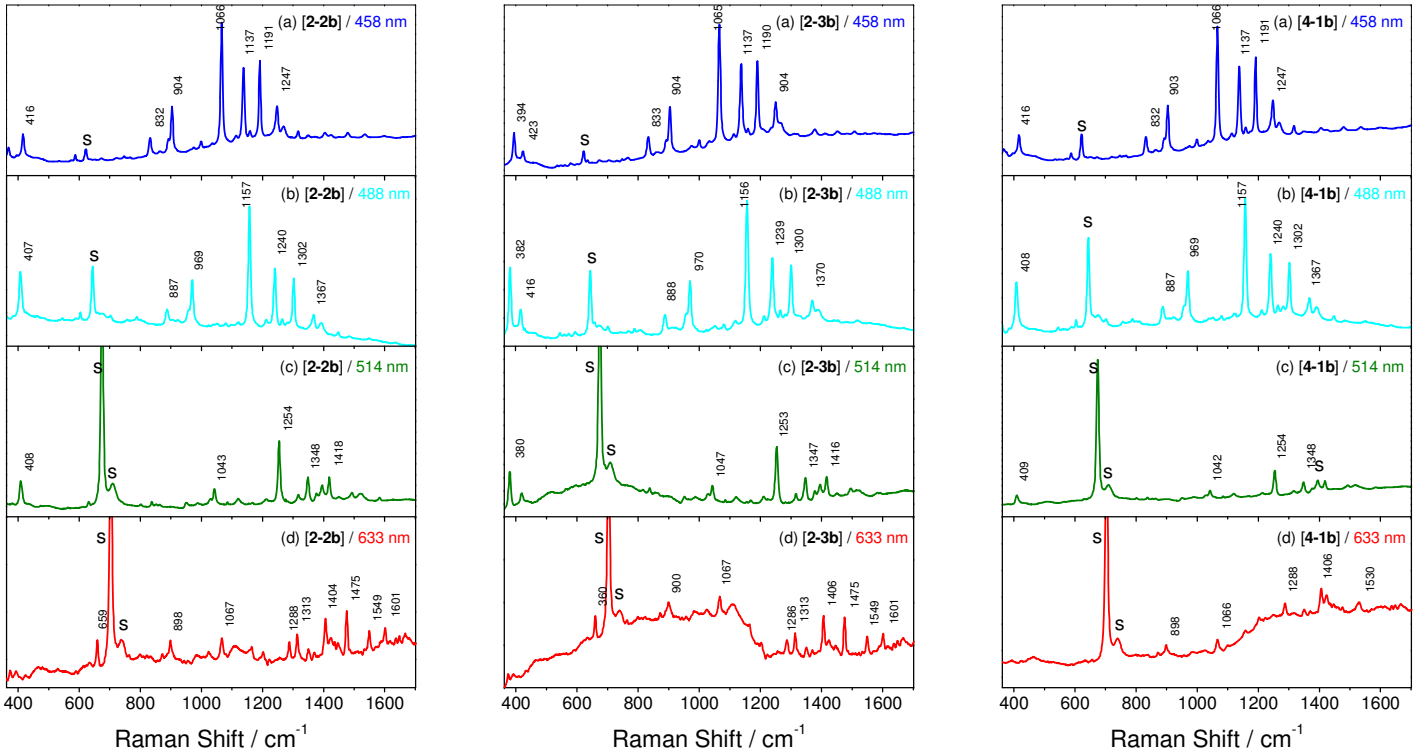


**Figure 3.12** Resonance Raman spectra of [Ru(bipy)(COOH-dp)$_2$] [**2-1c**] in dmso and [Ru(bipy)(COOMe-dp)$_2$] [**2-1b**], [Ru(bipy)(Ph-dp)$_2$] [**2-2b**], [Ru(bipy)(Ph$_2$N-dp)$_2$] [**2-3b**] and [Ru(dcbipy)(Ph-dp)$_2$] [**4-1b**] in dichloromethane at stated excitation wavelengths. S denotes a solvent band, and asterisks denote where laser lines have been removed.

of dipyrrin vibrational modes. Like the Dye One group complexes, these observations confirm the origin of the two absorption bands and imply that the dipyrrin and MLCT chromophores in the Dye Two group complexes are also localized and non-interacting as was outlined in Chapter 3.2.2. Also analogous to the Dye One group complexes, it is unsurprising that the peak assignments and Raman shift values are again nearly identical for each of the three dipyrrinato functional groups, due to the lack of differentiation between the absorption spectra for the three complexes.

The spectra of the Dye Two group complexes are nearly identical to those seen for the Dye One group complexes, strongly suggesting that the absorption bands around 480 and 488 nm and also around 514 and 633 nm for the each group of complexes originate from similar transitions, namely, dipyrrin $\pi$-$\pi^*$ and MLCT d- $\pi^*$ respectively.

Interestingly it is also apparent from Figure 3.12 that substituting the bipyridine ligand for a carboxylic acid derivative of the same ligand (as is the case in the Dye Four group complex [Ru(dcbipy)(Ph-dp)$_2$] [**4-1b**]) does not have any effect upon excitation into the low energy bands ($\lambda_{ex}$) 514 and 633 nm, or the high energy bands at ($\lambda_{ex}$) 458 and 488 nm. The positions and shapes of the peaks observed for [Ru(dcbipy)(Ph-dp)$_2$] [**4-1b**] are nearly identical to those observed for the Dye Two group complexes, and as they show the same distinct differentiation between the spectra for the high and low energy bands (excitation wavelengths), therefore must also arise from dissimilar vibrational modes as has been described for the Dye Two group complexes.

## 3.4. Electrochemistry Study

Electrochemistry is the study of chemical reactions which take place in a solution placed at the interface of an electrode (conducts electrons) such as a metal or semiconductor and an electrolyte (conducts free ions), and which involve the transfer of electrons between either the electrode and electrolyte, or between the electrode and chemical solution. Electrochemistry is often recorded in the form of a cyclic voltammogram, which is a trace produced from a plot of the current (A, amps) supplied at the working electrode against the applied voltage (V, volts). The cyclic voltammogram provides information on redox

processes, that is the processes of reduction (electron gain) and oxidation (electron loss). Reduction and oxidation occurs when an electron is transferred to or from a molecule or ion respectively, thus changing its oxidation state. For example $Ru^{2+}$ has an oxidation state of (II) (i.e. its valence shell has only six electrons, and needs a further two to make a full valence shell), and may be reduced to $Ru^{+}$ (ruthenium(I) - seven valence electrons) or oxidised to $Ru^{3+}$ (ruthenium(III) - five valence electrons).

Cyclic voltammograms were recorded for millimolar solutions of each of the complexes across the applied voltage range of -1.7 to 1.5 V vs. an Ag/AgCl reference electrode. Each wave in the voltammograms represents a reversible single-electron process and consists of both an oxidation and reduction component. Oxidation and reduction peaks were identified, and attributed to certain molecular entities and oxidation state transformations. Quantitative data was extracted from the cyclic voltammograms for the purpose of comparing the dye group complexes. Data is presented in two forms. Firstly as raw data, where values are expressed as peak potentials for the oxidation ($E_{ox(p)}$, V) and reduction ($E_{red(p)}$, V) component of each relative to both the silver reference electrode, and to ferrocence, which was used as the external standard in the electrochemical experiments using the equation $E_{red/ox(p)} = E_{complex(p)} - E_{ferrocene(p)}$ (Equation 3.2). And in processed form, where values are expressed as the half-wave potential ($E_{1/2(p)}$) for each wave. The half-wave potential is the midpoint between the oxidation and reduction components of each wave and is calculated using Equation 3.3.

$$E_{1/2(p)} = \frac{E_{ox(p)} + E_{red(p)}}{2} \qquad \textbf{Equation 3.3}$$

In this thesis the purpose of the electrochemical study is to determine if the complexes possess a suitably high redox potential to be able to be regenerated by the $I^-/I_3^-$ redox couple, therefore help ascertain if the complexes are suitable as dyes for DSSCs.

### 3.4.1. Dye One Group Complexes

Figure 3.13 (next page) illustrates the cyclic voltammograms for the Dye One group complexes, with the peak potentials listed in Table 3.2 and the $E_{1/2}$ values listed in Table 3.3 (following page).

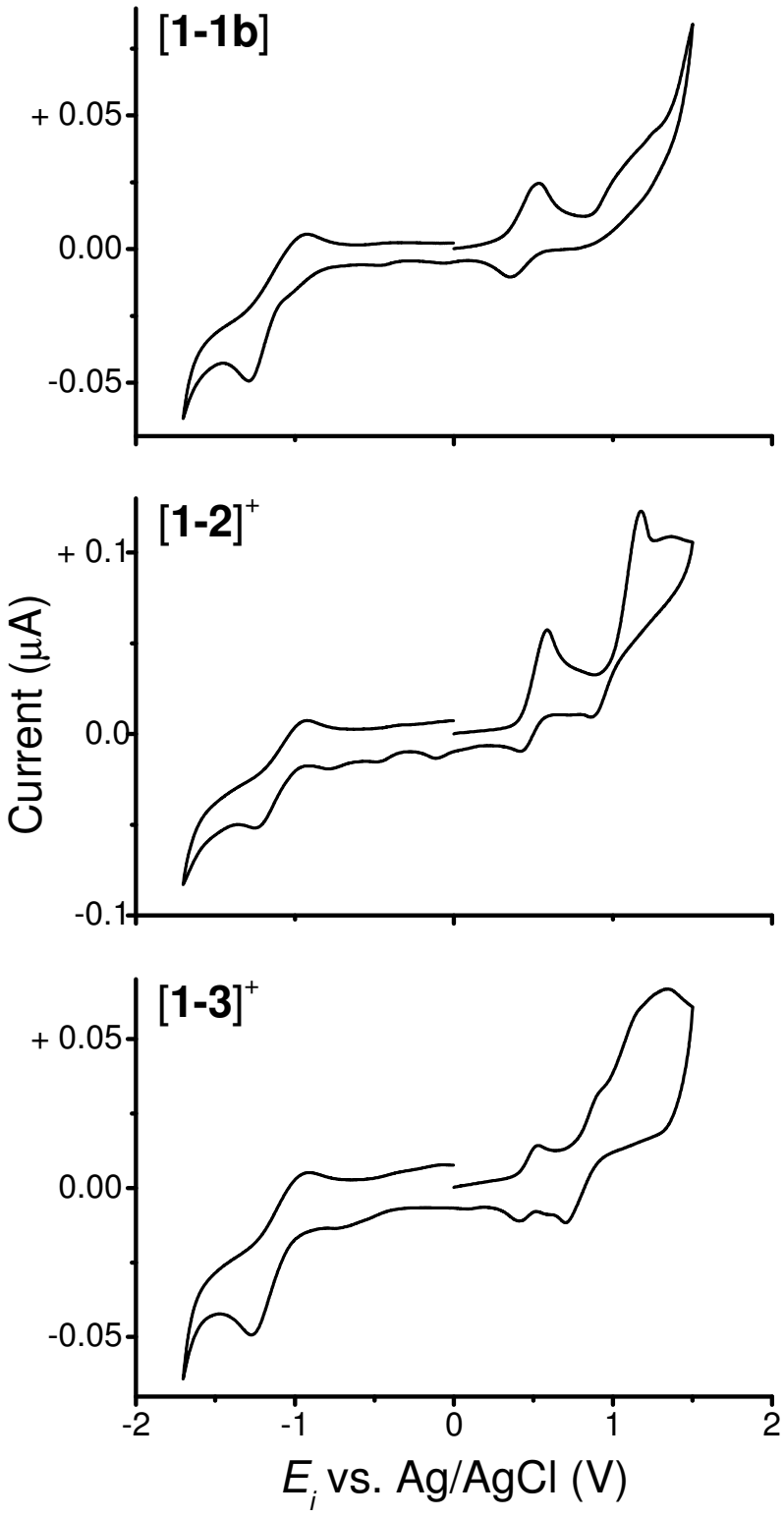


**Figure 3.13** Cyclic voltammograms for the Dye One group complexes

| | Peak Position $E_{i(p)}$ | | | | | |
|---|---|---|---|---|---|---|
| **Complex** | $E_{red(1)}$ | $E_{ox(1)}$ | $E_{red(2)}$ | $E_{ox(2)}$ | $E_{red(3)}$ | $E_{ox(3)}$ |
| $E_i$ vs Ag pseudo reference electrode: | | | | | | |
| **[1-1b]** | -1.29 | -0.93 | +0.35 | +0.53 | - | - |
| **[1-2]$^+$** | -1.25 | -0.93 | +0.42 | +0.59 | +0.87 | +1.18 |
| **[1-3]$^+$** | -1.27 | -0.92 | +0.41 | +0.53 | +0.70 | +0.91 |
| **Ferrocene** | -1.06 | - | +0.13 | +0.28 | - | - |
| $E_i$ vs Fc/Fc$^+$: | | | | | | |
| **[1-1b]** | -0.23 | - | +0.22 | +0.25 | - | - |
| **[1-2]$^+$** | -0.19 | - | +0.29 | +0.28 | - | - |
| **[1-3]$^+$** | -0.21 | - | +0.28 | +0.25 | - | - |

**Table 3.2** Peak potentials for the Dye One group complexes (stated in V).

All three of the Dye One group complexes display reversible or quasi-reversible oxidation and reduction processes. The reversible oxidation processes take place on the *d*-orbitals of the Ru(II) metal centre and are indicative of the processes occurring at the HOMO, whereas the reversible reduction processes take place on a ligand $\pi^*$-orbital and are indicative of the processes occurring at the LUMO. The lowest energy electronic transition is presumed to be the Ru(II)-bipyridine MLCT, and as the electrochemistry involves the same molecular orbitals (the HOMO and the LUMO) we can presume that all of the electrochemical peaks are attributable to the MLCT, and that it is the metal-centred redox processes that are observed in the cyclic voltammograms. The lowest energy electronic transition is presumed to be the MLCT, and as the electrochemistry involves the same molecular orbitals (the LUMO) we can presume that all of the electrochemical peaks are attributable to the MLCT, and that it is the metal-centred redox processes that are observed in the cyclic voltammograms. These presumptions are based on those reported in Xia et al[35]. The electrochemical peaks characteristic of the Ru(II)-bipyridine MLCT in the unexcited Dye One complexes are $E_{red(2)}$ and $E_{ox(2)}$. $E_{red(1)}$ and $E_{ox(1)}$ correlate to the addition of an electron to one of the ligands (most likely the dipyrrinato ligand, or more specifically the electron withdrawing functionality on the ligand), while $E_{red(3)}$ and $E_{ox(3)}$ correlate to the oxidation (loss of an electron) of the ruthenium metal centre ($Ru^{2+} \leftrightarrow Ru^{3+}$) MLCT. The assignments discussed here are based

on those reported in the literature[35] for mixed ligand polypyridine Ru(II) complexes, which display very similar characteristics to the Dye One complexes.

Two waves, and therefore two single-electron processes, are observed for $[Ru(bipy)_2(COO^-\text{-dp})]$ [**1-1b**], while $[Ru(bipy)_2(Ph\text{-dp})]^+$ [**1-2**]$^+$ and $[Ru(bipy)_2(Ph_2N\text{-dp})]^+$ [**1-3**]$^+$ exhibit a third. The greater electron withdrawing effect provided by the phenyl groups on the dipyrrin ligands in these complexes is the cause for the additional wave. In comparing solely the second wave values (as this is the only completely reversible single-electron oxidation process shown by the ferrocene redox couple) it is clear that all three of the Dye One complexes possess more positive peak potentials than ferrocene.

| Complex | $E_{1/2(1)}$ | $E_{1/2(2)}$ | $E_{1/2(3)}$ |
|---|---|---|---|
| **[1-1b]** | -1.11 | +0.44 | - |
| **[1-2]$^+$** | -1.09 | +0.51 | +1.03 |
| **[1-3]$^+$** | -1.10 | +0.47 | +0.81 |
| **Ferrocene** | | +0.21 | - |

**Table 3.3** Half-wave potentials for the Dye One group complexes (stated in V).

It is notable from the half-wave potentials ($E_{1/2(p)}$) that the phenyl-type complex $[Ru(bipy)_2(Ph\text{-dp})]^+$ [**1-2**]$^+$ is the most positive of the three Dye One complexes, followed by the diphenylamino-type complex $[Ru(bipy)_2(Ph_2N\text{-dp})]^+$ [**1-3**]$^+$. The more positive potentials were obtained for these complexes because the phenyl group(s) on the dipyrrinato ligand can stabilise the metal-centred Ru(II), and therefore make oxidation of the phenyl- and diphenylamino-type complexes more difficult. Not surprisingly, the $E_{1/2(p)}$ values are more than twice that for ferrocene. In stark contrast the $E_{1/2(p)}$ values for the Dye One complexes are significantly smaller than that stated in the literature for the well-documented complex $[Ru(bipy)_3]^{2+}$, which has an $E_{1/2}$ of 2.30 V[35]. This result is consistent with the red-shifted absorbance spectra displayed by the Dye One complexes with respect to $[Ru(bipy)_3]^{2+}$ (refer to Chapter 3.2.1), and therefore also the negative shifting of the HOMO by the bipyridine ligands.

It is also important to note that the size of the discrepancy between the half-wave potentials for the three complexes (i.e. $\Delta E_{1/2}$) increases substantially from wave to wave,

with the difference between the half-potentials for the first wave ($E_{1/2(1)}$) being the smallest. The cause for this change is again the electron-withdrawing effect provided by the phenyl groups on the dipyrrin ligands of the complexes, where the presence of electron-withdrawing groups lowers the potential for the first wave.

The combination of the results from Tables 3.2 and 3.3 and the features discussed above both from the individual peak potentials and from the half-wave potentials suggests that the Dye One group complexes are less easily reduced, and therefore have a higher LUMO than ferrocene, with the phenyl-type complex $[Ru(bipy)_2(Ph\text{-}dp)]^+$ [**1-2**]$^+$ having the highest LUMO. From this we may deduce that that the Dye One group complexes all have a sufficiently high redox potential, and therefore a suitably high energy LUMO for efficient charge injection into the $TiO_2$ conduction band in a DSSC to create a circuit, but also a HOMO low enough in energy to allow practically 100% regeneration of the dye complex from an electrolyte such as the $I^-/I_3^-$ redox couple used in most DSSCs following excitation to complete the circuit and to facilitate optimum energy transfer, with the phenyl-type complex $[Ru(bipy)_2(Ph\text{-}dp)]^+$ [**1-2**]$^+$ appearing to be the best to achieve this.

### 3.4.2. Dye Two Group Complexes

Figure 3.14 (next page) illustrates the cyclic voltammograms for the Dye Two group complexes, with the redox potentials listed in Table 3.4 and the $E_{1/2}$ values listed in Table 3.5.

All three of the Dye Two group complexes display reversible or quasi-reversible oxidation and reduction processes. The reversible oxidation processes take place on the *d*-orbitals of the Ru(II) metal centre and are indicative of the processes occurring at the HOMO, whereas the reversible reduction processes take place on a ligand $\pi^*$-orbital and are indicative of the processes occurring at the LUMO. The lowest energy electronic transition is presumed to be the Ru(II)-bipyridine MLCT, and as the electrochemistry involves the same molecular orbitals (the HOMO and the LUMO) we can presume that all of the electrochemical peaks are attributable to the MLCT, and that it

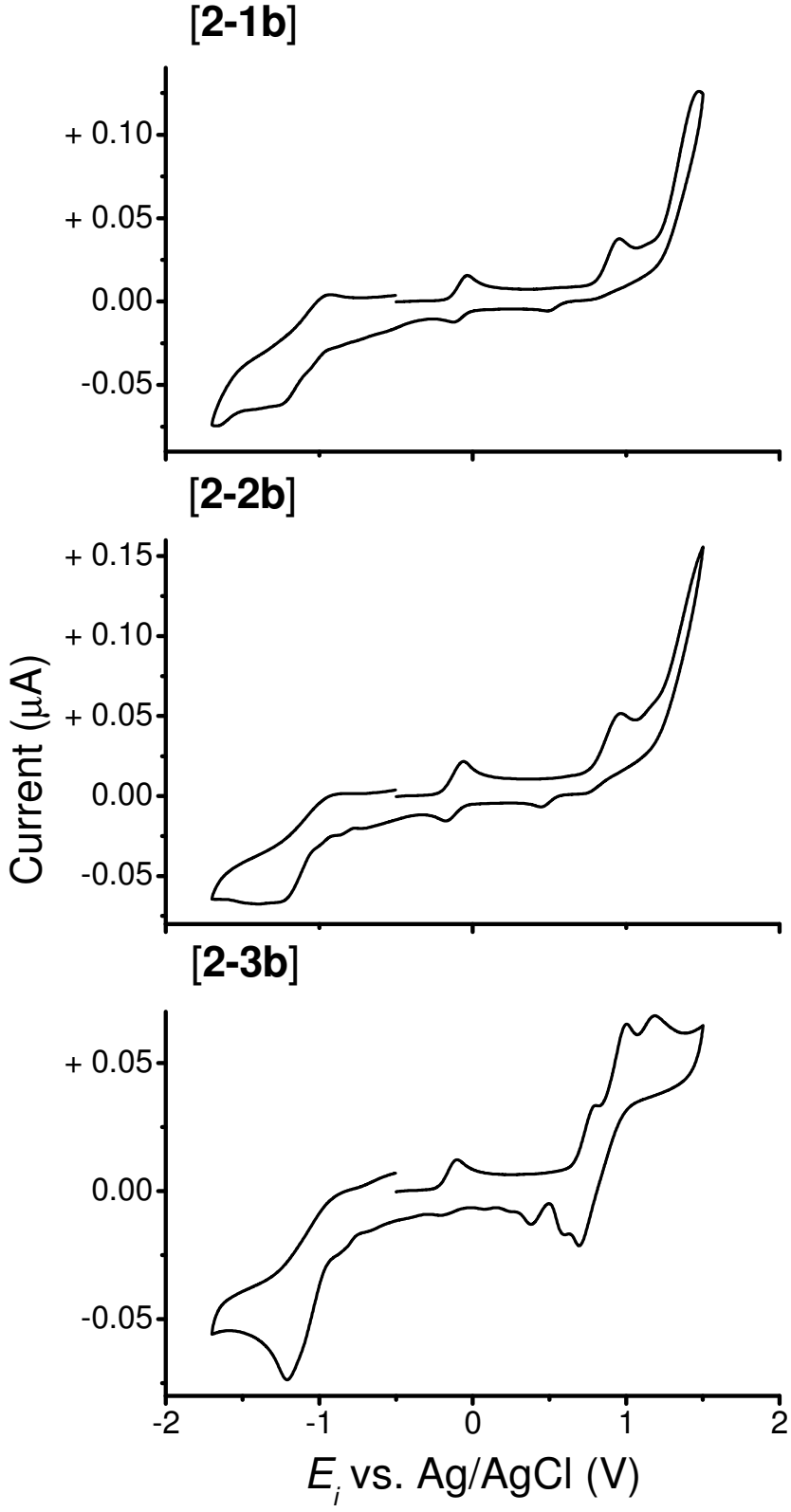


**Figure 3.14** Cyclic voltammograms for the Dye Two group complexes

is the metal-centred redox processes that are observed in the cyclic voltammograms. The lowest energy electronic transition is presumed to be the MLCT, and as the electrochemistry involves the same molecular orbitals (the LUMO) we can presume that all of the electrochemical peaks are attributable to the MLCT, and that it is the metal-centred redox processes that are observed in the cyclic voltammograms. These presumptions are based on those reported in Xia et al[35]. The electrochemical peaks characteristic of the Ru(II)-bipyridine MLCT in the unexcited Dye One complexes are $E_{red(2)}$ and $E_{ox(2)}$. $E_{red(1)}$ and $E_{ox(1)}$ correlate to the addition of an electron to one of the ligands (most likely the dipyrrinato ligand, or more specifically the electron withdrawing functionality on the ligand), while $E_{red(3)}$ and $E_{ox(3)}$ correlate to the oxidation (loss of an electron) of the ruthenium metal centre ($Ru^{2+} \leftrightarrow Ru^{3+}$) MLCT. The assignments discussed here are based on those reported in the literature[35] for mixed ligand polypyridine Ru(II) complexes, which display very similar characteristics to the Dye Two complexes.

| | **Peak Position $E_i$** | | | | | | | |
|---|---|---|---|---|---|---|---|---|
| **Complex** | $E_{red(1)}$ | $E_{ox(1)}$ | $E_{red(2)}$ | $E_{ox(2)}$ | $E_{red(3)}$ | $E_{ox(3)}$ | $E_{red(4)}$ | $E_{ox(4)}$ |
| $E_i$ vs Ag pseudo reference electrode: | | | | | | | | |
| **[2-1b]** | -1.25 | -0.93 | -0.13 | -0.04 | +0.49 | +0.95 | - | - |
| **[2-2b]** | - | - | -0.18 | +0.06 | +0.45 | +0.96 | - | - |
| **[2-3b]** | -1.21 | -0.10 | +0.38 | +0.80 | +0.60 | +1.00 | +0.70 | +1.19 |
| **Ferrocene** | -0.77 | - | +0.12 | +0.28 | - | - | - | - |
| $E_i$ vs $Fc/Fc^+$: | | | | | | | | |
| **[2-1b]** | -0.48 | - | -0.15 | -0.08 | - | - | - | - |
| **[2-2b]** | - | - | -0.10 | -0.06 | - | - | - | - |
| **[2-3b]** | -0.44 | - | +0.1 | +0.68 | - | - | - | - |

**Table 3.4** Peak potentials for the Dye Two group complexes (stated in V).

Three waves, and therefore three single-electron processes, are observed for [Ru(bipy)(COOMe-dp)$_2$] [**2-1b**], and [Ru(bipy)(Ph-dp)$_2$] [**2-2b**], while [Ru(bipy)(Ph$_2$N-dp)$_2$] [**2-3b**] exhibits a fourth. The greater electron withdrawing effect provided by the diphenylamino group on the dipyrrin ligand in the latter complex is the cause for the

additional wave. In comparing solely the second wave values (as this is the only completely reversible single-electron oxidation process shown by the ferrocene redox couple) it is clear that only the diphenylamino-type of the Dye Two complexes [Ru(bipy)($Ph_2$N-dp)$_2$] [**2-3b**] possesses more positive peak potentials than ferrocene.

| Complex | $E_{1/2(1)}$ | $E_{1/2(2)}$ | $E_{1/2(3)}$ |
|---|---|---|---|
| **[2-1b]** | -1.09 | +0.23 | - |
| **[2-2b]** | - | +0.26 | - |
| **[2-3b]** | -0.66 | +0.70 | +0.95 |
| **Ferrocene** | -0.39 | +0.06 | - |

**Table 3.5** Half-wave potentials for the Dye Two group complexes (stated in V).

It is notable from the half-wave potentials ($E_{1/2(p)}$) that the diphenylamino-type complex [Ru(bipy)($Ph_2$N-dp)$_2$] [**2-3b**] is the most positive of the three Dye Two complexes. The more positive potential was obtained for this complex because the diphenylamino group on the dipyrrinato ligand can stabilise the metal-centred Ru(II), and therefore makes oxidation of the diphenylamino-type complex [Ru(bipy)($Ph_2$N-dp)$_2$] [**2-3b**] more difficult. Not surprisingly, the $E_{1/2(p)}$ values for all the Dye Two complexes are greater than for ferrocene, with the $E_{1/2(p)}$ values for the ester- and phenyl-type complexes ([Ru(bipy)(COOMe-dp)$_2$] [**2-1b**] and [Ru(bipy)(Ph-dp)$_2$] [**2-2b**], respectively) four times greater than that for ferrocene and an astounding almost twelve times greater for the diphenylamino-type complex ([Ru(bipy)($Ph_2$N-dp)$_2$] [**2-3b**]). In stark contrast the $E_{1/2(p)}$ values for the Dye Two complexes are significantly smaller than that stated in the literature for the well-documented complex $[Ru(bipy)_3]^{2+}$, which has an $E_{1/2}$ of 2.30 V[35]. This result is consistent with the red-shifted absorbance spectra displayed by the Dye Two complexes with respect to $[Ru(bipy)_3]^{2+}$ (refer to Chapter 3.2.2), and therefore also the negative shifting of the HOMO by the bipyridine ligand.

It is also important to note that the size of the discrepancy between the half-wave potentials for the three complexes (i.e. $\Delta E_{1/2}$) increases substantially from wave to wave, with the difference between the half-potentials for the first wave ($E_{1/2(1)}$) being the smallest. The cause for this change is again the electron-withdrawing effect provided by

the phenyl groups on the dipyrrin ligands of the complexes, where the presence of electron-withdrawing groups lowers the potential for the first wave.

The combination of the results from Tables 3.3 and 3.4 and the features discussed above both from the individual peak potentials and from the half-wave potentials suggests that the Dye Two group complexes are less easily reduced, and therefore have a higher LUMO than ferrocene. This is analogous to the Dye One group complexes, except that for the Dye Two group complexes it is the diphenylamino-type complex [Ru(bipy)($Ph_2$N-dp)$_2$] [**2-3b**] that has the highest LUMO. From this we may deduce that that the only Dye Two group complex to have a sufficiently high redox potential, and therefore a suitably high energy LUMO for efficient charge injection into the $TiO_2$ conduction band in a DSSC to create a circuit, but also a HOMO low enough in energy to allow practically 100% regeneration of the dye complex from an electrolyte such as the $I^-/I_3^-$ redox couple used in most DSSCs following excitation to complete the circuit and to facilitate optimum energy transfer, is the diphenylamino-type complex [Ru(bipy)($Ph_2$N-dp)$_2$] [**2-3b**].

### 3.4.3. Cross-Examination of the Dye Group Complexes

It is notable that the reduction potentials for the Dye Two group complexes are all substantially higher than those for the Dye One group complexes with the same dipyrrin group. The higher redox potentials (ie. more positive) than ferrocene suggest that the dipyrrin ligands are creating metal centres indicative of a hard donor ligand environment. This is due to the stabilising effect that the dipyrrin ligands have upon the Ru(II) metal centre, where the Ru(II) oxidation state is strongly stabilized relative to soft donor NN ligands such as bipyridine[36] (e.g. the $E_{ox}$ for $[Ru(bipy)_3]^{2+}$ and $[Ru(phen)_3]^{2+}$ versus the reference electrode Ag/AgCl are 1.05 and 1.06 V respectively;[37] while the $E_{ox}$ for $[Ru(bipy)_3]^{2+}$ and $[Ru(phen)_3]^{2+}$ versus the ferrocence redox couple $Fc/Fc^+$ are 0.91 and 0.92 V respectively[37]). There is also a greater stabilising effect in the Dye Two group complexes that arises from the extra conjugation provided from having two dipyrrin ligands and one bipyridine, rather than one dipyrrin ligand and two bipyridines as in the Dye One group complexes. This additional stabilisation causes the Dye Two group complexes to be more difficult to oxidise than the Dye One group complexes and

therefore have more positive peak potentials and $E_{1/2}$ values particularly for the second wave ($E_{red(2)}$, $E_{ox(2)}$ and $E_{1/2(2)}$) i.e. $Ru^{2+} \leftrightarrow Ru^{3+}$.

Furthermore a trend exists where the complex containing the diphenylamino functional group (i.e. [Ru(bipy)($Ph_2$N-dp)$_2$] [**2-3b**]) possesses the highest reduction potential of the three dipyrrins. This trend was anticipated, and is believed to be due to two reasons. Firstly, the predisposition of the diphenylamino group towards electron donation was expected to boost the magnitude of the MLCT, and therefore lead to higher oxidation potentials. The fact that the diphenylamino-type Dye Two complex [Ru(bipy)($Ph_2$N-dp)$_2$] [**2-3b**] is three times higher than the other Dye Two complexes provides evidence for this. The second reason for the trend is the additional phenyl rings on the diphenylamino functionality giving rise to a boost in the stabilising effect the dipyrrin ligand has upon the Ru(II) metal centre.

We may surmise from the discussion and data given here that Dye Two group complexes would be better at promoting this process than the Dye One group complexes, with the diphenylamino-type Dye Two complex [Ru(bipy)($Ph_2$N-dp)$_2$] [**2-3b**] proving to be the best overall.

## 3.1. Potential for Dye-Sensitised Solar Cells

The intention when designing the target complexes for this research project was to ultimately use the complexes synthesised as dyes in DSSCs. Some preliminary experiments were carried out at the Nanomaterials Research Centre in the Institute of Fundamental Sciences (now the Institute of Fundamental Sciences MacDiarmid Centre) at Massey University in Palmerston North (New Zealand). The complexes [Ru(bipy)$_2$($COO^-$-dp)] [**1-1b**] and [Ru(dcbipy)(Ph-dp)$_2$] [**4-1b**] were adsorbed to pre-prepared $TiO_2$ plates, which were then placed into the open-cell photovoltaic circuit apparatus at the Centre and illuminated with the equivalent input current to that provided by the sun. Measurements were taken of the open-circuit voltage ($V_{oc}$, mV) and short-circuit current ($J_{sc}$, mA $cm^{-2}$) that were produced by the cell upon illumination, which were used to calculate the power ($P_{max}$, mW $cm^{-2}$) output (Equation 3.4), and subsequently the solar energy conversion efficiency ($\eta$%) (Equation 3.5) of each dye complex.

$$P_{max} = V_{oc} \times J_{sc}$$ **Equation 3.4**

$$\eta\% = \frac{P_{max}}{P_{source}}$$ **Equation 3.5**

A series of different conditions were tested for each dye complex in order to find the most effective combination of variables, including dissolution in different solvents before adsorption (ethanol, THF, ethanol/THF), the use of different electrolytes (E-Zn3(III), Eth1, G), and using a slightly different light source (A, B). Four separate plates were created and tested for each combination of variables, and an average efficiency recorded. Details of the series of conditions that were tested the DSSC experiments are provided in Chapter 5.1.8.

For the complex $[Ru(bipy)_2(COO^-\text{-}dp)]$ [**1-1b**] the optimum conditions were when the complex was dissolved in a mixture composed of 8% Ethanol/92% THF prior to adsorption to the $TiO_2$ plates, and when using Eth-1 as the electrolyte. When these particular conditions were employed a solar energy conversion of 0.356% was obtained. For the complex $[Ru(dcbipy)(Ph\text{-}dp)_2]$ [**4-1b**] the optimum conditions were when the complex was dissolved in 100% THF prior to adsorption to the $TiO_2$ plates, and hen using Zn3(III) as the electrolyte. When these particular conditions were employed a solar energy conversion of 0.110% was obtained.

It can be deduced from this data that both of these complexes hold promise as potential dyes in DSSC's simply because their solar cell conversion efficiencies are positive integers, i.e. $\eta > 0\%$. Further conclusions and discussion regarding these results is given in Chapter 4.2.1.

*Chapter 4*

# CONCLUSIONS AND FUTURE PERSPECTIVES

## 4.1. Conclusions

Prior to commencement of this research project it was planned to achieve three aims: to develop a series of dipyrrin complexes as dyes for DSSC's; to fully characterise these complexes and then to investigate the spectroscopic properties of each complex; and finally to ascertain the suitability of the complexes as dyes for DSSC's. In the course of this research project all three of those aims have been fully achieved.

The full set of Dye One group complexes have been shown to be easily synthesised using microwave irradiation, and have a well-defined purification procedure. This synthetic methodology has been shown to be applicable to three different dipyrrins, thus we can presume that it is a method that can be applied to synthesise the same complexes using dipyrrins with any functional group. The complexes have been fully characterised via the usual methods (summarised in Chapter 5 and discussed in Chapter 2). The complexes all conform to the set of attributes they must possess to be successfully used as dyes in DSSC's, evidence for which is provided in Chapter 3 from the electrochemical and spectroscopic data.

The full set of Dye Two group complexes has also been synthesised and fully characterised. The Dye Two group complexes have been shown to be synthesised using a straightforward two-step methodology, where an intermediate is formed from a conventional thermal reaction involving a dmso-ruthenium (II) building block and the dipyrrin ligand, and then the intermediate is reacted with molten bipyridine to give the desired complex. The purification of the Dye Two group complexes is also very well-defined. Like the Dye One group complexes, this synthetic methodology has been shown to be applicable to three different dipyrrins, thus we can presume that it is a method that can be applied to synthesise the same Dye Two group complexes using dipyrrins with any functional group. The complexes all conform to the set of attributes they must possess to

be successfully used as dyes in DSSC', evidence for which is also provided in Chapter 3 from the electrochemical and spectroscopic data.

The phenyl-type Dye Four group complex [Ru(dcbipy)(Ph-dp)$_2$] has been shown to be successfully synthesised by following a similar two-step methodology to the Dye Two group complexes. The first involves the formation of the very same intermediate complex as that formed for the phenyl-type Dye Two group complex [Ru(bipy)(Ph-dp)$_2$]. However, the subsequent molten reaction is carried out using an esterified bipyridine moiety which is later hydrolysed to give dicarboxybipyridine in the place of the bipyridine ligands. The carboxylic acid groups on the bipyridine ligands mean that a differing purification procedure must be carried out, but the precise process to achieve analytical purity was, regrettably, not fully resolved. This complex was characterised and investigated as much as possible within the limitations of impurity (i.e. $^{1}$H NMR, $^{13}$C NMR, ESI-MS, UV-vis and Raman were possible but not accurate, whereas elemental analysis and electrochemistry were not feasible).

The dipyrrin ligands that were used in the design of the series of target complexes for this thesis were chosen for their availability. Due to the functional groups on these dipyrrin ligands not all of the complexes have been able to contain a carboxylic acid group, necessary for anchorage to $TiO_2$. Those that do include a carboxylic acid moiety do hold the ability to the ability to bind strongly to $TiO_2$, which is the first in a list of attributes a compound must possess in order to be a good DSSC dye. Those without the carboxylic acid functional group conform to the list of attributes, with the ability to bind strongly to $TiO_2$ being the exception.

Regardless which set the complex belongs to, two distinct peaks are displayed in the visible region of the UV-visible spectrum: an intense narrow band attributed to a $S_o \rightarrow S_1$ ($\pi$-$\pi^*$) transition of the dipyrrin ligand, and a broader peak originating from a Ru(II)-to-bipy charge transfer (MLCT). The MLCT band is progressively red shifted in going from $[Ru(bipy)_3]^{2+}$ (found in the literature) to the Dye One group complexes to the Dye Two group complexes. All complexes have been shown to absorb strongly across the whole spectrum, particularly in the visible and near-IR regions, which is the second attribute that a compound must possess in order to be a good DSSC dye. It is assumed that because the

complexes strongly absorb artificial light characteristic of that produced by the sun, they will also strongly absorb solar radiation in a similar manner.

The Resonance Raman spectra were acquired at three excitation wavelengths corresponding to the two absorption bands in the UV-visible spectrum. The resulting Raman spectra are distinctly different. The longer wavelengths (54 and 633 nm) are associated with vibrational modes of the Ru-bipy MLCT chromophore, whereas the shorter wavelengths (458 and 488 nm) are associated with the dipyrrin vibrational modes. These assignments support those made for each of the peaks in the UV-visible spectra, and together (UV-visible and Resonance Raman collectively), suggest that the two chromophores are largely decoupled.

The electrochemistry has shown that all of the complexes are able to be oxidised (i.e. lose electrons) and then reduced (i.e. gain electrons). This is important because it indicates that they are all able to be regenerated by the $I^-/I_3^-$ redox couple: the volatile solvent solution electrolyte that has been proven to be the optimal HTM, and is found in most DSSCs. Therefore all complexes have been shown to possess a suitably high redox potential, which is the third attribute that a compound must possess in order to be a good DSSC dye.

As time did not permit the testing of the long-term stability of the complexes, it is not certain whether any or all of the complexes possess the fourth and final attribute of a good DSSC dye: the ability to be stable over many years of exposure to sunlight.

It was initially thought that the order of suitability of the sets of complexes as dyes for DSSCs would be: Dye Four > Dye Three > Dye Two > Dye One (where A > B means that A would be a better DSSC dye than B). It was also initially believed that within each set of complexes the suitability would very depending on the functional group on the dipyyrin ligand, where the order of suitability of the dipyrrin ligand would be: $Ph_2N$-dp > COOH-dp > Ph-dp (where, A > B means that A would be a better ligand than B, because A would result in a better DSSC dye than B). It is not possible to draw conclusions at this stage as to the order of suitability of the dye groups or the dipyrrinato functionalities as insufficient information has been collated to do this. It would be necessary to carry out DSSC testing on the full series of dye group complexes and the results evaluated before

conclusions may be drawn. However, based on the findings from the spectroscopic and electrochemical analysis discussed in Chapter 3 and which have been summarised further here in this Chapter, it is still supposed that the theories made at the outset of this research project regarding the order of suitability of each of the sets of complexes and the order of dipyrrin ligands within the series are correct, as there has been no result that has suggested otherwise.

## 4.2. Applications

There are three principal strategies that research into solar energy conversion follow: the direct conversion of light into electrical energy (i.e. photovoltaic devices), the production of biofuels from plants or waste agricultural by-products, and artificial photosynthesis[38]. The complexes discussed in this thesis have shown to be applicable to two of these principal strategies.

### 4.2.1. Dye-Sensitised Solar Cells

For the complex $[Ru(bipy)_2(COO^-\text{-}dp)]$ [**1-1b**] a preliminary solar energy conversion efficiency of 0.356% was obtained. A preliminary solar energy conversion efficiency of 0.110% was obtained for the complex $[Ru(dcbipy)(Ph\text{-}dp)_2]$ [**4-1b**].

It can be deduced from this data that both of these complexes hold promise as potential dyes in DSSC's simply because their solar cell conversion efficiencies are positive integers, i.e. $\eta > 0\%$.

Although it was expected that the complex $[Ru(dcbipy)(Ph\text{-}dp)_2]$ [**4-1b**] would have a superior solar energy conversion efficiency to complex $[Ru(bipy)_2(COO^-\text{-}dp)]$ [**1-1b**] due to the greater proportion of dipyrrin ligands to bipyridine ligands in conjunction with the positioning of the carboxylic acid group on the bipyridine instead of the dipyrrin ligand; this was not the case. However, it is necessary to note that, for reasons already discussed in previous Chapters, the sample used for the preliminary testing of complex $[Ru(dcbipy)(Ph\text{-}dp)_2]$ [**4-1b**] was not analytically pure. The large proportion of TnBA

hydroxide base that was still present in the [Ru(dcbipy)(Ph-dp)$_2$] [**4-1b**] sample at the time of testing would have prevented a significant proportion of the complex from binding to the $TiO_2$ plates, and therefore substantially decrease the conversion efficiency that may be produced.

Even though these conversion efficiencies are drastically lower than those published in the recent literature, it is necessary to take into consideration several crucial points before dismissing their potential as dyes for DSSCs. Firstly, the results published in the recent literature are those obtained from measurements made using a closed-cell apparatus. By using a closed-cell apparatus the amount of power from the source escaping from the sides of the cell is reduced, thus giving a more true indication of the ratio of power produced to that supplied by the source. Secondly, a very narrow range of experimental testing conditions were available and therefore trialled. A far more effective dissolution solvent and/or electrolyte may exist but was not employed, and so from this we must construe that the testing conditions are truly preliminary, and could be further optimised.

To get an idea of how truly comparable these dye complexes are to those published in the recent literature it would be necessary to acquire samples of Grätzels dyes (such as N3 or N719) and measure their solar energy conversion efficiencies using the same apparatus and conditions as those used for the aforementioned preliminary results. An even more accurate idea of the extent of comparability of the dyes to those published in the recent literature may be gained by sending samples to a Grätzel-accredited laboratory. It is hoped to send samples of [Ru(bipy)$_2$(COO$^-$-dp)] [**1-1b**] and [Ru(dcbipy)(Ph-dp)$_2$] [**4-1b**] to such a laboratory in Australia in the very near future.

### 4.2.2. Water Splitting

The focal reaction under study in artificial photosynthesis is the splitting of water. Through the process of photoexcitation and charge transfer, two half-cell reactions occur which either consume or generate electrons. Proton reduction and hydrogen evolution occurs at the electron acceptor, while water oxidation and oxygen evolution occurs at the electron donator (which accepts holes). Alternatively, water splitting can occur via a

thermally driven reaction which generates hydrogen, followed by a photolytic step that creates oxygen through decomposition of a hydrogen peroxide product.[38].

As ruthenium complexes have already been shown to successfully catalyse the water splitting process[39] it was hypothesised that the deprotonated form of the complex $[Ru(bipy)_2(COO^-\text{-}dp)]$ [**1-1b**] and the intermediate complex $[Ru(bipy)(COOMe\text{-}dp)_2]$ [**2-1b**] would be likely candidates to catalyse the photogeneration of $H_2$, and thus be successful in water splitting. Upon invitation samples of these complexes were sent to Dr Richard Eisenberg at the University of Rochester in New York (USA), who is a leading researcher in the field of water splitting. At the University of Rochester experiments were carried out by Dr Eisenberg's postdoctoral research student to test the aforementioned hypothesis. Details of the methodology of these experiments are provided in Appendix B.

Unfortunately, no $H_2$ was detectable after a set period of continuous irradiation, thus disproving the hypothesis that the particular complexes would be successful in splitting water. However, Eisenberg stated in his email accompanying the results that the negative outcome does raise some questions that will need to be addressed in further studies, and this area is ongoing.

## 4.3. Future Perspectives

Preliminary fluorescence measurements indicate that complexes [**1-1a**]$PF_6$, $[Ru(bipy)_2(COO^-\text{-}dp)]$ [**1-1b**], and $[Ru(bipy)(COOMe\text{-}dp)_2]$ [**2-1b**] exhibit either very weak or no fluorescence upon excitation into their dipyrrin absorption bands ($\lambda_{ex}$ = 460 nm). In the case of $[Ru(bipy)_2(COOMe\text{-}dp)_2]$ [**2-1b**], where the MLCT absorption band is energetically well separated from the dipyrrin band, excitation into the MLCT excited states also does not lead to any emission. As observed for related complexes, the excited states of these complexes may decay via low-lying ligand field states[40]. A full investigation of the emissive properties of these complexes, including any pH-dependent emission from $[Ru(bipy)_2(COO^-\text{-}dp)]$ [**1-1b**], is continuing.

Due to time limitations the Dye Three group complexes and the diphenylamino-type Dye Four group complex [Ru(dcbipy)($Ph_2N$-dp)$_2$]were not able to be successfully synthesised; and the phenyl-type Dye Four group complex [Ru(dcbipy)(Ph-dp)$_2$] was not able to be taken through to completion. Without theses complexes it is only possible to theorise the suitability of the full set of complexes as dyes for DSSC's. Further work regarding the methodology for the synthesis and purification of these missing compounds is required. Subsequently, DSSC testing upon these missing complexes may be undertaken, the results of which will either prove or disprove the conclusions drawn in this thesis.

To wholly complete the set and provide the full picture with regards to the characteristics of ruthenium (II) centred dipyrrin complexes, in addition to the target complexes specified in this thesis, a set of homoleptic Dye Five group complexes may be synthesised, consisting of three dipyrrin ligands. Although the phenyl- and diphenylamino-types of these Dye Five group complexes would not be able to be utilised as dyes for DSSC's due to the absence of any carboxylic acid groups on the ligands, the spectroscopic and electrochemical properties of such a group of complexes would be intriguing to study, particularly in comparison with those provided in this thesis. It is thought by the Author that these Dye Five group complexes would be straightforward to synthesise simply by reacting three equivalents of dipyrrin ligand with one equivalent of $RuCl_3 \bullet xH_20$ in a microwave synthesiser using the same sequence (30 minutes at 100°C) and solvent (ethylene glycol) as was used to successfully synthesise the Dye One group complexes. The Author believes that the crude product could be extracted into an organic solvent (dichloromethane) following the dilution of the ethylene glycol with excess water, and further purification could be achieved by employing similar procedures to those followed for the Dye One group complexes (column chromatography over lipophylic Sephadex and/or dry-packed deactivated neutral alumina).

It was also originally hoped that the series could be extended to include complexes coordinated to a range of metals including: ruthenium (II)/ruthenium (III), osmium (II)/osmium (III), and copper (I). Unfortunately, again due to time restrictions, all complexes synthesised in this research project were based only on ruthenium (II). This leaves a large, as yet untapped, collection of dipyrrin complexes which have the potential to act as suitable, possibly even competitive, DSSC dyes.

*Chapter 5*

# EXPERIMENTAL DETAILS

## 5.1. General Procedures

### 5.1.1. Solvents and Reagents

All solvents and reagents were purchased from standard chemical suppliers and were used without further purification unless stated. All syntheses were carried out with analytical grade solvents and reagents.

### 5.1.2. NMR Spectroscopy

$^{1}$H NMR and $^{13}$C NMR spectra were recorded on Bruker 500 MHz and 400 MHz spectrometers as stated. Chemical shift values are reported in parts per million (ppm). Samples were dissolved in the deuterated solvents as stated. Solvents were referenced as outlined in Table 5.1[41].

| | Reference (ppm) | |
|---|---|---|
| **Solvent** | **$^{1}$H NMR** | **$^{13}$C NMR** |
| $CD_3OD$ | 3.31 | 49.0 |
| $CDCl_3$ | 7.25 | 77.2 |
| $d^6$-Acetone | 2.05 | 29.8 |
| $d^6$-DMSO | 2.50 | 39.5 |

**Table 5.1** Solvent values used as reference points in NMR spectra.

### 5.1.3. Mass Spectroscopy

Mass spectra were recorded using a Micromass ZMD 400 electrospray mass spectrometer. Samples were dissolved in acetone or methanol, and where appropriate included 1% trifluroacetic acid or triethylamine.

### 5.1.4. Elemental Analyses

Microanalyses were carried out by Campbell Microanayltical Laboratory at the University of Otago in Dunedin, New Zealand.

### 5.1.5. UV/Visible Spectroscopy

UV/Visible spectroscopy was performed on a Varian Cary 1 UV/Visible spectrometer at room temperature. Quartz cells with a pathlength of 1 mm were used. For all samples the spectrometer was first zeroed and then a baseline was recorded while the spectrometer enclosed a solvent-only cell. The cell was emptied and rinsed with complex solution before filling with complex solution. The spectrum was recorded baseline correction mode so that the solvent and baseline were automatically subtracted from the complex spectrum.

### 5.1.6. Raman Spectroscopy

Continuous wave excitation was used for all Raman measurements. A ThorLabs HeNe laser provided 3-5 mW of 633 nm excitation at the sample. A Modu-Laser Stellar-Pro argon laser provided 6-8 mW of 514, 458, and 488 nm excitation at the sample. Raman and Rayleigh scattering light was collected from the sample cell using a 180° backscattering geometry. Rayleigh scattering was rejected using Raman edge filters from Iridian Technologies. The scattered photons were focussed onto the entrance slit (100 μm) of an Acton Spectra Pro® 2550i, 0.500 m imaging single stage monochromator/spectrograph and detected with a Roper Scientific Spec-10:100B CCD detector, controlled by WinSpec software. The detector was liquid nitrogen cooled to -110°C. Raman scattering was dispersed with a 1200 g/mm holographic diffraction grating. The entire Raman spectrum could not be collected in a single window. To obtain the entire spectrum the spectrograph position was moved in increments, ensuring good overlap with the previous window. A combination of cyclohexane and a 50/50 v/v mix of toluene and acetonitrile (ASTM E 1840 Raman Shift Standard) was used for the frequency calibration for each window. Frequency calibration was accurate to 0.5 $cm^{-1}$. Resolution ranged from 2 – 4 $cm^{-1}$ depending on spectral position.

### 5.1.7. Electrochemistry

Electrochemical measurements were performed using a computer controlled Autolab PGSTAT30 potentiostat and GPES software. Cyclic voltammograms were recorded at a scan rate of 100 $mVs^{-1}$ from 1 $mmolL^{-1}$ dry dichloromethane solutions using a glassy carbon working electrode, with platinum wire as the counter (auxiliary) electrode, and Ag/AgCl ($Ag/Ag^{+}$) in acetontrile as the reference electrode. 0.1 mol $NBut_4BF_4$ was added to each solution as the supporting electrolyte, and a 1 $mmolL^{-1}$ dry dichloromethane solution of Ferrocene was used as an external standard.

### 5.1.8. Solar Energy Conversion Efficiency Measurements

Preliminary experiments were carried out at the Nanomaterials Research Centre in the Institute of Fundamental Sciences (now the Institute of Fundamental Sciences MacDiarmid Centre) at Massey University in Palmerston North (New Zealand). Details of the series of conditions that were tested these preliminary DSSC experiments are outlined in Table 5.2.

| Variable | [1-1b] | [4-1b] |
|---|---|---|
| $TiO_2$ pre-treatment | 490℃ | 490℃ |
| Solvent | Ethanol, THF,Ethanol + 1% THF | THF |
| Concentration | 0.2 mM | 0.2 mM |
| Volume (number of plates) | 12 mL (4) | 12 mL (4) |
| Soaking Time | Overnight | Overnight |
| $TiO_2$ batch | STA (PJ) | STA (PJ) |
| $TiO_2$ area | 0.88 $cm^2$ | 0.88 $cm^2$ |
| Illumination intensity | 1.087 mA | 1.087 mA |
| Counter electrode | Platinum (solid) 1.3 x 1.2 mm | Platinum (solid) 1.3 x 1.2 mm |
| Electrolyte | E-Zn3 (III), Eth1, G | E-Zn3 (III), Eth1, G |

**Table 5.2** Details for the conditions employed in the preliminary DSSC tests.

## 5.2. Synthetic Details for Starting Materials

### 5.2.1. COOMe-dp

Synthetic route is illustrated by Scheme 2.1. Procedure and adaptation of that published by Rohand et al[19].

Methyl 4-formylbenzoate (8.02 g, 40 mmol) dissolved in minimum methanol was added dropwise to a stirring solution of freshly distilled pyrrole (11 mL, 159 mmol) in hydrochloric acid (400 mL). The mixture was stirred at room temperature for 4 hours. The precipitate was filtered and then washed with water and hexane before drying in a 40°C oven overnight. (Lavender-grey powder, 10.48 g, 77%)

A solution of COOMe-dpm (1.48 g, 5.31 mmol) in chloroform (35 mL) and acetone (13 mL) was cooled in an ice bath. A solution of DDQ (1.34 g, 5.92 mmol) in acetone (15 mL) was added dropwise with stirring, before the further addition of acetone (5 mL). The reaction mixture was stirred in an ice bath for 45 minutes, and then taken to dryness on a rotary evaporator. The resulting solid was suspended in a mixture of cold chloroform and dichloromethane, stirred at room temperature for 10 minutes then filtered off, washed thoroughly with chloroform, and dried under vacuum. Purification was achieved by dissolution in dichloromethane/triethylamine, adsorption onto deactivated alumina, then flash chromatography on deactivated alumina using dichloromethane as the eluent. The first yellow band was collected and the solvent removed to give a dark dichroic crystalline solid. Yield: 934 mg, 63%. (over two steps)). Spectroscopic data matched that previously published by Rohand et al[19]

### 5.2.2. Ph-dp

Synthetic route is illustrated by Scheme 5.1. Procedure is an adaptation of that published by Yu et al[42], where the only modification was the removal of the solvent tetrahydrofuran (THF) before extraction of the product in chloroform.

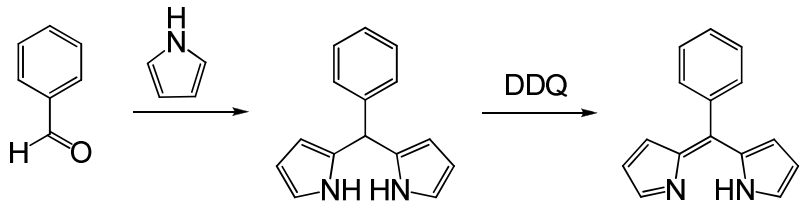


**Scheme 5.1** Synthesis of Ph-dp.

Benzaldehyde (5 mL, 4.92 mmol) was added dropwise to a stirring solution of freshly distilled pyrrole (14 mL, 197 mmol) in hydrochloric acid (175 mL). The mixture was stirred at room temperature for 1 hour. The product was extracted into dichloromethane and dried over magnesium sulphate. The solvent was removed on the rotary-evaporator and then dried on a vacuum pump. (Purple-black sludge, 17.7 g, 62%)

Ph-dpm (672 mg, 3.05 mmol) in was dissolved in THF (10 mL). A solution of DDQ (700 mg, 3.08 mmol) in THF (10 mL) was added dropwise with stirring. The reaction mixture was stirred at room temperature for 1 hour, and then poured into water. The THF was removed by rotary evaporation before the product was extracted with chloroform, dried over sodium sulphate and the solvent removed by rotary evaporattion. Purification was achieved by dissolution in methanol, adsorption onto silica, then flash chromatography on silica using chloroform initially, and then 99% chloroform/1% methanol as the eluent. A yellow band was collected and the solvent was removed. (Dichroic dark green-brown crystalline solid, 282 mg, 42% (over two steps)). Spectroscopic data matched that previously published by Yu et al[42]

### 5.2.3. $Ph_2N$-dp

Synthetic route is illustrated by Scheme 2.2.

A solution of dry dichloromethane (100 mL), freshly distilled pyrrole (50 mL, 704 mmol) and TFA (0.205 mL, 0.275 mmol) were dearated and flushed with argon. 4-diphenylaminobenzaldehyde (504 mg, 1.84 mmol) was dissolved in dry dichloromethane (10 mL) and added dropwise with stirring to the pyrrole solution. The mixture was stirred at room temperature under an inert atmosphere for 1 ½ hours. The reaction mixture was washed with 1 $MolL^{-1}$ aqueous potassium hydroxide before the dichloromethane was removed by rotary-evaporation. The resulting solution was dried over magnesium sulphate and the pyrrole removed by vacuum distillation. The residue was purified by dissolution in dichloromethane, then flash chromatography on deactivated neutral alumina using 60% dichloromethane/40%hexane as the eluent. The product was collected and the solvent was removed. (Black crystalline solid, 322 mg, 45%).

$Ph_2N$-dpm (714 mg, 1.84 mmol) was added dissolved in dry dichloromethane (50 mL). A solution of *p*-chloronil (632 mg, 2.58 mmol) dissolved in dry dichloromethane (5 mL) was added dropwise with stirring to the aldehyde solution, along with additional dichloromethane (5 mL). The mixture was stirred at room temperature under an inert atmosphere for 19 hours. The solution was then concentrated by rotary-evaporation and purified by column chromatography over deactivated neutral alumina, using 60% dichloromethane/40% hexane/0.1-0.2% methanol as the eluent. The product appeared as a purple band on the alumina column, but was bright yellow in solution. The product was collected and the solvent was removed. (Dichroic dark green-black crystalline solid, 519 mg, 73% (over two steps)). $^1$H NMR (500 MHz, acetone): δ (ppm) 7.71 (s, , J = 1.2 Hz, 1H), 7.39 (m, J = 6.1 Hz, 3H), 7.20 (d, J = 3.2 Hz, 2H), 7.12 (m, J = 6.6 Hz, 2H), 6.69 (dd, J = 1.7 Hz, 1H), 6.42 (dd, J = 1.9 Hz, 1H); $^{13}$C NMR (100 MHz, acetone): δ (ppm) 149.71, 148.07, 132.76, 131.29, 130.32, 129.06, 125.90, 124.56, 121.66, 118.04; ESI-MS ($CH_2Cl_2$) $m/z$ = 388.70 ($[M+H]^+$). UV-Vis ($CH_2Cl_2$) λmax/nm (log ε): 297 (5.82), 390 (5.03), 460 (5.56) 524 (5.09). Anal. Calcd for $Ph_2N$-dp·0.67$CH_3OH$• $C_{27.67}H_{22.67}N_3O_{0.67}$): C, 81.48; H, 5.60; N, 10.30. Found: C, 81.21; H, 5.71; N, 10.57.

### 5.2.4. Dimethylbipyridine

Followed the procedure published by Sprintschnik et al[29], illustrated by Scheme 5.2.

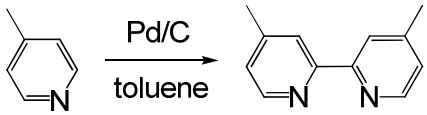


**Scheme 5.2** Synthesis of dimethlybipyridine.

4-picoline (1.54 mol) and palladium on activated charcoal (Pd/C) were refluxed for 3 days. Toluene (55 mL) was added and the solution refluxed for a further 2 hours. The solution was filtered through filter paper while still hot and washed with hot toluene. The filtrate and washings were combined before concentrating on a rotary-evaporator (~100 mL) and then filtering. The crude product was recrystallised from ethyl acetate. A second, smaller crop of crystals were obtained from the recrystallisation of the Pd/C + filter paper using ethyl acetate. (White crystals, 2.86 g, 1%). Spectroscopic data matched that previously published by Sprintschnik et al[29].

### 5.2.5. Dicarboxybipyridine (dcbipy)

Followed the procedure published by Oki & Morgan[24], illustrated by Scheme 5.3.

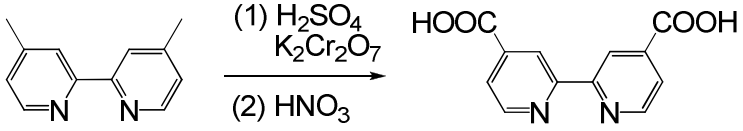


**Scheme 5.3** Synthesis of dicarboxybipyridine.

Dimethylbipyridine (5.43 mmol) was dissolved in a stirring solution of 98% sulphuric acid (25 mL). Potassium dichromate (16.3 mmol) was added in small portions with stirring so that the temperature of the reaction stayed between 70-85°C by cooling when necessary with an ice bath. The reaction mixture was poured into ice water and filtered, and then the precipitate was washed with water until the filtrate ran colourless before drying first under vacuum, and then in air overnight. The dry precipitate was then refluxed in 50% nitric acid (170 mL) for 7 hours, poured over ice again, and then diluted with deionised water (400 mL) before filtering. This solid was washed with water and acetone and finally air

dried. (Flaky white solid, 1.20 g, 90%). Spectroscopic data matched that previously published by Oki & Morgan[24].

### 5.2.6. Docosonate ester-bipyridine (COOR-bipy)

Synthetic route is illustrated by Scheme 5.4. Procedure is an adaptation of that published by Sprintschnik et al[29], where the only modification was the use of 1-docosonol as the alcohol.

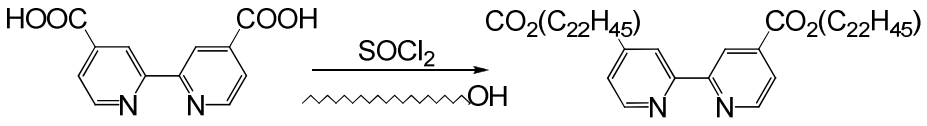


**Scheme 5.4** Synthesis of docosonate ester-bipyridine.

Dicarboxybipyridine (3.09 mmol) was dissolved in thionyl chloride (75 mL) in a clean, dry round-bottom flask. The solution was deaerated and then refluxed under argon for 5 hours. Excess thionyl chloride was removed via vacuum distillation. Dry toluene (90 mL) was added to the solid residue along with a slight excess of 1-docosonol (12.5 mmol). The new solution was briefly deaerated before refluxing under argon for a further 2 hours. Chloroform (200 mL) was added and the mixture was treated with cold aqueous sodium bicarbonate solution (200 mL). The organic phase was dried over magnesium sulphate and the solvent was removed on a rotary-evaporator. The resulting product was recrystallised from chloroform and ethyl acetate. (Flaky white solid, 1.56 g, 59%). $^1$H NMR (500 MHz, $CDCl_3$): δ (ppm) 8.91 (s, 1H), 8.84 (d, J = 5.0 Hz, 1H), 7.87 (d, J = 4.9 Hz, 1H), 3.61 (t, J = 6.5 Hz, 1H), 2.14 (s, 1H), 1.53 (s, 11H), 1.41 (m, J = 7.2 Hz, 3H), 1.22 (s, 65H), 0.84 (t, J = 6.8 Hz, 7H).

*Note: The hydrolysed form of docosonate ester-bipyridine (COOR-bipy) is dicarboxybipyridine (dcbipy).*

### 5.2.7. $[Ru(bipy)_2Cl_2]$

Followed the procedure published by Sullivan, Salmon & Meyer[21], illustrated by Scheme 5.5.

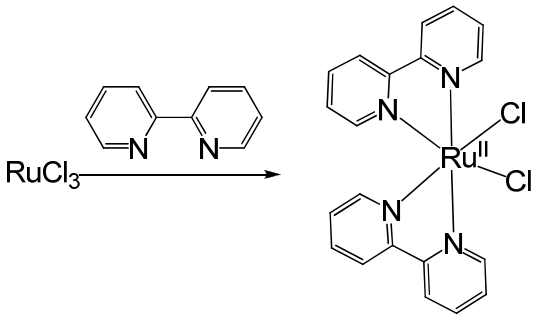


**Scheme 5.5** Synthesis of $[Ru(bipy)_2Cl_2]$.

Ruthenium trichloride (13.4 mmol), lithium chloride (89.4 mmol) and bipyridine (27.0 mmol) were dissolved in dearated, dry DMF (25 mL) and refluxed under argon for 8 hours. The mixture was cooled to room temperature before acetone (130 mL) was added and the solution left in a freezer overnight. The solution was filtered, and then washed with deionised water and diethylether before the product was vacuum dried. (Black crystalline solid, 69%). Spectroscopic data matched that that previously published by Sullivan, Salmon & Meyer[21].

### 5.2.8. $[Ru(dmso)_4Cl_2]$

Followed the procedure published by Kobayashi et al,[43] and Evans, Spencer & Wilkinson[44].

Ruthenium trichloride (4.11 mmol) was refluxed under argon in dimethylsulfoxide (5 mL) for 5 minutes. The solution was cooled and concentrated under vacuum on an oil pump (~2.5 mL) before acetone was added and the solution left to stir overnight. The solution was filtered and then washed with acetone and diethyl ether. Spectroscopic data matched that that previously published by Kobayashi et al,[43] and Spencer & Wilkinson[44].

## 5.3. Synthetic Details for Dye One Group Complexes

### 5.3.1. [Ru(bipy)$_2$(COOH-dp)]

Synthetic route is illustrated by Scheme 2.3.

Ru(bipy)$_2$Cl$_2$] (441 mg, 0.91 mmol), COOMe-dp (256 mg, 0.92 mmol) and triethylamine (0.64 mL) were dissolved in ethylene glycol (30 mL) and the solution was reacted in a microwave synthesiser at a controlled temperature of 100 °C for 35 minutes. $NH_4PF_6$ (1.50 g, 9.20 mmol) was dissolved in deionised water, and added to the reaction mixture along with further water. The suspension was left to stand overnight before the dark green precipitate was collected by filtration. Purification was achieved by dissolving the precipitate in acetonitrile and trituration with diethyl ether. The resulting precipitate was collected by filtration, washed thoroughly with diethyl ether and water, then dried at the pump then in a 40°C oven overnight. The mixture was identified by $^1$H NMR and ES-MS to be a mixture of [**1-1a**]$^+$ and [**1-1a'**]$^+$. The product mixture was dissolved in minimum of THF and added to 1 M aqueous potassium hydroxide solution (47 mL). The orange-red solution was refluxed overnight. The organic solvent was removed on a rotary-evaporator and the resulting suspension stood overnight before the precipitated product was collected by filtration. Purification was achieved by recrystallisation from hot methanol/water. (Metallic green solid, 314 mg, 51% (over two steps)).

$^1$H NMR (500 MHz, $CD_3OD$): δ (ppm) 8.74 (d, J = 8.1 Hz, 4H), 8.05 (m, 4H), 7.89 (d, J = 6.3 Hz, 4H), 7.77 (d, J = 5.5 Hz, 2H), 7.61 (t, J = 6.6 Hz, 2H), 7.44 (t, J = 7.2 Hz, 2H), 7.27 (d, J = 7.8 Hz, 2H), 6.47 (d, J = 4.3 Hz, 2H), 6.33 (m, 2H), 6.30 (d, J = 4.3 Hz, 2H); $^{13}$C NMR (100 MHz, $CD_3OD$): δ (ppm) 174.77, 159.67, 159.65, 158.80, 153.03, 152.07, 150.00, 148.00, 141.98, 139.16, 137.29, 136.78, 132.41, 130.84, 129.09, 127.69, 127.40, 124.54, 124.48, 119.10; ESI-MS (MeOH) $m/z$ = 677.31 ([M+H]$^+$); UV-Vis (MeOH) λmax/nm (log ε): 235 (4.54), 295 (4.70), 459 (4.62) 516 (4.04). Anal. Calcd for **1b**·5.5$H_2O$ ($C_{36}H_{37}N_6O_{7.5}Ru$): C, 55.81; H, 4.81; N, 10.85. Found: C, 55.97; H, 4.32; N, 10.21.

### 5.3.2. [Ru(bipy)$_2$(Ph-dp)]

Synthetic route is illustrated by Scheme 2.4.

[Ru(bipy)$_2$Cl$_2$] (260 mg, 0.54 mmol), Ph-dp (120 mg, 0.55 mmol) and triethylamine (0.08 mL) were dissolved in ethylene glycol (20 mL) and the solution was reacted in a microwave synthesiser at a controlled temperature of 100 °C for 35 minutes. $NH_4PF_6$ (3.44 g, 21.1 mmol) was dissolved in deionised water, and added to the reaction mixture along with further water. The suspension was left to stand overnight. The product was extracted with dichloromethane, dried over magnesium sulphate, and dried on a rotary-evaporator. Purification was achieved by a series of procedures. First, the product was eluted using 75% acetonitrile/25% water over a column containing Sephadex-SP C-25 resin. The acetonitrile was removed by rotary-evaporation, and then the product was extracted in dichloromethane, dried over magnesium sulphate and dried on a rotary evaporator. The product went through a second column, this time containing LH-20 lipophilic Sephadex and using 100% acetonitrile as the eluent. The final purification step was achieved by column chromatography over deactivated neutral alumina, using 80% hexane/20% dichloromethane initially to remove all slow moving impurities and then 95% dichloromethane/5% methanol to remove the product. The product was collected and the solvent was removed. The final product was dried by a high vacuum pump for several days. (Dichroic dark green-black crystalline solid, 359 mg, 85%).

$^1$H NMR (500 MHz, acetone): δ (ppm 7.37 (dd, J = 1.4 Hz, 2H), 8.08 (m, 3H), 8.02 (dd J = 0.6 Hz, 1H), 7.57 (t, J = 2.4 Hz, 1H), 7.46 (m, J = 3.1 Hz, 3H), 6.53 (d, J = 1.3 Hz, 1H), 6.48 (t, J = 1.4 Hz, 1H), 6.29 (d, J = 1.5 Hz, 1H); $^{13}$C NMR (100 MHz, acetone): δ (ppm) 158.45, 158.41, 152.75, 152.21, 149.84, 137.20, 136.55, 136.50, 132.14, 131.01, 130.36, 128.05, 127.67, 127.41, 124.45, 124.31, 124.26, 118.96, 118.89; ESI-MS ($CH_3OH$) $m/z$ = 633.64 ($M^+$); UV-Vis ($CH_2Cl_2$) λmax/nm (log ε): 297 (5.67), 346 (4.89), 460 (5.56) 525 (5.05). Anal. Calcd for [**1-2**]$PF_6$•1$CH_3OH$ ($C_{36}H_{31}F_6N_6OPRu$): C, 53.40; H, 3.86; N, 10.38. Found: C, 53.54; H, 3.60; N, 1034.

### 5.3.3. $[Ru(bipy)_2(Ph_2N\text{-}dp)]$

Synthetic route is illustrated by Scheme 2.5.

$[Ru(bipy)_2Cl_2]$ (191 mg, 0.39 mmol), $Ph_2N$-dp (150 mg, 0.39 mmol) and triethylamine (0.05 mL) were dissolved in ethylene glycol (20 mL) and the solution was reacted in a microwave synthesiser at a controlled temperature of 100 °C for 35 minutes. $NH_4PF_6$ (630 mg, 3.87 mmol) was dissolved in deionised water, and added to the reaction mixture along with further water. The suspension was left to stand overnight. The product was extracted with dichloromethane, dried over magnesium sulphate, and dried on a rotary-evaporator. Purification was achieved by a series of procedures. First, the product was eluted using 75% acetonitrile/25% water over a column containing Sephadex-SP C-25 resin. The acetonitrile was removed by rotary-evaporation, then the product was extracted in dichloromethane, dried over magnesium sulphate and dried on a rotary evaporator. Second, the product was recrystallised from hot dichloromethane/cyclohexane. The final purification step was achieved by column chromatography over deactivated neutral alumina, using 80% hexane/20% dichloromethane initially and then 100% dichloromethane to remove all the remaining impurities, switching to 95% dichloromethane/5% methanol to remove the product. The product was collected and the solvent was removed. The final product was dried by a high vacuum pump for several days. (Dichroic dark green-black crystalline solid, 140 mg, 44%). %).

$^1$H NMR (500 MHz, acetone): δ (ppm) 8.69 (t, J = 3.7 Hz, 2H), 8.05 (dd, J = 4.8 Hz, 4H), 7.55 (t, J = 2.9 Hz, 1H), 7.46 (t, J = 2.4 Hz, 1H), 7.35 (m, J = 3.0 Hz, 3H), 7.18 (d, J = 1.6 Hz, 1H), 7.17 (d, J = 1.08 Hz, 1H), 7.10 (m, J = 2.0 Hz, 2H), 6.74 (d, J = 1.3 Hz, 1H), 6.48 (t, J = 1.4 Hz, 1H), 6.32 (d, J = 1.5 Hz, 1H); $^{13}$C NMR (100 MHz, acetone): δ (ppm) 159.20, 158.48, 152.96, 152.79, 152.46, 152.20, 149.52, 149.13, 148.41, 147.97, 137.11, 136.74, 136.56, 133.56, 133.12, 132.44, 132.20, 130.40, 127.72, 127.35, 125.60, 124.39, 124.30, 122.12, 118.85, 55.46; ESI-MS (acetone) $m/z$ = 800.82 ($M^+$); UV-Vis ($CH_2Cl_2$) λmax/nm (log ε): 297 (5.82), 390 (5.03), 460 (5.56) 524 (5.09). Anal. Calcd for 3[**1-3**]$PF_6$•2$CH_3OH$ ($C_{47.7}H_{38.7}F_6N_7O_{0.67}PRu$): C, 59.5; H, 4.03; N, 10.15. Found: C, 59.50; H, 4.02; N, 10.06.

## 5.4. Synthetic Details for Dye Two Group Complexes

### 5.4.1. [Ru(bipy)(COOH-dp)$_2$]

Synthetic route is illustrated by Scheme 2.6.

$Ru(dmso)_4Cl_2$] (0.66 mmol), COOMe-dp (1.37 mmol) and triethylamine (0.70 mmol) were dissolved in deaerated absolute ethanol (17 mL) and the solution refluxed under argon (with its own headspace) overnight. Purification was achieved by column chromatography on dry-packed deactivated alumina, using 60% hexane/ 40% dichloromethane/1% ethanol as the eluent. (Fine red-brown solid, 322 mg, 60%).
$^1$H NMR (500 MHz, $CDCl_3$): δ (ppm) 8.83 (m, 2H), 8.07 (d, J = 7.9 Hz, 2H), 8.04 (d, J = 8.0 Hz, 2H), 7.42 (d, J = 8.1 Hz, 2H), 7.39 (d, J = 8.0 Hz, 2H), 6.56 (d, J = 3.6 Hz, 4H), 6.46 (m, 2H), 6.37 (d, J = 3.7 Hz, 2H), 6.22 (d, J = 3.7 Hz, 2H), 3.96 (s, 6H), 2.81 (s, 6H), 2.54 (s, 6H); $^{13}$C NMR (100 MHz, $CDCl_3$): δ (ppm) 166.96, 156.07, 152.45, 145.32, 143.71, 136.25, 135.21, 132.66, 132.21, 130.79, 130.13, 130.06, 128.69, 128.54, 118.90, 118.73, 52.54, 45.87, 45.63; UV-Vis ($CH_3OH$) λmax/nm (log ε): 333 (4.54), 300 (4.00), 439 (4.38). Anal. Calcd for [**2-1a**]•$H_2O$ ($C_{38}H_{40}N_4O_7RuS_2$): C, 54.99; H, 4.86; N, 6.75. Found: C, 55.06; H, 4.81; N, 6.52.

**[2-1a]** (162 mg, 0.20 mmol) and 2,2'-bipyridine (781 mg, 5.00 mmol) were mixed together under vacuum before placing in an oil bath preheated to 100°C. The reaction mixture was heated under vacuum overnight. The reaction mixture was taken up in dichloromethane to give a green solution, which was washed with 1 M aqueous hydrochloric acid solution. The organic layer was dried over magnesium sulphate before the solvent was removed on a rotary-evaporator. Purification was achieved by flash chromatography on deactivated alumina using 100% dichloromethane as the eluent. Further purification was achieved by recrystallisation from hot chloroform/methanol. The fine green solid was collected by filtration, washed with methanol, then dried in a 40°C oven overnight. (Dichroic turquoise crystalline solid, 106 mg, 65%).
$^1$H NMR (500 MHz, $CDCl_3$): δ (ppm) 8.24 (d, J = 6.2 Hz, 2H), 8.05 (d, J = 7.8 Hz, 6H), 7.62 (d, J = 7.4 Hz, 2H), 7.51 (d, J = 7.4 Hz, 4H), 7.15 (d, J = 6.5 Hz, 2H), 6.69 (d,

J = 7.0 Hz, 2H), 6.50 (d, J = 4.5 Hz, 2H), 6.37 (d, J = 5.8 Hz, 4H), 6.33 (d, J = 4.4 Hz, 2H), 6.16 (d, J = 4.2 Hz, 2H), 3.95 (s, 6H); $^{13}$C NMR (100 MHz, $CDCl_3$): δ (ppm) 167.04, 159.33, 152.74, 152.23, 147.45, 144.61, 144.21, 135.22, 135.11, 131.98, 130.75, 130.59, 130.24, 129.32, 128.45, 128.34, 128.20, 125.00, 121.57, 118.15, 116.34, 30.94; ESI-MS ($CH_3OH$) $m/z$ = 812.70 ($M^+$); UV-Vis ($CH_2Cl_2$) λmax/nm (log ε): 238 (4.74), 298 (4.57), 453 (4.85) 638 (3.91). Anal. Calcd for [**2-1b**]•$CH_3OH$•$0.5H_2O$ ($C_{45}H_{39}N_6O_{5.5}Ru$): C, 62.43; H, 4.90; N, 9.50. Found: C, 62.16; H, 4.43; N, 9.55.

**[2-1b]** (149 mg, 0.18 mmol) was dissolved in minimum of THF and added to 1 M aqueous potassium hydroxide solution (30 mL). The green solution was refluxed for three nights. 1 M aqueous hydrochloric acid solution was added until the pH was ~2.5 on the pH meter and the organic solvent was removed on a rotary-evaporator. TnBA hydroxide was added. The resulting salt was extracted into dichloromethane, washed with excess water and dried over anhydrous sodium sulphate. Purification was achieved by recrystallisation from hot methanol/water to give a metallic green solid. (Yield: 91 mg, 63% (over three steps)).

$^1$H NMR (400 MHz, DMSO): δ (ppm) 8.03 (d, J = 8.5 Hz, 1H), 7.99 (dd, J = 5.6 Hz, 3H), 7.85 (t, J = 7.8 Hz, 1H), 7.03 (m, J = Hz, 3H), 6.64 (s, 1H), 6.36 (dd, J = 5.8 Hz, 3H), 6.26 (d, J = 4.1 Hz, 1H), 6.17 (d, J = 4.3 Hz, 1H); $^{13}$C NMR (100 MHz, DMSO)*: δ (ppm) 134.5, 128.0, 126.5, 120.5, 115.5, 113.5, 3.0, 1.0, -3.0; ESI-MS (MeOH) m/z = 784.86 ($[M+H]^+$); UV-Vis (MeOH) λmax/nm (log ε): 298 (5.88), 454 (6.12), 635 (5.28). Anal. Calcd for [**2-1c**]•$3CH_3OH$•$1H_2O$ ($C_{36}H_{37}N_6O_{7.5}Ru$): C, 60.19; H, 4.94; N, 9.36. Found: C, 59.88; H, 4.52; N, 9.06.

*$^{13}$C NMR values estimated from cross examination of HMQC. Multiple $^{13}$C NMR spectra were recorded but for some unexplainable reason only displayed solvent peaks.

### 5.4.2. [Ru(bipy)(Ph-dp)$_2$]

Synthetic route is illustrated by Scheme 2.7.

$[Ru(dmso)_4Cl_2]$ (177 mg, 0.36 mmol), Ph-dp (160 mg, 0.73 mmol) and triethylamine (0.10 mL) were dissolved in deaerated absolute ethanol (30 mL) and the solution refluxed

under argon (with its own headspace) overnight. Purification was achieved by column chromatography on dry-packed deactivated alumina, using 60% hexane/ 40% dichloromethane/1% ethanol as the eluent. (Fine red-brown solid, 230 mg, 45%)

**[2-2a]** (132 mg, 0.19 mmol) and 2,2'-bipyridine (1.19 g, 7.6 mmol) were weighed into a clean, dry reaction vessel and then mixed together . The vessel was placed under vacuum briefly before placing in an oil bath preheated to 100°C and flushing with a stream of argon. The reaction mixture was heated under argon overnight. The reaction mixture was taken up in dichloromethane to give a green solution, which was washed with 1 M aqueous hydrochloric acid solution. The organic layer was dried over magnesium sulphate before the solvent was removed on a rotary-evaporator. Purification was achieved by flash chromatography on deactivated alumina using 100% dichloromethane as the eluent. Further purification was achieved by recrystallisation from hot chloroform/methanol. The suspension was centrifuged, the liquid removed, and the supernatant taken up in dichloromethane. The solvent was removed by rotary evaporation and the remaining fine green solid was suspended in hexane, and collected by filtration. The final product was dried by a high vacuum pump for several days. (Green crystalline solid, 25 mg, 10% (over two steps)).

$^{1}$H NMR (500 MHz, acetone): δ (ppm) 8.46 (d, J = 8.0 Hz, 1H), 8.19 (d, J = 5.0 Hz, 1H), 7.80 (t, J = 3.4 Hz, 1H), 7.44 (m, J = 2.4 Hz, 6H), 7.36 (t, J = 2.4 Hz, 1H), 6.75 (t, J = 1.3 Hz, 1H), 6.49 (d, J = 1.9 Hz, 1H), 6.43 (t, J = 2.7 Hz, 1H), 6.37 (d, J = 1.9 Hz, 1H), 6.30 (d, J = 1.9 Hz, 1H), 6.14 (d, J = 1.4 Hz, 1H); $^{13}$C NMR (100 MHz, acetone)*: δ (ppm)150.06, 151.00, 149.50, 148.23, 146.36, 143.52, 142.43, 141.18, 140.93, 139.06, 136.06, 133.69, 131.73, 131.20, 131.07, 129.64, 128.55, 127.89, 127.05, 126.11, 122.40, 122.00, 123.21, 118.28, 117.29, 113.57; UV-Vis ($CH_2Cl_2$) λmax/nm (log ε): 218 (5.64), 299 (5.53), 450 (5.89) 642 (4.94). Anal. Calcd for **[2-2b]**•0.5$CH_3OH$•1$H_2O$ ($C_{41}H_{35}N_6O_{1.5}Ru$): C, 66.83; H, 4.79; N, 11.41. Found: C, 66.70; H, 4.78; N, 10.92.

*$^{13}$C NMR values estimated from cross examination of HMQC. Multiple $^{13}$C NMR spectra were recorded but for some unexplainable reason only displayed solvent peaks.

### 5.4.3. [Ru(bipy)($Ph_2$N-dp)$_2$]

Synthetic route is illustrated by Scheme 2.8.

[$Ru(dmso)_4Cl_2$] (117 mg, 0.24 mmol), $Ph_2$N-dp (187 mg, 0.48 mmol) and triethylamine (0.67 mL) were dissolved in deaerated absolute ethanol (50 mL) and the solution refluxed under argon (with its own headspace) overnight. Purification was achieved by column chromatography on dry-packed deactivated alumina, using 60% hexane/ 40% dichloromethane/1% ethanol as the eluent. (Fine red-brown solid, 158 mg, 61%).

**[2-3a]** (200 mg, 0.19 mmol) and 2,2'-bipyridine (1.57 g, 10.1 mmol) were weighed into a clean, dry 50 mL round bottom flask and then mixed together . The vessel was placed under vacuum briefly before placing in an oil bath preheated to 100°C and flushing with a stream of argon. The reaction mixture was heated under argon over two nights. The reaction mixture was taken up in dichloromethane to give a green solution, which was washed with 1 M aqueous hydrochloric acid solution. The organic layer was dried over magnesium sulphate before the solvent was removed on a rotary-evaporator. Purification was achieved by a series of procedures. Initial purification was achieved by flash chromatography on deactivated alumina using 100% dichloromethane as the eluent. Secondly, the product was eluted using 100% acetone over a lipophilic Sephadex column and then dried on a rotary-evaporator. The final purification step was achieved by column chromatography over deactivated neutral alumina, using 80% hexane/20% dichloromethane initially and then 100% dichloromethane to remove all the remaining impurities, switching to 95% dichloromethane/5% methanol to remove the product. The product was collected and the solvent was removed. The final product was dried by a high vacuum pump for several days. (Green crystalline solid, 46 mg, 19% (over two steps)).
$^1$H NMR (500 MHz, acetone): δ (ppm) 8.45 (d, J = 7.9 Hz, 1H), 8.14 (d, J = 5.4 Hz, 1H), 7.79 (t, J = 4.2 Hz, 1H), 7.34 (dd, J = 7.4 Hz, 7H), 7.16 (d, J = 7.6 Hz, 4H), 7.09 (m, J = 6.4 Hz, 4H), 6.67 (s, 1H), 6.60 (d, J = 3.5 Hz, 1H), 6.52 (d, J = 3.4 Hz, 1H), 6.39 (s, 1H), 6.27 (d, J = 1.1 Hz, 1H), 6.14 (d, J = 1.4 Hz, 1H); $^{13}$C NMR (100 MHz, acetone)*: δ (ppm), 160.49, 153.16, 151.84, 148.55, 148.37, 147.97, 146.24, 136.43, 134.96, 133.37, 132.27, 131.29, 130.25, 129.56, 125.98, 125.23, 123.96, 123.10, 122.46, 118.08, 117.09; UV-Vis ($CH_2Cl_2$) λmax/nm (log ε): 217 (5.89), 300 (5.89),

451 (5.88) 641 (4.98). Anal. Calcd for [**2-3b**]•1$CH_3OH$ ($C_{65}H_{52}N_8ORu$): C, 73.78; H, 4.94; N, 10.57. Found: C, 73.79; H, 4.97; N, 10.60.

*$^{13}$C NMR values estimated from combination of $^{13}$C MNR spectral analysis and cross examination of HMQC. Multiple $^{13}$C NMR spectra were recorded but for some unexplainable reason did not display all peaks.

## 5.5. Synthetic Details for Dye Four Group Complexes

### 5.5.1. [Ru(dcbipy)(Ph-dp)$_2$]

Synthetic route is illustrated by Scheme 2.10.

[**2-1a**] (see section 2.32 of this thesis for the synthetic details of this particular complex) (175 mg, 0.25 mmol) and COOR-bipy (648 mg, 0.75 mmol) were weighed into a clean, dry reaction vessel and then mixed together. The vessel was placed under vacuum before placing in an oil bath preheated to 100°C. The reaction mixture was heated under continuous vacuum for three nights. The reaction mixture was taken up in dichloromethane to give a green solution which was centrifuged to remove insoluble residue and concentrated on a rotary-evaporator. Purification was achieved by flash chromatography on deactivated alumina using 100% dichloromethane as the eluent. Further purification was achieved by flash chromatography on deactivated alumina using 80% hexane/20% dichloromethane as the eluent.

[**4-1a**] was dissolved in minimum of THF (5 mL) and added to 1 M aqueous potassium hydroxide solution (15 mL). The green solution was refluxed overnight. The organic solvent was removed on a rotary-evaporator before TnBA hydroxide was added. The resulting salt was extracted into dichloromethane, washed with excess water and dried over anhydrous sodium sulphate. The solution was concentrated on a rotary-evaporator to a thick oil. Pentane was added to the oil and the solution was sonicated. The resulting precipitate was filtered (quickly) and washed with pentane. The final product was dried by a high vacuum pump for several days. (Metallic green solid, 35 mg, 18% (over two steps)).

$^{1}$H NMR (500 MHz, acetone): δ (ppm) 8.20 (d, J = 5.3 Hz, 1H), 7.75 (d, J = 5.4 Hz, 1H), 7.44 (m, J = 4.2 Hz, 5H), 6.75 (s, 1H), 6.50 (d, J = 3.6 Hz, 1H), 6.39 (s, 1H), 6.33 (d, J = 3.4 Hz, 1H), 6.29 (dd, J = 1.8 Hz, 1H), 6.07 (d, J = 3.6 Hz, 1H); $^{13}$C NMR (100 MHz, acetone)$^{*}$: δ (ppm) 100.26, 116.0, 117.0, 126.0, 128.0, 129.0, 130.0, 131.0, 147.5, 151.0, 152.0; ESI-MS (MeOH) $m/z$ = 723.89 ($M^{+}$); UV-Vis ($CH_2Cl_2$) λmax/nm (log ε): 308 (4.92), 451 (5.26) 643 (4.46).

*$^{13}$C NMR values estimated from cross examination of HMQC. Multiple $^{13}$C NMR spectra were recorded but for some unexplainable reason only displayed solvent peaks.

# REFERENCES


1. Gratzel, M., Solar energy conversion by dye-sensitized photovoltaic cells. *Inorganic Chemistry* **2005,** 44, (20), 6841-6851.
2. Brückner, C.; Zhang, Y.; Rettig, S. J.; Dolphin, D., Synthesis, derivatization and structural characterization of octahedral tris(5-phenyl-4,6-dipyrrinato) complexes of cobalt(III) and iron(III). *Inorganica Chimica Acta* **1997,** 263, (1-2), 279-286.
3. Wood, T. E.; Thompson, A., Advances in the chemistry of dipyrrins and their complexes. *Chemical reviews* **2007,** 107, (5), 1831-1861.
4. Hall, J. D.; McLean, T. M.; Smalley, S. J.; Waterland, M. R.; Telfer, S. G., Chromophoric Dipyrrin Complexes Capable of Binding to TiO2: Synthesis, Structure and Spectroscopy. *Dalton Transactions* **(accepted for publication on 6 October 2009)**.
5. Falk, H., *The Chemistry of Linear Oligopyrroles and Bile Pigments*. Springer-Verlag/Wien: New York, 1989.
6. Gilles, U.; Raymond, Z.; Anthony, H., The Chemistry of Fluorescent Bodipy Dyes: Versatility Unsurpassed13. *Angewandte Chemie - International Edition* **2008,** 47, (7), 1184-1201.
7. Smalley, S. J.; Waterland, M. R.; Telfer, S. G., Heteroleptic Dipyrrin/Bipyridine Complexes of Ruthenium(II). *Inorganic Chemistry* **2008,** 48, (1), 13-15.
8. Kennelly, T.; Gafney, H. D.; Braun, M., Photoinduced disproportionation of Ru(bpy)32+ on porous Vycor glass. *Journal of the American Chemical Society* **2002,** 107, (15), 4431-4440.
9. Fuller, Z. J.; Bare, W. D.; Kneas, K. A.; Xu, W. Y.; Demas, J. N.; DeGraff, B. A., Photostability of Luminescent Ruthenium(II) Complexes in Polymers and in Solution. *Analytical Chemistry* **2003,** 75, (11), 2670-2677.
10. Sauvage, J. P.; Collin, J. P.; Chambron, J. C.; Guillerez, S.; Coudret, C.; Balzani, V.; Barigelletti, F.; De Cola, L.; Flamigni, L., Ruthenium(II) and Osmium(II) Bis(terpyridine) Complexes in Covalently-Linked Multicomponent Systems: Synthesis, Electrochemical Behavior, Absorption Spectra, and Photochemical and Photophysical Properties. *Chemical Reviews* **2002,** 94, (4), 993-1019.
11. Komatsuzaki, N.; Katoh, R.; Himeda, Y.; Sugihara, H.; Arakawa, H.; Kasuga, K., Structure and photochemical properties of ruthenium complexes having dimethyl-substituted DPPZ or TPPHZ as a ligand. *Journal of the Chemical Society, Dalton Transactions* **2000**, (18), 3053-3054.
12. Bonnet, S.; Collin, J.-P., Ruthenium-based light-driven molecular machine prototypes: synthesis and properties. *Chemical Society Reviews* **2008,** 37, (6), 1207-1217.
13. Hara, K.; Arakawa, H., Dye-sensitised Solar Cells (Chapter 15). In *Handbook of Photovoltaic Science and Engineering*, Luque, A.; Hegedus, S., Eds. John Wiley & sons, Ltd: West Sussex, England, 2003.
14. Fanni, S.; Keyes, T. E.; O'Connor, C. M.; Hughes, H.; Wang, R.; Vos, J. G., Excited-state properties of ruthenium(II) polypyridyl complexes containing asymmetric triazole ligands. *Coordination Chemistry Reviews* **2000,** 208, (1), 77-86.
15. Chiba, Y.; Islam, A.; Watanabe, Y.; Komiya, R.; oide, N.; Han, L., Dye-Sensitized Solar Cells with Conversion Efficiency of 11.1%. *Japanese Journal of Applied Physics* **2006,** 45, (25), L638-L640.

16. SANYO Electric Co., L. SANYO Develops HIT Solar Cells with World's Highest Energy Conversion Efficiency of 23.0%. http://us.sanyo.com/News/SANYO-Develops-HIT-Solar-Cells-with-World-s-Highest-Energy-Conversion-Efficiency-of-23-0- (21 May),
17. Robertson, N., Optimizing dyes for dye-sensitized solar cells. *Angewandte Chemie - International Edition* **2006,** 45, (15), 2338-2345.
18. Campbell, W. M.; Burrell, A. K.; Officer, D. L.; Jolley, K. W., Porphyrins as light harvesters in the dye-sensitised TiO2 solar cell. *Coordination Chemistry Reviews* **2004,** 248, (13-14), 1363-1379.
19. Rohand, T.; Dolusic, E.; Ngo, T. H.; Maes, W.; Dehaen, W., Efficient synthesis of aryldipyrromethanes in water and their application in the synthesis of corroles and dipyrromethenes. *ARKIVOC* **2007**, 307-324.
20. Littler, B. J.; Miller, M. A.; Hung, C. H.; Wagner, R. W.; O'Shea, D. F.; Boyle, P. D.; Lindsey, J. S., Refined synthesis of 5-substituted dipyrromethanes. *Journal of Organic Chemistry* **1999,** 64, (4), 1391-1396.
21. Sullivan, B. P.; Salmon, D. J.; Meyer, T. J., Mixed phosphine 2,2'-bipyridine complexes of ruthenium. *Inorganic Chemistry* **1978,** 17, (12), 3334-3341.
22. Hydrogen bonds. http://www.bio.brandeis.edu/classes/biochem104/hydrogen_bonds.pdf (21 October 2009),
23. Ophardt, C. H. hydrogen bonding. http://www.elmhurst.edu/~chm/vchembook/161Ahydrogenbond.html (21 October 2009),
24. Oki, A. R.; Morgan, R. J., An efficient preparation of 4, 4-dicarboxy-2, 2-bipyridine. *Synthetic Communications* **1995,** 25, (24), 4093 - 4097.
25. Liska, P.; Vlachopoulos, N.; Nazeeruddin, M. K.; Comte, P.; Gratzel, M., Cis - diaquabis( 2,2'-bipyridyL4,4'-dicarboxylate)-ruthenium(I1) sensitizes wide band gap oxide semiconductors very efficiently over a broad spectral range in the visible. *Journal of the American Chemical Society* **1988,** 110, 3686-3687.
26. Bessho, T.; Yoneda, E.; Yum, J.-H.; Guglielmi, M.; Tavernelli, I.; Imai, H.; Rothlisberger, U.; Nazeeruddin, M. K.; GraÌˆtzel, M., New Paradigm in Molecular Engineering of Sensitizers for Solar Cell Applications. *Journal of the American Chemical Society* **2009,** 131, (16), 5930-5934.
27. Klein, C.; Nazeeruddin, M. K.; Di Censo, D.; Liska, P.; Gratzel, M., Amphiphilic Ruthenium Sensitizers and Their Applications in Dye-Sensitized Solar Cells. *Inorganic Chemistry* **2004,** 43, (14), 4216-4226.
28. *Aldrich Handbook of Fine Chemicals*. Sigma-Aldrich Co.: Australia/New Zealand, 2007-2008.
29. Sprintschnik, G.; Sprintschnik, H. W.; Kirsch, P. P.; Whitten, D. G., Preparation and photochemical reactivity of surfactant ruthenium(II) complexes in monolayer assemblies and at water-solid Interfaces. *Journal of the American Chemical Society* **1977,** 99, (15), 4947-4954.
30. Horváth, O.; Huszánk, R.; Valicsek, Z.; Lendvay, G., Photophysics and photochemistry of kinetically labile, water-soluble porphyrin complexes. *Coordination Chemistry Reviews* **2006,** 250, (13-14), 1792-1803.
31. Klassen, D. M.; Crosby, G. A., Spectroscopic Studies of Ruthenium(II) Complexes. Assignment of the Luminescence. *The Journal of Chemical Physics* **1968,** 48, (4), 1853-1858.

32. Mabrouk, P. A.; Wrighton, M. S., Resonance Raman spectroscopy of the lowest excited state of derivatives of tris(2,2'-bipyridine)ruthenium(II): substituent effects on electron localization in mixed-ligand complexes. *Inorganic Chemistry* **2002,** 25, (4), 526-531.
33. Smith, E.; Dent, G., *Modern Raman Spectroscopy - A Practical Approach*. Jon Wiley & Sons, Ltd: West Sussex, England, 2005.
34. McCreery, R. L., *Raman Spectroscopy for Chemical Analysis*. John Wiley & Sons, Ltd: Columbus, Ohio, 2000; Vol. 157.
35. Xia, H.; Zhu, Y.; Lu, D.; Li, M.; Zhang, C.; Yang, B.; Ma, Y., Ruthenium(II) Complexes with the Mixed Ligands 2,2â€˜-Bipyridine and 4,4â€˜-Dialkyl Ester-2,2â€˜-bipyridine as Pure Red Dopants for a Single-Layer Electrophosphorescent Device. *The Journal of Physical Chemistry B* **2006,** 110, (37), 18718-18723.
36. Cohen, S. M.; Halper, S. R., Dipyrromethene complexes of iron. *Inorganica Chimica Acta* **2002,** 341, 12-16.
37. Cooke, M. M.; Doeven, E. H.; Hogan, C. F.; Adcock, J. L.; McDermott, G. P.; Conlan, X. A.; Barnett, N. W.; Pfeffer, F. M.; Francis, P. S., Comparison of homoleptic and heteroleptic 2,2'-bipyridine and 1,10-phenanthroline ruthenium complexes as chemiluminescence and electrochemiluminescence reagents in aqueous solution. *Analytica Chimica Acta* **2009,** 635, (1), 94-101.
38. Eisenberg, R., CHEMISTRY: Rethinking Water Splitting. *Science* **2009,** 324, (5923), 44-45.
39. Kohl, S. W.; Weiner, L.; Schwartsburd, L.; Konstantinovski, L.; Shimon, L. J. W.; Ben-David, Y.; Iron, M. A.; Milstein, D., Consecutive Thermal H2 and Light-Induced O2 Evolution from Water Promoted by a Metal Complex. *Science* **2009,** 324, (5923), 74-77.
40. Wacholtz, W. M.; Auerbach, R. A.; Schmehl, R. H.; Ollino, M.; Cherry, W. R., Correlation of ligand field excited-state energies with ligand field strength in (polypyridine)ruthenium(II) complexes. *Inorganic Chemistry* **2002,** 24, (12), 1758-1760.
41. Gottlieb, H. E.; Kotlyar, V.; Nudelman, A., NMR Chemical Shifts of Common Laboratory Solvents as Trace Impurities. *The Journal of Organic Chemistry* **1997,** 62, (21), 7512-7515.
42. Yu, L.; Muthukumaran, K.; Sazanovich, I. V.; Kirmaier, C.; Hindin, E.; Diers, J. R.; Boyle, P. D.; Bocian, D. F.; Holten, D.; Lindsey, J. S., Excited-State Energy-Transfer Dynamics in Self-Assembled Triads Composed of Two Porphyrins and an Intervening Bis(dipyrrinato)metal Complex. *Inorganic Chemistry* **2003,** 42, (21), 6629-6647.
43. Kobayashi, T.; Nishina, Y.; Shimizu, K.; Sato, G. P., Diacetonitrilbis(beta-diketonato)ruthenium(II) complexes. Their preparation and use as intermediates for the synthesis of mixed-ligand beta-diketonato ruthenium(III) complexes. *Chemistry Letters* **1988**, 1137-1140.
44. Evans, I. P.; Spencer, A.; G. Wilkinson, Dichlorotetrakis(dimethyl sulphoxide)ruthenium(II) and its use as a source material for some new ruthenium(II) complexes. *J C S Dalton* **2007**, 204-209.

# APPENDIX A

## X-ray Crystallographic Data

### A1 [Ru(bipy)$_2$(COOH-dp)]

Crystal data structure refinement for [Ru(bipy)$_2$(COOH-dp)] ([**1-1b**]).

| | |
|---|---|
| Identification code | ss125 |
| Empirical formula | $C_{36}H_{26}N_6O_2Ru$, $CH_4O$, 6($H_2O$) |
| Formula weight | 815.83 |
| Temperature | 150(2) K |
| Wavelength | 0.71073 A |
| Crystal system | triclinic |
| Space group | P-1 |
| Crystal size | 0.26 x 0.22 x 0.16 mm |
| Crystal colour | black |
| Crystal form | prism |
| Unit cell dimensions | a = 8.76980(10) Å alpha = 108.0700(10) °<br>b = 12.46720(10) Å beta = 90.1170(10) °<br>c = 17.3089(2) Å gamma = 92.8580(10) ° |
| Volume | 1796.58(3) Å$^3$ |
| Z, calculated density | 2, 1.512 Mg/m$^3$ |
| Absorption coefficient | 0.501 mm$^{-1}$ |
| Absorption correction | empirical |
| F(000) | 848 |
| Theta range for data collection | 0.992 to 30.06° |
| Limiting indices | -12<h<12, -17<k<17, -24<l<24 |
| Reflections collected/unique | 73884/10474 [R(int) = 0.038 ] |
| Completeness to theta = 30.06 | 99.2% |
| Maximum and minimum transmission | 0.8807 and 0.9241 |
| Refinement method | Full matrix least-squares on $F^2$ |
| Data/restraints/parameters | 10474/18/512 |
| Goodness-of-fit on $F^2$ | 1.062 |

| | |
|---|---|
| Final R indices [I>2sigma(I)] | R1 = 0.0472, wR2 = 0.1288 |
| R indices (all data) | R1 = 0.0550, wR2 = 0.1341 |
| Largest difference peak and hole | 1.81/-1.32 |

## A2 [Ru(bipy)(COOH-dp)$_2$]

Crystal data structure refinement for [Ru(bipy)(COOH-dp)$_2$] ([**2-1c**]).

| | |
|---|---|
| Identification code | ss261 |
| Empirical formula | 0.5($C_{42}H_{30}RuN_6O_4$), ($C_5H_{12}$) |
| Formula weight | 928.08 |
| Temperature | 123(2) K |
| Wavelength | 1.54178 A |
| Crystal system | orthorhombic |
| Space group | *P*bcn |
| Crystal size | 0.20 x 0.20 x 0.02 mm |
| Crystal colour | green |
| Crystal form | plate |
| Unit cell dimensions | a =12.4091(12) Å alpha = 90.00°<br>b = 10.8412(8) Å beta = 90.00°<br>c = 33.848(3) Å gamma = 90.00° |
| Volume | 4553.6(7) Å$^3$ |
| Z, calculated density | 4, 1.354 Mg/m$^3$ |
| Absorption coefficient | 3.203 mm$^{-1}$ |
| Absorption correction | multi-scan |
| F(000) | 1936 |
| Theta range for data collection | 13.39 to 143.42° |
| Limiting indices | -13<h<11, -12<k<11, -37<l<27 |
| Reflections collected/unique | 21994/3247 [R(int) = 0.1231] |
| Completeness to theta = 58.93 | 99.6% |
| Maximum and minimum transmission | 0.5667 to 0.9387 |
| Refinement method | Full matrix least-squares on F$^2$ |
| Data/restraints/parameters | 3247/19/278 |
| Goodness-of-fit on F$^2$ | 1.066 |

| | |
|---|---|
| Final R indices [I>2sigma(I)] | R1 =0.1215, wR2 = 0.2716 |
| R indices (all data) | R1 = 0.1393, wR2 = 0.2901 |
| Largest difference peak and hole | 1.74/-1.39 |

## A3 [Ru(bipy)(Ph-dp)$_2$]

Crystal data structure refinement for [Ru(bipy)(Ph-dp)$_2$] ([**2-2b**]).

| | | |
|---|---|---|
| Identification code | ss235 | |
| Empirical formula | $C_{40}H_{30}N_6Ru$ | |
| Formula weight | 695.77 | |
| Temperature | 123(2) K | |
| Wavelength | 1.54178 A | |
| Crystal system | monoclinic | |
| Space group | $P2_1c$ | |
| Crystal size | 3.00 x 0.07 x 0.01 mm | |
| Crystal colour | green | |
| Crystal form | needle | |
| Unit cell dimensions | a = 8.9691(74) Å | alpha = 90.00° |
| | b = 24.668(20) Å | beta = 97.30(1)° |
| | c = 14.653(12) Å | gamma = 90.00° |
| Volume | 3216(4) Å$^3$ | |
| Z, calculated density | 4, 1.437 Mg/m$^3$ | |
| Absorption coefficient | 4.248 mm$^{-1}$ | |
| Absorption correction | multi-scan | |
| F(000) | 1424 | |
| Theta range for data collection | 13.12 to 63.91° | |
| Limiting indices | -8<h<8, -24<k<23, -14<l<14 | |
| Reflections collected/unique | 16361/3346 [R(int) = 0.175] | |
| Completeness to theta = 50.41 | 99.5% | |
| Maximum and minimum transmission | 0.42 to 1.0 | |
| Refinement method | Full matrix least-squares on F$^2$ | |
| Data/restraints/parameters | 3346/240/424 | |
| Goodness-of-fit on F$^2$ | 0.996 | |

| | |
|---|---|
| Final R indices [I>2sigma(I)] | R1 =0.1035, wR2 = 0.2225 |
| R indices (all data) | R1 =0.1627, wR2 = 0.2683 |
| Largest difference peak and hole | 1.38/-0.78 |

# APPENDIX B

## Water Splitting Procedure and Results Carried Out by Eisenberg.

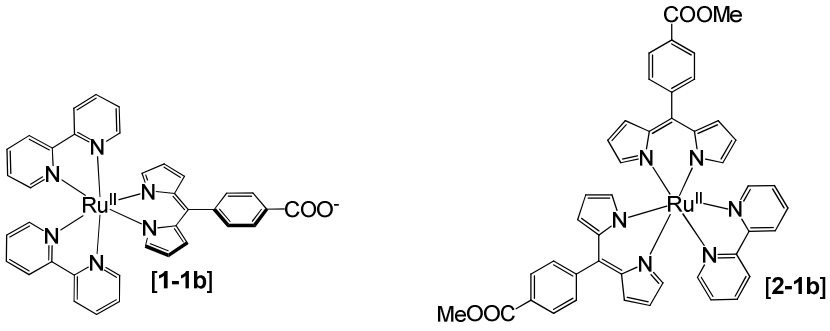


**Figure B.1** The compounds sent to Dr Eisenberg to test for water splitting ability.

20 mg of 0.5% w/w $Pt/TiO_2$ were suspended in 20 ml of a $5x10^{-5}$ M solution of compound [**1-1b**] in MeCN/10% v/v TEOA in $H_2O$ (1:1) (adjusted to pH = 7 with HCl). The resulting suspension was purged with $N_2$ for 10 min and then irradiated $\lambda > 420$ nm using a Xenon-Mercury arc lamp and a cut off filter. Every 60 min a gas sample was taken from the reaction vessel and was analysed in a gas chromatograph. No $H_2$ was detected after ~ 24 h of continuous irradiation.

In the case of compound [**2-1b**], the solvent mixture used was MeCN/10% v/v TEOA in $H_2O$ (9:1) due to poor solubility of the compound in aqueous media. Otherwise the procedure was identical to that for compound [**1-1b**]. No $H_2$ was detected after ~ 24 h of continuous irradiation.

# APPENDIX C/INSERT

## Systems Key

This insert provides details of the structures of the complexes used in this thesis, their abbreviations and numbering schemes. The purpose of this insert is to provide an easy reference for the reader to clarify discussions regarding the spectroscopic analysis of the complexes (Chapter 3).

## C1 Dipyrrin Ligands

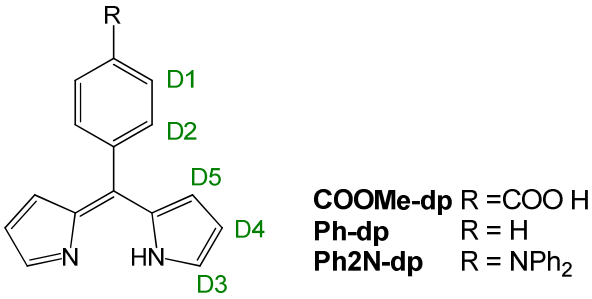


COOMe-dp ester-type dipyrrin ligand

Ph-dp phenyl-type dipyrrin ligand

$Ph_2N$-dp diphenylamino-type dipyrrin ligand

## C2 Dye One Group Complexes

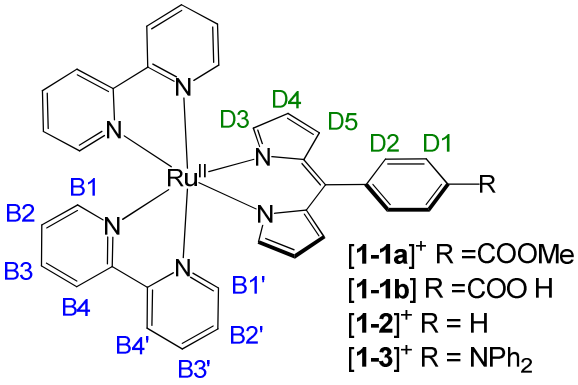


**[1-1a]**. $[Ru(bipy)_2(COOMe\text{-}dp)]$ ester-type Dye One group complex

**[1-1b]**. $[Ru(bipy)_2(COOH\text{-}dp)]$ carboxylic acid-type Dye One group complex

**[1-2]$^+$**. $[Ru(bipy)_2(Ph\text{-}dp)]$ phenyl-type Dye One group complex

**[1-3]$^+$**. $[Ru(bipy)_2(Ph_2N\text{-}dp)]$ diphenylamino-type Dye One group complex

## C3 Dye Two Group Complexes

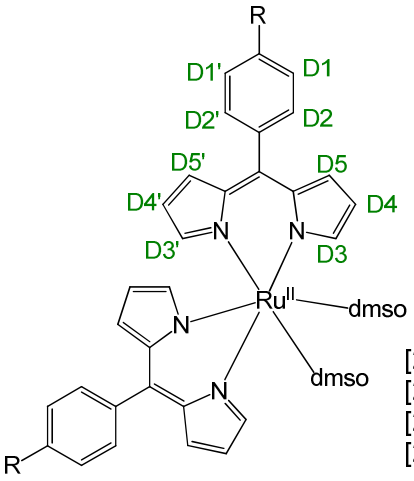


[**2-1b**] R =COO Me
[**2-1c**] R =COO H
[**2-2b**] R = H
[**2-3b**] R = $NPh_2$

**[2-1a]**. [Ru(dmso)$_2$(COOMe-dp)$_2$] the ester-type intermediate complex

**[2-2a]**. [Ru(dmso)$_2$(Ph-dp)$_2$] phenyl-type intermediate complex

**[2-3a]**. [Ru(dmso)$_2$($Ph_2$N-dp)$_2$] diphenylamino-type intermediate complex

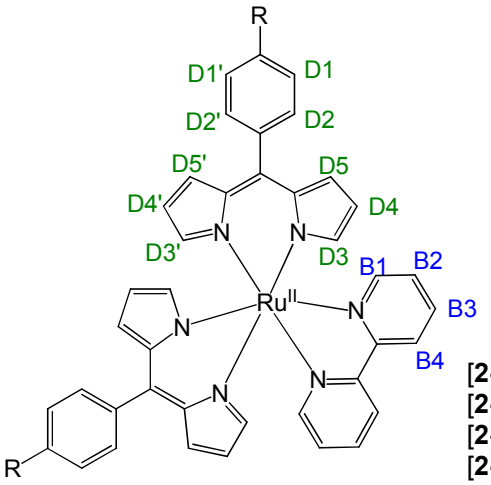


[**2-1b**] R =COO Me
[**2-1c**] R =COO H
[**2-2b**] R = H
[**2-3b**] R = $NPh_2$

**[2-1b]**. [Ru(bipy)(COOMe-dp)$_2$] ester-type Dye Two group complex

**[2-1c]**. [Ru(dmso)$_2$(COOMe-dp)$_2$] carboxylic acid-type Dye Two group complex

**[2-2b]**. [Ru(bipy)(Ph-dp)$_2$], the phenyl-type Dye Two group complex

**[2-3b]**. [Ru(bipy)($Ph_2$N-dp)$_2$] diphenylamino-type Dye Two group complex

## C4 Dye Four Group Complexes

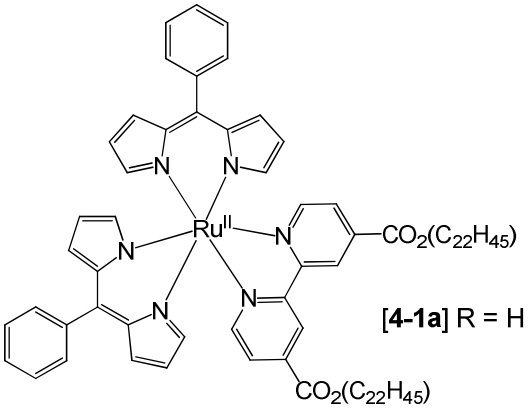


**[4-1a]**. [Ru(COOR-bipy)(Ph-dp)$_2$] phenyl-type Dye Four group precursor complex

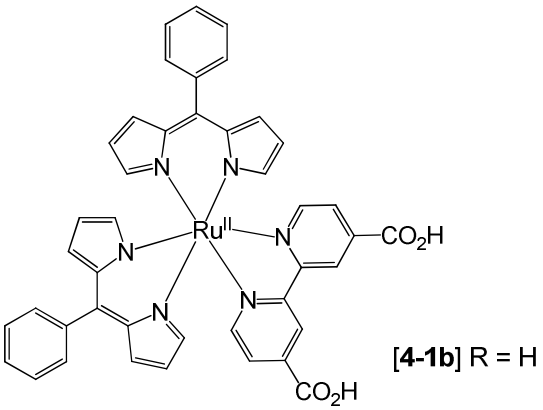


**[4-1b]**. [Ru(dcbipy)(Ph-dp)$_2$] phenyl-type Dye Four group complex